UNIVERSITY OF CALIFORNIA

Santa Barbara

Programmed Secretion Arrest and Receptor-Triggered Restart of CdiA during Contact-Dependent Growth Inhibition

A dissertation submitted in partial satisfaction of the
requirements for the degree Doctor of Philosophy
in Biochemistry and Molecular Biology

by

Kiho Song

Committee in charge:
Professor Christopher S. Hayes, Chair
Professor David A. Low
Professor Kevin W. Plaxco
Professor Anthony De Tomaso

September 2020

The dissertation of Kiho Song is approved.

_____

David A. Low

_____

Kevin W. Plaxco

_____

Anthony De Tomaso

_____

Christopher S. Hayes, Chair

July 2020

ACKNOWLEDGEMENTS

I thank God for His abundant blessings throughout my PhD manifested through the following wonderful people.

Professor Chris Hayes made my accomplishments possible. When my first PI left academia and closed his lab, I was ready to give up pursuing research. Chris adopted me into his group and jumpstarted my passion. He has continuously fueled my love for science for the past 4 years. I am deeply grateful for him.

My committee members (Professors David Low, Kevin Plaxco, and Tony De Tomaso) have supported me throughout these years. They were especially supportive when I made the shift to Chris's lab. I will always be thankful for them.

None of my works would have been possible without Dr. Zach Ruhe and Dr. Fernando Garza. They have been immensely instrumental in my development as a researcher. Besides their rich technical expertise, I appreciate their friendship. I also thank all former and current members of the Hayes lab. I have learned so much from them. Working with them has been a big part of why I loved coming to the lab.

I thank my family and friends for their love and support. My parents, Rev. Chae Myong Song and Kyung Hee Song, taught me the joy of learning and working with others. Unlike the CDI+ cells, they have shown me what it means "to love your neighbor as yourself."

Finally, I thank my loving wife, Hansol Jang. She has patiently endured many date night plans change because of my experiments. She has given me unconditional love and unwavering support throughout my PhD. It's difficult to describe how much I love her, but she is the only reason I rush my western blots to come home to.

VITA OF KIHO SONG
July 2020

Education

University of California, Santa Barbara
B.S. in Biochemistry & Molecular Biology July 2020
Cumulative GPA: 3.99/4.00

University of California, Davis
B.S. in Biochemistry & Molecular Biology June 2012
Cumulative GPA: 3.79/4.00 High Honors

Research Experience

University of California, Santa Barbara
PhD Candidate
Christopher Hayes, UCSB MCDB Jun 2016-Present

- Mechanism of toxin delivery by bacterial surface protein CdiA
- Investigated the programmed secretion arrest and restart of CdiA

PhD Student
Patrick Daugherty Lab, UCSB Chemical Engineering Jun 2015-Jun 2016

- Guided selection of random peptide library displayed on bacterial surface
- Developed peptides which bind to synthetic polymer membrane

Marrone Bio Innovations Inc. Davis, California
Associate Research Scientist
Nematology/Soil-borne Pathogens Jun 2012-Jun 2014

- Designed bioassays to aid in developing bio-nematicides and bio-fungicides
- Modes of action studies of active compounds

University of California, Davis
Undergraduate Researcher
Valerie Williamson Lab, UC Davis Nematology Oct 2009-Jun 2012

- PCR-based diagnostic test to determine root-knot nematodes species based on the mitochondrial DNA

Teaching Experience

University of California, Santa Barbara
Contemporary Nutrition, Immune Systems and AIDS, Microbiology Lab

University of California, Davis
Biochemistry Lab

Awards/Honors

University of California, Santa Barbara
Academic Senate Outstanding Teaching Assistant Award Nominee, 2020
Graduate Division Dissertation Fellowship, 2020
MCDB-BMSE Friday Noon Seminar Best 5th Year Presentation, 2019
Ellen Schamberg Burley Graduate Scholarship, 2019
Doreen J. Putrah Cancer Research Foundation Conference Fellowship, 2018
MCDB-BMSE Friday Noon Seminar Best 3rd Year Presentation, 2017

University of California, Davis
College of Biological Sciences Citation Award, 2012
Biological Sciences Dean's List, 2008-2011
First Year Scholar, 2009
Honor Roll by Congressman Dennis Cardoza, 2008

Publications

Zachary C. Ruhe*, Poorna Subramanian*, **Kiho Song***, Josephine Y. Nguyen, Taylor A. Stevens, David A. Low, Grant J. Jensen, and Christopher S. Hayes. "Programmed Secretion Arrest and Receptor-Triggered Toxin Export during Antibacterial Contact-Dependent Growth Inhibition." Cell (2018). 175, 921–933. https://www.cell.com/cell/pdf/S0092-8674(18)31386-2.pdf (*equal contributions)

Nicholas L. Bartelli, Sheng Sun, Grant C. Gucinski, Hongjun Zhou, **Kiho Song**, Christopher S. Hayes, Frederick W. Dahlquist. "The Cytoplasm-Entry Domain of Antibacterial CdiA Is a Dynamic α-Helical Bundle with Disulfide-Dependent Structural Features." JMB (2019) 431, 3203-3216. https://doi.org/10.1016/j.jmb.2019.05.049

Presentations

Oral presentation. "Programmed Secretion Arrest and Restart in the Bacterial Surface Protein, CdiA." *Molecular Genetics of Bacteria and Phages Meeting* (Aug 5-9, 2019)

Poster presentation. "CdiA Mutants Reveal a Complex Mechanism of Toxin Delivery." *Molecular Genetics of Bacteria and Phages Meeting* (Aug 7-12, 2017)

Oral presentation. "CdiA Mutants Reveal a Complex Mechanism of Toxin Delivery." *West Coast Bacterial Physiologists* (Dec 15-17, 2017)

ABSTRACT

Programmed Secretion Arrest and Receptor-Triggered Restart of CdiA during Contact-Dependent Growth Inhibition

by

Kiho Song

Many Gram-negative bacteria utilize contact-dependent growth inhibition (CDI) systems to deliver toxins to nearby cells using a large (~350kD) filamentous protein, CdiA, expressed on their cell surface. Recently, we discovered that biogenesis of CdiA is tightly regulated such that the N-terminal half of CdiA is first exported to form a 33nm stick on the cell surface, while the C-terminal half remains in the periplasm. When CdiA recognizes a receptor on a neighboring cell, the periplasmic half resumes secretion and penetrates the neighboring cell's outer membrane to deliver the C-terminal toxin domain. This mode of programmed secretion is crucial for CdiA function because prematurely secreting its C-terminal half releases CdiA off the cell surface and renders it ineffective. Since there is no obvious source of energy or potential difference across the outer membrane, it is intriguing how secretion of a large protein like CdiA is arrested at a precise configuration only to be resumed by a receptor-binding event.

This thesis will highlight the recent findings about this mechanism of programmed secretion of CdiA. Deletions and sequence-replacement mutants have identified a 50-residue

long, Tyr-Pro enriched, region in the periplasmic half of the protein responsible for secretion arrest. The CdiA receptor-binding event specifically relays a signal to release this arrest and resume secretion. Studies with a chimeric CdiA-DHFR have shown that the periplasmic CdiA domain must first unfold in order to resume export. Substrate-induced folding of the periplasmic DHFR fusion disrupts secretion restart. Interestingly, enzymatic fusions to CdiA demonstrate that the system functions as a nanoscale switch to direct the enzymatic activity to the extracellular space only when CdiA binds a receptor. Lastly, the filamentous N-terminal CdiA is a robust toxin delivery machine which tolerates shortening and severing at its base.

TABLE OF CONTENTS

Chapter 1. Introduction

The plasma membrane forms a minimal boundary which defines a living cell. Gram-negative bacteria have additional asymmetric outer membrane (OM) with phospholipids in the inner leaflet and lipopolysaccharides in the outer leaflet (1,2). The outer membrane of Gram-negative bacteria serves as the first barrier to protect the organism from external threats such as bacteriocins and antimicrobial compounds (1), (3). However, bacteria must selectively secrete protein products across the outer membrane to carry out crucial cellular functions such as motility, adhesion, pathogenicity, bacterial communications, adaptation and survival (4,5).

Protein secretion across the lipid bilayer is a challenging task, and bacteria have developed diverse protein secretion systems to accomplish it. Many secretion systems have been identified and named as type I secretion system (T1SS) to type IX secretion system (T9SS) (4,6–11). Of the nine secretion systems, T1SS-T6SS have been well-characterized in Gram-negative bacteria (4,7). The chaperone-usher pathway is named T7SS and T8SS each dedicated to export of type I pili and curli, respectively (9,11). A unique early secretory antigenic target (ESAT6) protein family secretion (ESX) systems in *Mycobacteria* is also named as the T7SS (6), but an equivalent system is not found in Gram-negative bacteria (11). T9SS is the most recently discovered protein secretion that is found only in some species of *Bacteroidetes* phylum (12–14). I will discuss the T1SS-T6SS for a brief review of secretion systems in Gram-negative bacteria.

A. One-step transport systems

The T1SS, T3SS, T4SS, and T6SS are known as one-step transport systems because they deploy both IM and OM machinery to export proteins directly from the cytoplasm to the extracellular space.

The type I secretion system (T1SS) is composed of three essential components: an inner membrane component (IMC), an outer membrane factor (OMF), and a membrane fusion protein (MFP) which bridges the IMC and the OMF (15). The IMC is an ABC (ATP-binding cassette) transporter that provides an IM channel and serves as an energy source (4)(15). The IMC-MFP component recognizes a specific substrate for export but the OMF, TolC, is a promiscuous OM pore also involved in other efflux pump machinery (4,15). Hemolysin HlyA from *E. coli* is a well-studied model T1SS hemolysin. HlyB-HlyD, the IMC-MFP component of HlyA, forms a tunnel with TolC (16). This channel recognizes the C-terminal signal of HlyA to export into the medium where it lyses red blood cells (17).

The type III secretion system (T3SS) is composed of more than 25 conserved proteins to form a double-membrane spanning nanomachine (4,18). Many pathogenic Gram-negative bacteria utilizes T3SS in effector protein delivery to eukaryotic target cells (4,18). The plague-causing *Yersinia pestis* outer membrane proteins (Yops) are well-studied examples of T3SS (18). Deployment of Yops involves an impressive coordination between a cytoplasmic chaperone SycD which prevents tight folding of Yops (19,20), cytoplasmic ATPase YscN to energize export (19), and multi-component injectisome. The injectisome is built with basal rings at both the IM and the OM and needle-like structure formed by YscF (21–24). Upon construction of this needle, T3SS secret YopB and YopD which localizes in the target cytoplasm to form a channel. Finally, the Yops effectors are secreted through the T3SS

needle to reach the host cytoplasm (25). Activation of this secretion system usually requires a prior contact with the host cell (26).

Similarly, the type IV secretion system (T4SS) also forms a multi-component nanostructure spanning both the IM and the OM (4,18). T4SS has a unique ability to translocate DNA by conjugating DNA to an exported protein (4,18). The VirB/D system of *Agrobacterium tumefaciens* which delivers tumor-inducing Ti plasmid to plant cells is an example of best-studied T4SS (4,18). The VirB/D system consists of 12 proteins: VirB1-VirB11 and VirD4 (4). The major translocation apparatus is formed by VirB3 and VirB6-VirB10 complex (27). VirB2 and VirB5 form the pilus extending to the extracellular space through this apparatus (28). Formation of this pilus requires degradation of the peptidoglycan layer by VirB1 (28). Ti plasmid is covalently to VirD2 (18). C-terminal tail of VirD2 is recognized by VirD4 and recruited to the apparatus (29,30). Subsequent export of Ti plasmid-VirD2 through the pilus is powered by ATPase activities from VirB4, VirB11, and VirD4 (28).

The type VI secretion system (T6SS) interestingly combines homologous structures from other systems with a new twist. The T6SS is composed of 13 conserved, essential proteins (31,32) that make two main complexes: a membrane complex and a tail complex (4,33). Components making the membrane complex are homologous to the T4SS apparatus and they anchor the tail complex in the OM (34,35). The tail complex is evolutionarily related to the contractile phage tail (36). Similar to bacteriophage tails, the T6SS tail is composed of a tube in a sheath assembled on a baseplate (36). The tail tube is built from polymerized haemolysin co-regulated protein (Hcp) hexamers arranged in a tube-like fashion (36), (37). The Hcp tube is loaded with VgrG trimer spike and PAAR-repeat protein thought

to sharpen the spike (38). The effector protein is loaded to this spike for delivery to a target cell (38). TssB-TssC heterodimers polymerize around the Hcp tube to form a sheath (37,39). A rapid contraction of this sheath physically expels the tube, and the effector protein at the spike is delivered to the target host cell (33,39).

B. Dedicated secretion systems across the inner membrane

Unlike the one-step transport systems, two-step transport systems (T2SS and T5SS) export proteins sequentially first by an IM transport pathway then by another OM secretion mechanism. These secretion systems rely on two common protein export mechanisms across the inner membrane: Sec and Tat systems. The general secretory (Sec) pathway transports unfolded proteins through the SecYEG translocase, a tripart inner membrane channel (5). Proteins designated for Sec-dependent translocation carry ~20 residue-long N-terminal signal sequences composed of positively charged residues followed by a hydrophobic core and a polar carboxyl-terminal (5). A chaperone protein, SecB binds to pre-secretory proteins to keep them unfolded and compatible for subsequent export (40)(41)(42). Then SecB transfers the proteins to SecA which guides proteins to the SecYEG channel and catalyzes translocation (43,44). The secreted protein then folds in the periplasm unless directed otherwise (45).

The SPR pathway also utilizes the Sec system to transport and insert inner membrane proteins (18,46). Instead of SecB, signal recognition particle (SRP) composed of 4.5S RNA and a polypeptide Ffh binds to the hydrophobic domains of membrane proteins (47). Since the hydrophobic transmembrane proteins are unstable in the cytoplasm, secretion occurs co-translationally (18,46). The SRP-ribosome-protein complex is directed to the SRP receptor

FtsY which then delivers the ribosome-protein complex to the SecYEG channel for translocation. (5,47).

In contrast to the Sec pathway, the twin arginine translocation (Tat) pathway exports folded proteins across the inner membrane. Many proteins which requires binding to co-factors for correct folding and function are translocated by the Tat pathway (18,46). TatB and TatC recognize the Tat-signal peptides, S-R-R-x-F-L-K where x is a polar amino acid (48). Subsequently, the protein is transported by TatA which forms channel complexes of varying sizes, but the exact mechanism of the translocation remains unknown (18,49). Tat-secreted proteins are localized in the periplasm and can further be exported through the outer membrane by the type II secretion system [12].

The type II secretion system (T2SS) can export both unfolded proteins from the Sec pathway and folded proteins from the Tat pathway (4), (18). The T2SS is composed of 12-15 components known as the general secretion pathway (Gsp) proteins. These Gsp proteins make four major parts of the T2SS: an OM complex, an IM platform, a pseudopilus, and a cytoplasmic ATPase (4). The OM complex is made of a dodecameric protein GspD, also known as the T2SS secretin (50). GspD is connected to the IM platform composed of GspC, GspF, GspL and GspM (51–53). The major pseudopilus component GspG is anchored to the IM and the pseudopilus is confined to the periplasm (54). Then minor pseudopilins, GspH, GspI, GspJ and GspK, are assembled on the GspG pseudopilus filament to complete pseudopilus assembly (54,55). The substrates for T2SS are inserted into the secretin channel (4,18). ATP hydrolysis powers the extension of the pseudopilus in a piston-like manner to push the substrate out through the channel. Although it is unclear how the substrate is loaded to the channel, the pseudopilus seems to interact with GspC and GspD to facilitate substrate

loading (56). The T2SS substrates may have a structural motif to be presented to the secretin (57–60).

C. Type V Secretion Systems

The rest of this thesis will discuss the Type V secretion systems (T5SS). The T5SS are fully dedicated to protein secretion to the extracellular space using an OM component and solely rely on the Sec pathway for IM translocation. T5SS can be largely grouped into autotransporters and two-partner secretion (TPS) systems. Autotransporters carry their own β-barrel domain to secrete themselves (18,46), (61). In TPS, two separate proteins, TpsB and TpsA, make up the transporter and cargo, respectively (18,46), (61). TpsB and TpsA proteins carry the N-terminal signal sequence required for the Sec-dependent export to the periplasm (62,63). TpsB is a β-barrel outer membrane protein (OMP) responsible for TpsA export (64). Exported TpsA proteins then carry out diverse functions such as adherence, cytolysis, binding to heme, auto-aggregation and contact-dependent inhibition (65–67).

There are variations on the orientation and localization of the TpsA cargos upon secretion. For example, the filamentous hemagglutinin (FHA) in *Bordetella pertussis* is thought to have the N-terminus anchored in the periplasm. Then FhaB is displayed in a hairpin-like fashion with the C-terminus looping around and gets processed, causing FhaB to be released from the cell surface (68). However HMW1 adhesin, a TpsA cargo from *Haemophilus influenzae* has a C-terminal disulfide peptide loop which prevents release from its transporter partner, HMW1B (69).

Contact-dependent growth inhibition (CDI), the focus of this thesis, is orchestrated by TPS family. The details of how TpsB forms a β-barrel and exports the TpsA cargo will be discussed using CDI system as an example.

D. CDI operon

CDI was discovered in *E. coli* strain EC93, a dominant isolate from a rat intestine (70). Like many natural isolates, EC93 significantly outgrows *E. coli* K-12 lab strains (70). Interestingly, EC93 does not rely on secreted colicins for its growth advantage but directly inhibits growth of K12 strains upon cell-cell contact (70). CDI activity is attributed to *cdiBAI* gene cluster (70). Transformation of K-12 lab strain with this *cdiBAI* loci confers EC93-like inhibitory activity (70).

This CDI activity of target cell inhibition is carried out by CdiB/CdiA protein pair belonging to two-partner secretion (TPS) family (70)(71)(72). CdiB is a β-barrel TpsB protein which recognizes and transports CdiA, a TpsA cargo (70)(71)(72). Once exported CdiA forms a FHA-like β-helical filament on cell surface. This surface protein promotes receptor-binding in cell-cell contact and delivers the C-terminal toxin effector to inhibit the growth of the target cell (73). CDI+ cells also carries a third gene, *cdiI*, which encodes an immunity protein to prevent self-inhibition (70)(65).

These *cdi* genes are widely spread among alpha-, beta-, and gammaproteobacteria (74). Tentative *cdi* genes were also identified in distant Fusobacteria and the Negativicutes (73). All *cdi* genes in *E. coli* and other gammaproteobacteria are arranged as *cdiBAI.* But this arrangement is not conserved in betaproteobacteria; for example, Burkholderia *cdi* genes are arranged as *cdiBAI* (73)(75)

E. Biogenesis of CdiB

CdiB like other TpsB transporters are inserted to the outer membrane by the β-barrel assembly machinery (BAM) (71). The BAM complex is composed of the central pore protein BamA and four accessory lipoproteins (BamB-E) (76). How the BAM complex assembles other β-barrel proteins has been an active field of research (77–80). Recent works have revealed insights on the importance of key regions of BamA which itself is a β-barrel protein. Previous works have identified a lateral gate of BamA formed between β-strand 1 and β-strand 16 and have proposed that the lateral gate opens to insert a mature β-barrel protein in the membrane (81–84). BamA also contains periplasmic polypeptide transport-associated (POTRA) domains, and this region has been shown to be structurally dynamic to correctly guide substrate β-barrel proteins to the established β-barrel of BamA (76,81,85).

Interactions between a substrate β-barrel and the BamA lateral gate was experimentally shown for mitochondrial Sam50, a homolog of BamA (86). After the substrate β-barrel protein enters the lumen of Sam50, its C-terminal β-signal interacts with β-strand 1 of the lateral gate (86). Then the new β-barrel forms from CT to NT fashion to eventually leave through the lateral gate and gets inserted in the outer membrane which is significantly thinned at the opening to assist insertion (86).

Unlike the Sec translocon which uses the ATPase activity of SecA to insert inner membrane proteins (87), the BAM complex does not require ATP, and its energy source remains unclear (76,88). Recent discovery of the dynamic structural changes of BamA and BamD have been proposed to facilitate conducive folding of the substrate (76).

Although a crystal structure of CdiB has not been solved, structure of a closely related homolog from *Bordetella pertussis*, FhaC is available (89). FhaC is a 35 Å high monomeric β-barrel composed of 16 antiparallel β-strands (89). The N-terminal domain of FhaC seem to form an α-helical plug domain which can be removed to make a ~8 Å large pore (89). Other biochemical experiments have demonstrated that *Haemophilus influenzae* TpsB (HMW1B) and *Serratia marcescens* TpsB (ShlB) form β-barrels with predicted pore sizes smaller than 2.7 nm (90,91). Chapter 3 of this thesis will discuss the role of CdiB in exporting CdiA with a novel feature of arresting the export. Chapter 4 will discuss the limitations of the cargo transport via CdiB.

F. Biogenesis of CdiA

Following a successful insertion by the BAM complex, the periplasmic POTRA domain of CdiB is poised to interact with CdiA to initiate cargo export. The POTRA domains of TpsB proteins mediate protein-protein interactions to initiate TpsA export (92,93). This interaction of TpsA proteins requires a conserved 250 residues N-terminal TPS domain (94),(64). This TPS domain can further be divided to alternating regions of conserved sequences and less-conserved sequences (94). The conserved regions of TPS likely harbors a general secretion domain that TpsB utilizes while the less-conserved regions could dictate specificity of the TpsA cargo (94), (95,96). In agreement with the predicted region of specificity, TpsB does not export non-cognate TpsA cargo (97). Upon TPS recognition, TpsB β-barrel serves as the channel for TpsA export in an extended manner (64). The N-terminus of TPS domain adapts a β-helical fold and this folding has been proposed to nucleate folding of the rest of TPS domain and TpsA protein in a vectoral manner (95).

Most of the CdiA is highly conserved among different species except the central receptor-binding domain (RBD) and the C-terminal toxin effector (CdiA-CT) (73). The conserved regions of CdiA are dominated by FHA-1 and FHA-2 peptide repeats first identified in well-studied model TpsA from *Bordetella pertussis*, FhaB (98). FHA peptide repeats are degenerate 20-residue sequences predicted to form right-handed parallel β-helices with each repeat rising 4.8 Å in length (99,100). The N-terminal half of CdiA between the TPS domain and the central RBD is mostly composed of FHA-1 repeats [30]. The β-helical folding of FHA-1 repeats into a long filament probably provides the energy for translocation (100–102). The C-terminal half of CdiA between the RBD and CdiA-CT is dominated by FHA-2 repeats which are distinct from FHA-1. FHA-2 repeats are also predicted to take β dominant secondary structure, but it is unknown whether it will fold into FHA-1 like filament. Previous models of CdiA has proposed that all of CdiA is exported to form a long filamentous structure with the C-terminal toxin pointing away from the cell surface (73,103). The length of these CdiA filaments can be predicted based on the number of FHA peptide repeats. CdiA has a wide range of predicted lengths ranging from ~180kD in *Moraxella* to over 630kD in *Pseudomonas* (73).

Based on the location of the central RBD, Ruhe et al. have proposed that CdiA adopts a hairpin-like structure to display the RBD at the distal tip of FHA-1 filament (104). Chapter 2 of this thesis will reveal an updated model of CdiA biogenesis, whereby a programmed secretion arrest halts export to retain the C-terminal half in the periplasm. We also propose a previously unknown function for the FHA-2 domain in delivery of the CdiA-CT across the outer membrane of target bacteria.

G. Contact-dependent toxin delivery of CdiA

Two regions of CdiA sequences are highly vairable: the receptor-binding domain (RBD) and the C-terminal toxin domain (CdiA-CT) (73),(74). CdiA promotes adhesion to a target cell using the RBD in the middle of the primary sequence (104). Delivery of the CdiA-CT is directed to an intended target by the receptor-binding event (104). CdiA receptors are often outer membrane channel proteins such as BamA (71), Tsx (105), and OmpF/OmpC heterotrimer (106). Structural occlusion of the receptor by antibody binding prevents CdiA RBD from recognizing the receptor and blocks CDI (71). Some CdiA receptors are species specific. Replacing *E. coli* BamA with *E. cloacae* BamA deems $CdiA^{EC93}$, which targets *E. coli* BamA, inactive (104). This directs toxin delivery to related non-isogenic *E. coli.* The receptor binding domain is modular and can be swapped to target different OMPs (105).

It is tempting to speculate that CdiA hijacks the pore of these OMP receptors to infiltrate into the target's periplasm. However, a large body of evidence rejects such a model. For example, the lumen of BamA is not open to the extracellular space (107), and CDI translocation is independent of the transport activities of its OMP receptors (71,106). A recent discovery of CDI class which appears to use bacterial lipopolysaccharides as its receptor argues against the model of CdiA-CT translocation through receptor channels (108).

Receptor-dependent toxin delivery is conceptually similar to how colicin enters cells. Colicins bind to OMP receptors and parasitize Tol or Ton system to fuel its translocation across target's outer membrane through either the OMP lumen or the interface between the OMP and the lipid bilayer (109,110). However, CdiA uses a distinct toxin translocation mechanism, because Δ*tolA* and Δ*tonB* target cells are fully susceptible to CDI (71,111). In

the absence of the pmf, CdiA still delivers toxin across the target cell's outer membrane (111).

Surprisingly, CdiA-CT fragment of uropathogenic *E.coli* strain EC536 was reported to translocate to target cells without the rest of $CdiA^{EC536}$ protein (112)(113). Normally, $CdiA^{EC536}$ uses OmpC/OmpF heterotrimer as its receptor to deliver the CdiA-CT (106). Yet when expressed, the C-terminal toxin of $CdiA^{EC536}$ readily entered the cells and inhibit growth (112). However, this phenomenon is mediated by a distinctive ability of CdiA-CT^{EC536} to bind to F pilus and exploit its retraction mechanism (112). This unforeseen pathway to bypass the typical receptor binding is not relevant to normal $CdiA^{EC536}$ activity. The full-length $CdiA^{EC536}$ fails to deliver toxin without its OmpC/OmpF receptor regardless of F pilus (112). Thus, a general mechanism underlying CdiA toxin delivery across the outer membrane remains unknown.

H. CdiA-CT and CdiI

CdiA-CT is demarcated by a conserved VENN motif in enterobacteria (74) and the ELYN sequence in *Burkholderia* species (114). CdiA is remarkably modular. CdiA-CT can be exchanged and loaded onto a different CdiA at the VENN motif. Such chimeric CdiAs successfully inhibit target cells (74,111,113).

Toxin activity of CdiA-CT varies. CdiA-CT from the well-studied $CdiA^{EC93}$ reduces cellular respiration, dissipates pmf, and lowers ATP level of target cells (65). Upon BamA-dependent delivery, $CdiA^{EC93}$-CT requires an inner membrane efflux pump AcrB (71) (115). AcrB is a proton antiporter (116,117) which forms a small molecule exporting pump with

AcrA and TolC (118). Although it is unclear how CdiA^{EC93} toxin utilizes AcrB to inhibit growth, it could be forcing open the AcrB proton channel to dissipate pmf in target cells (65).

Many other CdiA toxins are nucleases that cleave DNA or RNA inside target cytoplasm (74,111,119–122). These toxins must further be translocated through the inner membrane of the target cell to reach the cytoplasm. CdiA-CT can further be categorized into two domains (112,114,119). The N-terminal domain of CdiA-CT binds to integral membrane protein (IMP) receptors to facilitate inner membrane translocation while the C-terminal domain of CdiA-CT carries the actual toxin activity (112,114). Exchange of the NT and CT domains of CdiA-CT also makes functional chimeras which hijack a specific IMP receptor to deliver toxin to the cytoplasm (114). Therefore, CdiA-CT after the VENN motif must be the minimal unit to be translocated through the outer membrane for a successful downstream toxin activity. And the delivery of CdiA-CT has been visualized in target cytoplasm (113). Highly modular nature of CdiA-CT again resembles colicins (123). In fact, crystal structures of some CdiA-CT domains show great structural homology to colicin E5 (119,124). Unlike CdiA-CT delivery across the outer membrane, the inner membrane translocation of the toxin requires the pmf (111). This suggests that IM translocation of CdiA-CT is a distinct process from the receptor-dependent OM translocation.

Apart from pore-formers and nucleases, bioinformatic analysis suggests some CdiA-CTs have peptidase and deaminase activities (124,125). But their activities have not been confirmed experimentally. Despite the diversity of toxin activity, CDI system carries corresponding c*diI* immunity gene to protect CDI+ cells from self-inhibition. Crystal structures of CdiA-CT and CdiI pairs reveals that mechanism to neutralize the toxin greatly differ between CdiI proteins. For example, CdiA-CT$_{II}^{Bp1026b}$ from *Burkholderia pseudomallei*

and CdiA-CT_{o11}^{EC869} from *E. coli* strain EC869 fold into remarkably similar structures of nucleases (121). However, $CdiI_{II}^{Bp1026b}$ directly binds to and occludes the active site of its cognate CdiA-CT while $CdiI_{o11}^{EC869}$ binds a β-hairpin exosite without directly altering the active site of CdiA-CT_{o11}^{EC869} (121). CdiI specifically mitigates CdiA-CT activity and cannot cross-protect (121).

CDI is thought to be deployed by CDI^+ cells to confer competitive advantage. Upon cell-to-cell contact, CDI^+ strain inhibits growth of neighboring CDI^- cells and greatly outcompetes them (70). Unstable minimal F plasmid, which quickly disappears in *E.coli* population within 50 generations, can be stabilized for over 100 generations by carrying the *cdiBAI* operon due to the competitive advantage CDI confers (126). Interestingly however, CdiA recognizes OMP of closely related species which narrows its target range (71,104). CdiA also wields adhesion-like activity via CdiA-receptor and homotypic CdiA-CdiA interactions (70,127). These observations raised recent interest in novel roles of CDI in kin communication and communal behavior (65),(104,122,127).

I. Thesis overview

CDI is an interesting mechanism of protein secretion widespread among Gram-negative bacteria which delivers toxin to neighboring cells in a contact-dependent manner. Since the exciting discovery of the CDI system in EC93, significant research has revealed much about the *cdiBAI* operon, the central receptor-binding domain, and the C-terminal toxin domain as well as the CdiI immunity. At the time I joined the Hayes lab, the topology of CdiA on surface was still unclear. It was also unknown how receptor-binding directs toxin delivery.

Chapter II of this thesis highlights a recent collaborative discovery of CdiA topology and mechanism. Secretion of CdiA is arrested so that C-terminal half remains in periplasm while the N-terminal CdiA forms a 33nm long filament on cell surface. Receptor-binding alleviates secretion arrest and exports periplasmic CdiA to deliver CdiA-CT to a target cell. We also proposed a previously unknown role of FHA2 and pre-toxin domain in CdiA-CT delivery.

Chapter III dissects the mechanism of CdiA secretion arrest. I have identified a 50-residue stretch called the YP region which is crucial to arrest CdiA secretion and to anchor it cell-bound. I also show a new role of CdiB which works in conjunction with the YP region to arrest secretion in the middle of the CdiA.

In chapter IV, I show that receptor-induced export of periplasmic CdiA occurs in an unfolded state. An enzymatic domain which readily unfolds can be fused to CdiA to make a receptor-dependent trigger.

Chapter V explores limitations and robustness of the N-terminal CdiA filament. I show that the TPS domain is exported to extracellular space. CdiA filament can tolerate severing and shortening to robustly deliver CdiA-CT to a target cell.

Chapter II. Programmed Secretion Arrest and Receptor-Triggered Toxin Export during Antibacterial Contact-Dependent Growth Inhibition

This research was published in *Cell* (2018). I collaborated with Zach Ruhe and Poorna Subramanian on this project. I contributed to the project by making/analyzing the in-frame deletions of CdiA to describe the toxin delivering mechanism of CdiA. I also discovered the function of a novel YP domain. The original manuscript was written by Prof. Christopher Hayes.

A. Introduction

Bacteria have long been known to release diffusible antibiotics and bacteriocins that inhibit competitor cells. Recent research has revealed that bacteria also commonly antagonize their neighbors through direct inter-cellular transfer of protein toxins. In Gram-negative bacteria, type I (128), type II (129), type IV (130), type V (70), and type VI (131,132) secretion systems have all been shown to deploy toxic antibacterial effectors. Gram-positive species exploit distinct mechanisms, using cell-wall-associated YD-repeat proteins (133) and type VII secretion systems (134,135) to deliver toxins into target bacteria. Direct inter-bacterial toxin exchange was first discovered in *Escherichia coli* isolate EC93, which uses the CdiB- CdiA two-partner secretion (TPS) system to inhibit other *E. coli* strains in a process called contact-dependent growth inhibition (CDI) (70). CdiB is an outer-membrane localized Omp85 b-barrel protein that exports and presents the toxic CdiA effector on the cell surface. CdiA is a very large protein hundred (~320 kDa) that is predicted to form a filament extending several Å from the cell surface (70,100). CdiA recognizes target bacteria through

specific binding interactions with a receptor. Upon binding to receptor, CdiA transfers its C-terminal toxin domain (CdiA-CT) into the target cell to inhibit growth (71). To prevent self-inhibition, *E. coli* EC93 also produces an immunity protein, CdiI, which specifically neutralizes CdiA-CT toxins delivered from neighboring sibling cells. Thus, *E. coli* EC93 uses CDI to suppress the growth of non-isogenic *E. coli* strains, presumably to compete for limited environmental resources.

Since its discovery in *E. coli* EC93, CDI systems have been identified in many other Gram-negative bacteria and are particularly common in pathogens (74,124,125). Though CdiA is not known to intoxicate eukaryotic cells, the effectors contribute to virulence by promoting bacterial auto-aggregation and biofilm formation (136,137). CdiA proteins are heterogeneous in sequence and length, ranging from ~180 kDa in *Moraxella* to over 630 kDa in some Pseudomonas species (73). Despite this diversity, CdiA proteins share the same general domain architecture. The N terminus carries a signal peptide for Sec-dependent secretion into the periplasm and a conserved TPS transport domain for CdiB-mediated export across the outer membrane (Figure 1A). The N-terminal half of CdiA is dominated by FHA-1 hemagglutinin peptide repeats (Pfam: PF05594) (Figure 1A). These motifs were first identified in the filamentous hemagglutinin (FHA) adhesins produced by Bordetella species (98). Structural modeling and electron microscopy of FHA indicate that FHA-1 repeats form an elongated β-helix, with each ~20-residue motif extending the helix ~4.8 Å (99,100). The C-terminal half of CdiA contains a second repeat domain composed of uncharacterized FHA-2 repeats (PF13332) (Figure 1A). FHA-2 repeats are predicted to adopt β secondary structure, but these sequences are distinct from FHA-1, and it is unclear whether this domain is filamentous. The receptor-binding domain (RBD) of CdiA resides between the two FHA

repeat regions. RBD sequences can differ between otherwise closely related CdiA proteins, enabling the effectors to recognize unique receptors (105). In *E. coli*, three RBD classes have been characterized that bind to BamA (71), heterotrimeric OmpF/OmpC (106), and the Tsx nucleoside transporter (105)(Figure 1A). Lastly, growth inhibition activity resides within the CdiA-CT region, which often varies dramatically in sequence between bacteria (74). *E. coli* isolates collectively encode at least 18 CdiA-CT sequence types that exhibit distinct toxic activities. For example, CdiA-CT^{EC93} from *E. coli* EC93 dissipates the proton gradient in target bacteria (65), whereas CdiA-CT^{STECO31} from *E. coli* STEC_O31 contains an EndoU RNase domain that cleaves tRNAGlu (138) (Figure 1A). CdiA-CT regions are typically demarcated by conserved peptide motifs, such as the ELYN sequence in *Burkholderia* species or VENN in enterobacteria (73). The latter VENN motif is part of a larger ‘‘pre-toxin’’ (PT) domain annotated as the PT-VENN region (PF04829)(124)(Figure 1A). The function of the PT domain is unknown, but its location suggests it could mediate auto-proteolysis to release the toxin for transport into target bacteria.

Although CdiA is thought to form a cell-surface filament, its orientation and architecture have yet to be examined experimentally. The original ‘‘toxin-on-a-stick’’ model proposed that CdiA extends its C terminus away from the cell to facilitate toxin transfer into target bacteria (103). This model implies that the FHA-1 and FHA-2 domains form a continuous filament, with the C-terminal toxin near the distal tip. This scenario appears to be incongruent with the recent discovery that the RBD is located between the FHA repeat regions (105), which would place the RBD in the middle of the filament. The mechanisms governing CdiA-CT delivery are also poorly understood. *E. coli* CdiA proteins recognize various OMPs as receptors, suggesting that these β-barrel proteins could also be exploited as

toxin translocation conduits. However, the *E. coli* BamA β-barrel is not open to the cell surface (139), and the narrow (~3-5 Å) hydrophobic lumen of Tsx presumably restricts the passage of peptides (140). Further, some CdiA proteins use lipopolysaccharide as a receptor (108), suggesting that OMPs are not necessarily required for toxin translocation. CDI toxin transport across the target-cell cytoplasmic membrane is also dependent on specific receptors. The CdiA-CT region is typically composed of two variable do- mains, with the extreme C-terminal domain constituting the actual toxin (73)(Figure 1A). Genetic evidence suggests that the N-terminal domain of the CdiA-CT hijacks integral membrane proteins to transport the tethered C-terminal toxin into the target-cell cytoplasm (114). Each N-terminal ‘‘translocation’’ domain recognizes a different membrane protein. For example, the PtsG glucose transporter is required for CdiA-CT^{STECO31} delivery (Figure 1A), but CdiA- CT^{Dd3937} from *Dickeya dadantii* 3937 uses the ribose ABC transporter RbsC to enter the cytoplasm (114). Though the co-opted membrane proteins are commonly metabolite transporters, their solute-transport activities are not required for toxin import.

Here, we uncover several new and unexpected insights into CdiA secretion and toxin delivery. Electron cryotomography (ECT) reveals that individual CdiA proteins form thin, 33-nm long filaments on the cell surface. Remarkably, CdiA export across the outer membrane is arrested during biogenesis, and the extracellular filament corresponds solely to the N-terminal half of the effector. We identify and delineate a previously unrecognized CdiA domain that is required for this secretion arrest. This Tyr/Pro-enriched region ensures that the C-terminal half of CdiA—including its toxin domain—remains sequestered within the periplasm prior to target-cell recognition. CdiA export resumes upon binding receptor, and the FHA-2 region is deposited directly onto the surface of target bacteria. The FHA-2

domain associates stably with the target-cell outer membrane, and this interaction is required for CdiA-CT transport into the periplasm of target bacteria. We propose that FHA-2 forms a membrane-embedded structure for CdiA-CT translocation. This unprecedented mechanism presumably contributes to CdiA modularity, enabling the effectors to deliver diverse cargoes.

B. Results

CdiA forms a filament on the cell surface

We used ECT to visualize $CdiA^{EC93}$ in its native context on the bacterial cell surface. To image effectors in the pre-delivery state, we used *E. coli* EC93 *bamA*^{LT2} cells, which express $BamA^{LT2}$ from Salmonella typhimurium LT2. The surface epitopes of $BamA^{LT2}$ differ significantly from $^{E.\ coli}$ BamA, thus preventing recognition by $CdiA^{EC93}$ (104,127). Tomography revealed poorly resolved filaments on EC93 cells (Figure S1A, Table S1). We reasoned that the surface O-antigen layer of *E. coli* EC93 could obscure the filaments, and therefore we produced CdiA in *E. coli* K-12 strains that lack both O-antigen and CdiA-receptors. $CdiA^{EC93}$ filaments were readily apparent on the surface of these latter cells (Figures 1B, S1B, Table S1, Movie S1), and this approach facilitated further experiments using minicells for higher resolution imaging (Figures1C, S1C, Movie S2). Similar filaments were also observed on bacteria and minicells that express $CdiA^{STECO31}$ from *E. coli* STEC_O31 (Figure 1D, Table S1, Movie S3). Notably, we did not detect filaments on control cells that lack *cdi* expression constructs (Table S1, Movie S4). Analysis of >100 $CdiA^{EC93}$ filaments revealed considerable heterogeneity. A few filaments were associated with additional periplasmic density (Figure 1E), and others projected from the cell surface at

an angle (Figure 1F). We also observed some bent structures (Figure S1D) and instances of twinned and clustered filaments (Figure S1E). The average length of CdiA^{EC93} filaments was 33 ± 4 nm (Figure 1G). Though filament width could not be determined at this resolution, it was clearly ≤4 nm, consistent with a parallel β-helix.

We previously showed that CdiA^{EC93} is also produced in a truncated form that lacks the FHA-2, PT and CdiA-CT domains (70,127). Although truncated CdiA^{EC93} cannot mediate CDI, it retains BamA-specific adhesin activity (127), indicating that it is presented on the cell surface. To determine whether truncation affects filament structure, we imaged CdiA^{EC93} truncated after residues Ser832, Gly1318, Val1929 and Thr2122 (Figure 1A). We did not detect surface structures with the two shortest constructs (Table S1), but proteins truncated after Val1929 and Thr2122 form filaments with the same dimensions as CdiA^{EC93} produced from the full-length construct (Figure 1G). Thus, the FHA-2, PT and CdiA-CT domains are not part of the surface structure, indicating that the extracellular filament corresponds to the N-terminal half of CdiA.

CdiA surface topology

ECT indicates that the C-terminal half of CdiA is either sequestered within the cell or not resolved because it is disordered or flexible. To distinguish between these possibilities, we examined CdiA surface topology using biochemical approaches. CdiA^{STECO31} was used for these experiments, because antisera to its N- and C-terminal regions are available. Immunoblotting showed that CdiA^{STECO31} is produced in both full-length and truncated forms when expressed in cells that lack its receptor Tsx (Figure 2A, lanes 1 & 4). The N-terminal TPS domain can be digested with extracellular proteinase K (Figure 2A, lane 2), but a C-

terminal fragment of >180 kDa is resistant to proteolysis (Figure 2A, lane 5). Trypsin generates a similar C-terminal fragment, but the TPS domain is resistant to this protease (Figure 2A, lanes 3 & 6). These results suggest that FHA-2 and CdiA-CT are intracellular, but it is also possible that these domains are simply protease resistant. Therefore, we developed a fluorescent dye-labeling approach to differentiate periplasmic and extracellular residues. We first showed that the outer membrane is impermeable to maleimide-conjugated IRDye® 680LT using His6-tagged maltose-binding protein (MBP) engineered to carry a single Cys residue. Periplasmic MBP-Cys-His6 is not labeled when whole cells are treated with dye but becomes labeled when the outer membrane is permeabilized with polymyxin B (Figure 2B, lanes 1 & 2). The cytoplasmic membrane remains intact during polymyxin treatment, because MBP-Cys-His6 lacking a signal peptide is not labeled under these conditions (Figure 2B, lanes 2 & 5). Cytoplasmic MBP becomes accessible to dye only when cells are completely disrupted (Figure 2B, lane 6). Thus, polymyxin selectively permeabilizes the outer membrane and can be used to probe the periplasm.

We then introduced Cys residues along $CdiA^{STECO31}$ for dye-labeling studies (Figure 2C). Each Cys-substituted effector retains growth inhibition activity against target bacteria (Figure S2A), demonstrating that the mutations do not perturb function. Wild-type $CdiA^{STECO31}$ contains four Cys residues that do not react with dye (Figure 2D, lanes 1 & 2), suggesting that they form disulfide bonds. Engineered Cys residues at positions 504, 1550 and 1693 label efficiently, with dye fluorescence superimposing with anti-TPS antibody signal (Figure 2D, lanes 3 - 8). These Cys residues are extracellular because they are accessible without polymyxin treatment. By contrast, positions 1726, 2502, 2731 and 3217 of $CdiA^{STECO31}$ are labeled only when the outer membrane is permeabilized (Figure 2D).

Position 1807 is relatively unreactive even with polymyxin treatment (Figure 2D, lanes 11 & 12), suggesting that its side-chain is occluded. These results indicate that the FHA-2, PT and CdiA-CT domains reside in the periplasm prior to target-cell recognition. The periplasmic region also contains a small cluster of FHA-1 motifs, which we have termed periplasmic FHA-1 repeats (pFR) (Figure 2C). The function of these repeats is unclear, but this region is conserved in other CdiA proteins (Figure S3).

CdiA-receptor binding interactions

The receptor-binding domain (RBD) of CdiA presumably forms the distal end of the filament. To localize the RBD, we incubated $CdiA^{EC93}$-expressing minicells with purified *E. coli* BamA and imaged using ECT. As predicted, BamA-containing micelles bind to the distal tips of the filaments, forming "lollipop"-like structures (Figures 3A & 3B). In some instances, filaments bundle together as they interact with larger micelles that presumably contain multiple receptors (Figures 3A & 3C). These interactions are BamA-dependent, because detergent micelles lacking BamA do not bind $CdiA^{EC93}$ and instead tend to interact with the cell surface (Figure 3D). Remarkably, BamA-bound filaments are significantly elongated, increasing approximately 5 nm to an average length of 38 ± 3.6 nm (Figure 1G, see Methods for statistical comparisons and p-values). We obtained similar results with target minicells that express *E. coli* BamA and captured an image of two minicells bridged by an individual filament (Figure 3E). However, most of the interactions involved vesicles that were presumably derived from the BamA-expressing target cells (Figures 3F & 3G). Given that the periplasmic space is often widened and distorted in minicells, these vesicles may have been stripped from target cells upon binding to $CdiA^{EC93}$. The vesicle-bound filaments

were also elongated to 38 ± 4.9 nm (Figure 1G). These data indicate that the RBD is at the distal end of the filament, suggesting that the TPS domain is associated with CdiB at the cell surface. Therefore, the CdiA chain must make a hairpin-turn at the RBD and return to the cell for the C-terminal domains to remain in the periplasm. Notably, only 176 residues separate position 1550 in the RBD from position 1726 in the periplasm, indicating that some portion of the intervening sequence must be extended (at ~3.5 Å per residue) to span the 33-nm filament. This region is enriched for Tyr (Y) and Pro (P) residues relative to the surrounding FHA repeat domains (Figure S4) and is abruptly demarcated from the variable RBD sequence by a conserved YPLP motif (Figure S3). This previously unrecognized "YP domain" is conserved in other species (Table S2 & Figure S3) and is of particular interest because dye-labeling indicates that this region crosses the outer membrane.

CdiA export resumes upon binding receptor

Filament elongation suggests that CdiA undergoes structural reorganization upon binding receptor. Moreover, effector topology must change dramatically for the C-terminal toxin domain to be transferred into target bacteria. Therefore, we used the dye-labeling approach to monitor topological changes in response to the addition of target bacteria. Immunoblotting revealed that the CdiA-CT region of $CdiA^{STECO31}$ is cleaved upon mixing with tsx+ target cells, but not with Δtsx mock targets (Figure 4A, lanes 1 & 2). Thus, this CdiA-CT processing is indicative of toxin delivery. The reactivity of extracellular positions 504 and 1693 is unaltered by target bacteria, but labeling at position 1550 is diminished in the presence of tsx+ targets (Figure 4A, lanes 5 & 6). Because residue 1550 lies within the RBD, it may become occluded through direct interaction with Tsx. Strikingly, positions

1726, 1807, 1959 and 2502 all become accessible to extracellular dye when tsx+ cells are introduced but remain periplasmic with mock Δtsx targets (Figure 4A). These data suggest that the C-terminal region is exported upon binding Tsx, but it is also possible that outer membranes become permeable to dye in response CdiA-receptor binding. This is not the case, however, as MBP-Cys-His6 in the inhibitor-cell periplasm remains unreactive when tsx+ targets are introduced (Figure 4B, lanes 3 & 4). In contrast to other Cys substitutions, residue 2731 in the PT domain remains unlabeled with tsx+ targets (Figure 4A, lanes 17 & 18), suggesting that it may be transferred into the target cell. We note that position 3217 cannot be detected because it lies within the cleaved CdiA-CT region. To monitor this latter position, we blocked CdiA-CT processing by mutating the VDNN motif to VDNA (Figure 4C, lanes 1 & 2), and repeated the topology mapping with a subset of Cys substitutions. The VDNA mutation has no effect on Cys reactivity at positions 504, 1550 and 2502 (Figure 4C, lanes 3 - 8). Positions 2731 and 3217 show some labeling in the presence of tsx+ targets, but at lower efficiencies than position 2502 (Figure 4C, compare lanes 8, 10 & 12). Residues 2731 and 3217 appear to be transferred into the periplasm of target cells, because they are labeled more efficiently when the mixed cell suspensions are permeabilized with polymyxin (Figure 4D, lanes 10 & 12). Together, these data indicate that CdiA export resumes upon binding receptor, with the PT and CdiA-CT domains being transferred into target bacteria. Because N-terminal residues remain extracellular, the CdiA chain must pass through the outer membrane of the target cell.

The YP domain is required for export arrest

We next disrupted the FHA-1, RBD, YP, FHA-2 and PT domains with 100-residue in-frame deletions to examine their functions during CDI (Figure 5A). The YP domain was dissected further with 50-residue deletions to test its extracellular region (ΔYP-N) and membrane-spanning segment (ΔYP-C). We also removed a portion of the periplasmic FHA-1 repeat (ΔpFR) region to probe its function. Though the ΔFHA-1 effector retains nearly wild-type inhibition activity, the other deletion constructs fail to inhibit target cells in shaking-broth co-cultures (Figure S2B). Receptor-binding function was then assessed by flow cytometry to monitor cell-cell adhesion. GFP-labeled inhibitor cells were mixed with DsRed-labeled target cells, and the mixtures analyzed by flow cytometry to quantify aggregates with dual green and red fluorescence. Cells expressing wild-type CdiA^{STECO31} bind ~80% of *tsx*+ target cells (Figure 5B). Adhesion is CDI-dependent because Δ*tsx* cells are bound at much lower levels, and mock inhibitors lacking CdiA^{STECO31} do not bind *tsx*+ targets (Figure 5B). As expected, the ΔRBD deletion abrogates target-cell binding, but effectors carrying YP domain deletions are also defective for adhesion (Figure 5B). The remaining effectors retain nearly wild-type cell-adhesion activity (Figure 5B). Immunoblotting showed low levels of ΔYP-C and ΔYP-100 relative to the other effectors, and these proteins were released into the culture supernatants (Figure S5A, lanes 5 & 6). This latter finding suggests that their defects in cell-cell adhesion are due to an unstable association with the inhibitor-cell surface. This phenomenon could also interfere with growth inhibition activity, particularly in shaking broth co-cultures. Therefore, we re-examined deletion construct activity on solid media, where inhibitor and target cells are held in close proximity within a structured environment. Strikingly, the YP deletion constructs inhibited target bacteria on solid media, with the ΔYP-100 effector exhibiting nearly wild-type growth-inhibition activity (Figure 5C). Further, this

activity is *tsx*-dependent (Figure 5C), demonstrating that the ΔYP-100 deletion does not disrupt the adjacent RBD. Thus, the YP domain is not necessary for toxin delivery, but is critical when cell-cell interactions are transient. Collectively, these results show that the membrane-spanning segment of the YP domain is required for stable presentation on the inhibitor-cell surface.

The FHA-2 domain is required for toxin delivery

To determine which steps in the CDI pathway are disrupted by the various deletions, we examined how each effector responds to target bacteria. Immunoblotting showed that Tsx-dependent CdiA-CT processing is defective for each effector except the ΔFHA-1 protein (Figure 5D, lanes 3 & 4). Notably, the ΔpFR and ΔFHA-2 proteins are cleaved at novel sites when mixed with *tsx*+ cells, but not mock targets (Figure 5D, white carets in lanes 14 & 16), suggesting aberrant processing during toxin delivery. We screened protease-deficient *E. coli* strains and found that OmpT is required for this activity. OmpT protease is embedded in the outer membrane with its active site facing the extracellular milieu (141,142). In principle, OmpT on either the inhibitor or target cell could catalyze cleavage, but CdiA degradation depends solely on OmpT in the target cell (Figure 5E, lanes 2, 4, 6 and 8). Further, OmpT-mediated cleavage releases C-terminal CdiA fragments into the culture supernatant (Figure S5B, lanes 10 & 12). The masses of the OmpT-dependent fragments indicate that the ΔpFR and ΔFHA-2 chains are each cleaved near their respective deletion sites, suggesting that the entire FHA-2 region is brought into close proximity with the target-cell surface. However, OmpT-mediated proteolysis does not explain the defects in inhibition activity, because *tsx*+ ΔompT target cells are not inhibited by the ΔpFR and ΔFHA-2 effectors, even when co-

cultured on solid media (Figure 5C). Moreover, the CdiA-CT toxin region is not processed when ΔpFR and ΔFHA-2 effectors bind to *tsx*+ ΔompT target cells (Figure 5E, lanes 3, 5, 7 and 9). Therefore, the pFR and FHA-2 regions are critical for CdiA-CT delivery into the target-cell periplasm.

We introduced Cys substitutions into the ΔRBD, ΔYP-N, ΔpFR, ΔFHA-2 and ΔPT effectors (Figure 6A) and monitored surface topology after addition of *tsx*$^{+}$ Δ*ompT* target cells. As expected, Cys residues in the ΔRBD protein show no changes in reactivity when target cells are introduced (Figure 6B). Similarly, the ΔYP-N protein shows only modest labeling of periplasmic residues 2502, 2731 and 3217 when mixed with targets (Figure 6C). In contrast, all periplasmic positions become accessible to extracellular dye when the ΔpFR and ΔFHA-2 effectors bind to target bacteria (Figures 6D & 6E), indicating that Tsx-interactions trigger export, but the PT and CdiA-CT domains are not transferred into target bacteria. Disruption of the PT domain also interferes with toxin delivery, because position 3217 in the toxin domain remains extracellular when the ΔPT effector binds target cells (Figure 6F, lane 12). However, labeling at position 2731 is suppressed in the ΔPT effector, similar to what is observed when this residue is probed in the context of full-length CdiA^{STECO31} (compare Figure 6F, lane 10 with Figure 4A, lane 18). This latter observation suggests that residue 2731, which is N-terminal to the ΔPT deletion, is still transferred into the target-cell periplasm. Therefore, the pFR, FHA-2 and PT disruptions have no effect on receptor-triggered export but prevent CdiA-CT delivery into target bacteria.

The ΔpFR and ΔFHA-2 deletions both prevent CdiA-CT transfer into the target-cell periplasm, and these effectors are susceptible to OmpT-mediated cleavage at the target-cell surface. These observations raise the possibility that FHA-2 integrates into the target-cell

outer membrane to form a translocon for toxin delivery. To explore this hypothesis, we incubated *tsx*$^{+}$ target cells with inhibitors that express Cys1959-substituted CdiA^{STECO31}, then incubated the suspension with maleimide-dye and proteinase K. Analysis of CdiA from this experiment revealed a large (>130 kDa) dye-labeled fragment that is resistant to proteolysis (Figure 6G, lane 4). Dye-labeling demonstrates that this fragment was derived from CdiA that was exported in response to target bacteria (Figure 6G, compare lanes 2 & 4). The dye-labeled fragment also reacted with PT/CdiA-CT antisera, indicating that it encompasses the entire FHA-2 region. Finally, we found that this fragment migrates in the outer-membrane fraction on sucrose gradients (Figure 6G), consistent with a stable interaction between FHA-2 and target-cell outer membranes. By contrast, a protease-resistant fragment was not detected with ΔFHA-2 effectors carrying the Cys1959 substitution (Figure 6H, lane 4). These results strongly suggest that an intact FHA-2 region is required for stable association with the target-cell outer membrane.

C. Discussion

Here, we present the first ultrastructural images of CdiA in its near-native state. ECT revealed that each CdiA effector forms a thin filament extending ~33 nm from the cell surface. These dimensions are consistent with the β-helix model (100), which predicts that the FHA-1 region of CdiA^{EC93} should form a ~27 nm filament. The TPS transport domain could account for another ~3 nm based on the crystal structures of homologous domains in *Bordetella* FhaB and *Haemophilus* HWM1 (95,143). Given our finding that the RBD forms the filament tip, the TPS domain must be at the other end of the filament, likely

associating with CdiB at the cell surface (Figure 7A). We also discovered that CdiA is subject to secretion arrest, and the entire C-terminal half of the effector is retained within the periplasm. Therefore, the extracellular CdiA filament must follow a hairpin-like trajectory, first extending outward to form the RBD, then returning back to the cell to enter the periplasm (Figure 7A). This topology imposes constraints on the sequence linking the distal RBD to the periplasmic FHA-2 domain. The peptide chain must be extended in this region to span the length of the extracellular filament. Because the YP domain traverses the outer membrane and is required for secretion arrest, we predict that it passes through the central lumen of CdiB to halt export and stabilize CdiA on the cell surface. Further, this export arrest appears to be universal, because similar YP domains are found in all recognizable CdiA proteins. Given that FHA-1 varies considerably in size between species (73), our model predicts that the extended return region should exhibit commensurate changes to accommodate different filament lengths. Indeed, analysis of 142 CdiA proteins from enterobacteria revealed that the size of the variable RBD is directly proportional to FHA-1 length (Figure 7B & Table S2). This correlation is remarkably robust ($r^2 = 0.87$) for filaments ranging from ~14 to 100 nm in predicted length. Therefore, the RBD must contribute significantly to the extended region, because the length of the YP domain is essentially invariant (Table S2). These observations suggest that the RBD, which is defined as the variable region between the FHA-1 and YP domains, may in fact contain two domains with distinct functions. We hypothesize that the N-terminal portion of the RBD makes direct contact with receptors based on sequence alignments showing limited homology in this region across species (Figure S3). This model predicts that the additional residues found in longer CdiA proteins do not contribute to receptor-binding *per se* but are required to span the

filament as the chain returns to the inhibitor-cell surface (Figure 7A). We also note that FHA-2 does not scale with filament length (Figures 7C & Table S2), demonstrating that size correlation is limited to the RBD and FHA-1. Together, these observations argue that all CdiA proteins adopt the same general surface topology.

Though CdiA undergoes export arrest, it remains poised to deliver toxin upon encountering target bacteria. Presumably, receptor-recognition generates a signal that causes CdiA export to resume. One possible mechanism involves receptor-induced folding of the RBD, which would exert a force on the extended region and release the YP domain from its "locked" state within CdiB (Figure 7A, step 2). This model may also explain why receptor-bound filaments become elongated. Alternatively, the additional length could correspond to the newly exported FHA-2 domain, which we showed makes contact with target bacteria and becomes stably associated with their outer membranes (see Figures 5E & 7G). Our results indicate that the FHA-2 domain likely passes through the target-cell outer membrane to deliver the CdiA-CT into the periplasm. The structure of FHA-2 is unknown, but the I-TASSER server (144) predicts that it could resemble the β-rich RsaA S-layer protein from *Caulobacter*, or the LptD lipopolysaccharide transporter from *Shigella*. The latter model is appealing because LptD forms a 26-stranded β-barrel in the outer membrane, which would be ideal for toxin translocation. Irrespective of its precise structure, we propose that FHA-2 interaction with the target-cell outer membrane is closely coupled with its export from the inhibitor cell (Figure 7A, step 3). This would allow FHA-2 to integrate as an unfolded chain emerging from the inhibitor cell. This hypothesis could explain why the constitutively released ΔYP-100 effector is inactive in shaking broth co-culture (see Figure S2B), yet retains nearly wild-type growth inhibition activity on solid media (see Figure 5C).

Following release into the medium, the FHA-2 domain is presumably free to adopt a conformation that precludes membrane integration. However, when released in a crowded sessile community, some of the CdiA will likely be deposited directly onto target bacteria before FHA-2 has the opportunity to fold. Thus, secretion arrest is not strictly required for CDI, but this feature is critical to ensure that the FHA-2 translocon is deployed only when a suitable target membrane is nearby.

The outer-membrane translocation mechanism proposed here is novel and distinct from other inter-bacterial competition systems. Type VI secretion systems rely on mechanical force to deliver toxic payloads. Type VI systems utilize a phage-related contractile apparatus to eject a toxin-laden spear that perforates the outer membranes of neighboring bacteria (145,146). This mechanism is sufficient to deliver lytic enzymes that degrade the bacterial cell wall and membrane lipids, but it remains unclear how these systems transfer nuclease toxins into the cytoplasm. Myxobacteria have the unique ability to merge outer membranes, thereby allowing lipids and OMPs to be shared freely between cells (147,148). Wall and coworkers have recently shown that polymorphic lipoprotein toxins are also transferred during this process, enabling cells to discriminate kin when engaging in this social behavior (149). Because the lipoprotein toxins are tethered to the inner leaflet of the outer membrane, they are able to flow between cells without physical translocation across a lipid bilayer. Toxin translocation has been studied most extensively with colicins. These diffusible protein toxins bind specific surface receptors, then recruit porins as portals for entry into the target-cell periplasm (150,151). Transport through the porin is powered by Tol and Ton system proteins, which harness energy from the proton gradient across the bacterial cytoplasmic membrane. Thus, colicins cannot penetrate the outer membrane when bacteria

are treated with uncoupling agents that dissipate the proton gradient. Intriguingly, Δ*tol* Δ*ton* mutants are completely resistant to colicin-mediated killing, but are fully sensitive to CDI (111)). Moreover, CdiA-CT toxins are readily delivered into the periplasm of de-energized cells, though the proton gradient is required for subsequent transport into the cytoplasm (111). These observations underscore fundamental differences between colicins and CDI, but also raise important unresolved questions about the thermodynamics of CdiA-CT transport across the outer membrane.

Finally, our results could have implications for the function of FHA adhesins in *Bordetella*. FHA is derived from the FhaB pre-protein, which is processed during biogenesis to remove its large C-terminal "prodomain" (152). The domain architecture of FhaB is quite similar to CdiA, and the prodomain contains an FHA-2 repeat region (70,73). In another parallel, Cotter and coworkers have shown that the FhaB prodomain resides in the periplasm during biogenesis (153). This phenomenon is thought to promote folding of the exported adhesin domain, after which the prodomain is degraded by periplasmic proteases to release mature FHA from the cell (152,153). Our work suggests an alternative function for the prodomain. We hypothesize that the FHA-2 repeats in FhaB are used to transport cargo across target-cell membranes. Instead of an antibacterial toxin, the prodomain of FhaB carries an unusual prolyl-rich domain adjacent to the FHA-2 region. The function of this prolyl-rich region is enigmatic, but recent work from the Cotter lab shows that it is important for bacterial persistence in the lower respiratory tract (152). Collectively, these observations raise the possibility that the prolyl-rich domain is delivered into host cells to modulate immune responses. Thus, *Bordetella* species may have repurposed the primordial antibacterial CDI mechanism to play a new role in pathogenesis.

D. Materials and methods

Bacterial growth conditions

Bacterial strains were derivatives of *E. coli* K-12 strains MG1655 and EPI100. Bacteria were cultured in lysogeny broth (LB) or on LB agar at 37 °C. Unless indicated otherwise, media were supplemented with antibiotics at the following concentrations: 150 μg/mL ampicillin (Amp), 100 μg/mL chloramphenicol (Cm), 50 μg/mL kanamycin (Kan), 200 μg/mL spectinomycin (Spc), and 25 μg/mL tetracycline (Tet).

Strain construction

E. coli strains are presented in Table 1. The *mreB(A125V)* allele (linked to Δ*yhdE::cat*) from *E. coli* DS612 (154) was transferred into *E. coli* CH9591 and CH9604 using phage Pi-mediated transduction. The Δ*yhdE::cat* Cm resistance cassette was subsequently removed using FLP recombinase expressed from pCP20 (155) to generate strains ZR82 and ZR83 (respectively). ZR82 was transformed with pZR108 (*minE* overexpression) and $CdiA^{EC93}$ expressing plasmids to generate minicell producing strains for ECT. The resulting strains were cultured in media supplemented with 0.4% L-arabinose to generate minicells. The Δ*wzb::kan*, Δ*tsx::kan* and Δ*ompT::kan* disruptions were introduced into *E. coli* MG1655 from the Keio collection (156) by phage P1-mediated transduction. For strains that carry multiple deletions, Kan resistance cassettes were removed with FLP recombinase.

Plasmid constructions

Cys substitutions were generated by PCR and the resulting fragments introduced into plasmid pET21b::*cdiBAI*^{STECO31} (pCH13604) using restriction endonuclease based cloning. The product from primers ZR260/ZR267 was ligated via NotI/KpnI to generate pZR432 (Ser504Cys). The product from CH403/ZR271 was ligated via SacI to generate pZR433 (Ser1550Cys). PCR fragments from primer pairs ZR268/ZR274 and ZR275/ZR287 were cloned sequentially into pBluescript II SK+ using KpnI/SalI and SalI/NotI, respectively. The KpnI/NcoI fragment was then subcloned to generate pZR434 (Ser1693Cys). PCR fragments from primer pairs ZR268/ZR277 and ZR281/ZR287 were cloned sequentially into pBluescript II SK+ using KpnI/XbaI and XbaI/NotI, respectively. The KpnI/NcoI fragment was then subcloned to generate pZR435 (Gly1726Cys). The product from ZR280/ZR261 was ligated via SexAI/Xho I to generate pZR437 (Ala1807Cys). The product from ZR286/ZR261 was ligated via NcoI/Xho I to generate pZR439 (Asp1959Cys). PCR fragments from primer pairs ZR347/ZR288 and ZR290/ZR261 were cloned sequentially into pBluescript II SK+ using NotI/EcoRI and EcoRI/XhoI, respectively. The NcoI/XhoI fragment was then subcloned to generate pZR441 (Thr2502Cys). PCR fragments from primer pairs ZR347/ZR348 and ZR349/ZR261 were cloned sequentially into pBluescript II SK+ using NotI/BamHI and BamHI/Xho I, respectively. The NcoI/XhoI fragment was then subcloned to generate pZR442 (Ser2731Cys). The product from ZR294/ZR261 was ligated via MfeI/XhoI to generate pZR444 (Ser3217Cys).

In-frame deletions within *cdiA*^{STECO31} were generated by PCR and introduced into plasmid pCH13604. The fragments from primer pairs ZR268/CH4240 and CH4241/ZR287 were cloned sequentially into pBluescript II SK+ using KpnI/XhoI and XhoI/NotI, respectively. The KpnI/NcoI fragment was then subcloned to generate pCH14028 (ΔFHA-1:

ΔAsp900-Ala999). The fragments from primer pairs ZR268/CH4243 and CH4244/ZR287 were cloned sequentially into pBluescript II SK+ via KpnI/XhoI and XhoI/NotI, respectively. The KpnI/NcoI fragment was then subcloned to generate pCH14029 (ΔRBD: ΔAsn1400-Ser1499). The fragments from primer pairs ZR268/CH4381 and CH4382/ZR287 were cloned sequentially into pBluescript II SK+ via KpnI/XhoI and XhoI/NotI, respectively. The KpnI/NcoI fragment was then subcloned to generate pCH14032 (ΔYP-100: Δpro1658-Asn1757). The fragments from primer pairs ZR268/CH4383 and CH4382/ZR287 were cloned sequentially into pBluescript II SK+ via KpnI/XhoI and XhoI/NotI, respectively. The KpnI/NcoI fragment was then subcloned to generate pCH14030 (ΔYP-N: ΔPro1658-Pro1707). The fragments from primer pairs ZR268/CH4383 and CH4384/ZR287 were cloned sequentially into pBluescript II SK+ via KpnI/XhoI and XhoI/NotI, respectively. The KpnI/NcoI fragment was then subcloned to generate pCH14031 (ΔYP-C: ΔGly1708-Asn1757). The product from ZR268/CH4245 was ligated via KpnI/NcoI to generate pCH14033 (ΔpFR: ΔGly1854-Ser1953). The product from ZR347/CH4247 was ligated via NcoI/AflII to generate pCH14034 (ΔFHA-2: ΔThr2324-Gln2423). The fragments from primer pairs CH4371/CH4372 and CH4373/ZR261 were cloned sequentially into pET21b via NheI/SacI and SacI/XhoI, respectively. The AflII/XhoI fragment was then subcloned to generate pCH14035 (ΔPT: ΔPro2781-Met2880).

The Asn2934Ala mutation in the VDNN motif was generated in three steps. Plasmid pCH13604 was digested with XbaI/SalI, end-filled with T4 DNA polymerase and re-ligated to remove restriction sites upstream of the *cdiBAI*$^{\text{SdTECO31}}$ gene cluster. An NheI restriction site was introduced into the resulting pCH13658 construct by ligating the PCR product of primers CH4282/CH4283 via AflII/XhoI to generate plasmid pCH13709. Finally, the product

from CH4412/CH4374 amplification was used as a template for a second PCR with CH4413/CH4374. The final product was ligated to pCH13709 via NheI/XhoI to generate pCH14036 (VDNA).

For cell-cell adhesion assays, the *cdiBAI*^{STECO31} gene cluster was over-expressed under an L-arabinose inducible promoter from plasmid pCH13602. Deletion constructs were introduced into pCH13602 through subcloning. The NotI/SacI fragment from pCH14028 was ligated to generate pCH14213 (ΔFHA-1: ΔAsp900-Ala999). The NotI/PmlI fragment from pCH14029 ligated to generate pCH14214 (ΔRBD: ΔAsn1400-Ser1499). SacI/XcmI fragments from pCH14030, pCH14031 and pCH14032 were ligated to generate plasmids pCH14215 (ΔYP-N: ΔPro1658-Pro1707), pCH14216 (ΔYP-C: ΔGly1708-Asn1757) and pCH14217 (ΔYP-100: Δpro-1658-Asn1757), respectively. NotI/XhoI fragments from pCH14033, pCH14034, pCH14035 and pCH14036 were ligated to generate pCH14218 (ΔpFR: ΔGly1854-Ser1953), pCH14219 (ΔFHA-2: ΔThr2324-Gln2423), pCH14220 (ΔPT: ΔPro2781-Met2880), and pCH14221 (VDNA: Asn2934Ala), respectively.

Cys substitutions were combined with the ΔAsn1400-Ser1499 (ΔRBD) deletion as follows. The NheI/KpnI fragment from pZR432 was ligated into pCH14029 to generate pCH14092 (S504C/ΔN1400-S1499). Plasmid pCH14029 was amplified with CH4239/CH4243 and pZR433 amplified with CH4244/ZR287, and the products ligated sequentially into pBluescript II SK+ with KpnI/XhoI and XhoI/NotI, respectively. The KpnI/NcoI fragment was then ligated to pCH13604 to generate pCH14093 (S1550C/ΔN1400-S1499). The KpnI/NcoI fragment from pCH14029 was ligated to plasmids pZR441, pZR442 and pZR444 to generate pCH14094 (T2502C/ΔN1400-S1499), pCH14095 (S2731C/ΔN1400-S1499) and pCH14096 (S3217C/ΔN1400-S1499), respectively.

Cys substitutions were combined with the ΔPro1658-Pro1707 (ΔYP-N) deletion as follows. The NheI/KpnI fragment from pZR432 was ligated into pCH14030 to generate pCH14202 (S504C/ΔP1658-P1707). Plasmid pZR433 was amplified with CH4239/CH4381 and with CH4382/ZR287, and the products ligated sequentially into pBluescript II SK+ via KpnI/XhoI and XhoI/NotI, respectively. The KpnI/NcoI fragment was then ligated to pCH13604 to generate pCH14203 (S1550C/ΔP1658-P1707). The KpnI/NcoI fragment from pCH14030 was ligated to plasmids pZR441, pZR442 and pZR444 to generate pCH14204 (T2502C/ΔP1658-P1707), pCH14205 (S2731C/ΔP1658-P1707), pCH14206 (S3217C/ΔP1658-P1707), respectively.

Cys substitutions were combined with the ΔGly1854-Ser1953 (ΔpFR) deletion as follows. The NheI/KpnI fragment from pZR432 was ligated into pCH14033 to generate pCH14102 (S504C/ΔG1854-S1953). The KpnI/PmlI fragment from pZR433 was ligated to pCH14033 to generate pCH14103 (S1550C/ΔG1854-S1953). AflII/XhoI fragments from plasmids pZR441, pZR442 and pZR444 were ligated to pCH14033 to generate pCH14104 (T2502C/ΔG1854-S1953), pCH14105 (S2731C/ΔG1854-S1953) and pCH14106 (S3217C/ΔG1854-S1953), respectively.

Cys substitutions were combined with the ΔThr2324-Gln2423 (ΔFHA-2) deletion as follows. The NheI/KpnI fragment from pZR432 was ligated to pCH14034 to generate pCH14107 (S504C/ΔT2324-Q2423). The KpnI/PmlI fragment from pZR433 was ligated to pCH14034 to generate pCH14108 (S1550C/ΔT2324-Q2423). AflII/XhoI fragments from plasmids pZR441, pZR442 and pZR444 were ligated to pCH14034 to generate pCH14109 (T2502C/ΔT2324-Q2423), pCH14110 (S2731C/ΔT2324-Q2423) and pCH14111 (S3217C/ΔT2324-Q2423). Plasmid pZR439 was amplified with CH4384/CH4247 and the

product ligated into pCH13604 via NcoI/AflII to generate pCH649 (D1959C/ΔT2324-Q2423).

Cys substitutions were combined with the ΔPro2781-Met2880 (ΔPT) deletion as follows. The NheI/KpnI fragment from pZR432 was ligated to pCH14035 to generate pCH14112 (S504C/ΔP2781-M2880). The KpnI/PmlI fragment from pZR433 was ligated to pCH14035 to generate pCH14113 (S1550C/ΔP2781-M2880). Plasmid pZR441 was amplified with CH4371/CH4372 and pZR432 with CH4373/ZR261, and the products ligated sequentially into pET21b via NheI/SacI and SacI/XhoI, respectively. The KpnI/NcoI fragment was then subcloned into pCH13604 to generate pCH14114 (T2502C/ΔP2781-M2880). Plasmid pZR442 was amplified with CH4371/CH4372 and pCH14035 with CH4373/ZR261, and the products ligated sequentially into pET21b via NheI/SacI and SacI/XhoI, respectively. The KpnI/NcoI fragment was then subcloned into pCH13604 to generate pCH14115 (S2731C/ΔP2781-M2880). The MfeI/XhoI fragment from pZR444 was ligated to pCH14035 to generate pCH14116 (S3217C/ΔP2781-M2880).

Cys substitutions were combined with the Asn2934Ala (VDNA) mutation as follows. The AflII/XhoI fragment from pCH14036 was ligated to plasmids pZR432 and pZR433 to generate pCH14117 (S504C/N2934A) and pCH14118 (S1550C/N2934A), respectively. Plasmid pZR441 was amplified with CH4371/CH4283 and the product ligated to pCH14036 via AflII/NheI to generate pCH14119 (T2502C/N2934A). Plasmid pZR442 was amplified with CH4371/CH4283 and the product ligated to pCH14036 via AflII/NheI to generate pCH14120 (S2731C/N2934A). The AflII/MfeI fragment from pCH14036 was ligated to pZR444 to generate pCH14121 (S3217C/N2934A).

The *E. coli minE* gene was amplified with CH2770/CH2771 and ligated to plasmid pTrc99a via NcoI/BamHI to generate pCH253. The NcoI/SbfI fragment from pCH253 was subcloned into

pCH450 (157) to generate pZR108. The *E. coli malE* gene was amplified with ZR295/ZR297 and ligated to pCH450 via NotI/XhoI to generate pZR462. The *malE* signal sequence was removed by cloning the product of ZR296/ZR297 into pCH450 via NotI/XhoI to generate pZR463. The *E. coli tsx* gene was amplified with ZR256/ZR257 and ligated to pZS21-MCS(Kan) (106) via EcoRI/XbaI to generate pCH14047. A fragment encoding the PT and CdiA-CT domains (Gly2648 – Lys3253) of cd/$A^{STECO31}$ and *cdil*^{STECO31} was amplified with primer pair ZR293/ZR261 and ligated to plasmid pCH7277 (158) via SpeI/Xhoi to generate pZR420. This latter plasmid was used to over-produce and purify His_6-tagged PT/CdiA-CT domains to raise polyclonal antisera in rabbits (Cocalico Biologicals, Stevens, PA).

Electron cryotomography

E. coli ZR82 cells carrying pCH253 and pDAL660 (full-length $CdiA^{EC93}$) were grown in LB media supplemented with Amp and Cm (100 μg/mL) at 37 °C, and minicell production induced with 1.5 mM isopropyl β-D-1-thiogalactopyranoside (IPTG). *E. coli* ZR82 strains carrying pZR108 and the various $CdiA^{EC93}$ truncation constructs were grown in LB media supplemented with Tet and Amp and induced with 0.2% L-arabinose to produce minicells. *E. coli* CH14017 cells carrying pZR108 and pCH13604 were used to visualize $CdiA^{STECO31}$ filaments. Lysed *E. coli* cells were prepared in 2 mg/mL lysozyme, 10 mM Tris-HCl (pH 8.0) at 37 °C for 30 min. The lysis mixture was adjusted to 2 mM $MgCl_2$, 250 μM $CaCl_2$ and treated with 1 mg/mL DNase I for 15 min at 37 °C. Cells were then collected by centrifugation and re-suspended in 10 mM Tris-HCl (pH 8.0) for imaging. All cell suspensions (16 μL) were mixed with bovine serum albumin (BSA)-treated 10-nm-diameter colloidal gold fiducial markers (159,160). This mixture (3 μL) was applied to a glow-discharged, X-thick carbon-coated, R2/2 200 mesh copper Quantifoil holey grid

(Quantifoil Microtools) in a Vitrobot Mark III (FEI Company, Hillsboro, OR). The Vitrobot chamber was maintained at 22 °C and 80% humidity. Excess liquid was blotte d from the grid with a blot time of 3 - 4 s and a drain offset of −3.5 or −4. The grid was then plunge-frozen in a liquid ethane-propane mixture and imaged by ECT (161). Imaging was performed on an FEI Polara G2 (FEI Company, Hillsboro, OR) 300-keV field emission gun electron microscope equipped with a Gatan image filter (Gatan, Pleasanton, CA) and K2 Summit counting electron detector camera (Gatan, Pleasanton, CA). Data were collected using the UCSF Tomo software (162), with each tilt series ranging from −60° to 60° (or −65° to 65°) in 1° increments, an under-focus of ~4-15 μm, and a cum ulative electron dose of ~190 e/Å^2 or less for each tilt series. The IMOD software package was used to calculate three-dimensional (3D) reconstructions (160).

To image BamA binding to CdiA^{EC93} by ECT, *E. coli* ZR82 strains carrying pCH253 and pDAL660 were grown and minicells produced as described above. Cells were collected by centrifugation, washed three times in 1× phosphate buffered saline (PBS) and re-suspended in 100 μg/mL BSA for 30 min at 4 °C. Purified *E. coli* BamA [50 nM in 20 mM Tris-HCl (pH 8.0), 0.5% Triton X-100] was also incubated with 100 μg/mL BSA for 30 min at 4 ° to prevent non-specific interactions with the cell surface. Cells were incubated with BamA-BSA for 1 h, collected by centrifugation at 3,000 × *g* for 5 min and re-suspended in PBS. For the negative control, the same procedure was conducted using a buffer-BSA solution that lacks purified BamA. Inhibitor cells (*E. coli* ZR82 carrying pCH253 and pDAL660) and BamA-expressing target cells (*E. coli* ZR83 carrying pCH253) were grown separately in LB media supplemented with the appropriate antibiotics as described above. Minicell production was induced with IPTG for 3.5 h, then cultures were mixed and

incubated with shaking at 240 rpm for 10 min and 75 rpm for 10 min. The suspension was incubated at 37 °C without shaking for 10 min prior to flash-freezing. Mixtures (4 μL) were applied to a glow-discharged, X-thick carbon-coated, R2/2 200 mesh copper Quantifoil holey grid in a Vitrobot Mark IV chamber maintained at 22 °C and 70% humidity. Excess liquid was blotted off the grid with a blot force of 6 or 3, a blot time of 3 or 2.5 s, and a drain time of 1 s. The grid was then plunge-frozen in a liquid ethane-propane mixture and imaged by ECT. Images were collected using either an FEI G2 300-keV field emission gun microscope or a FEI TITAN Krios 300-keV field emission gun microscope equipped with correction for lens aberration. Both microscopes were equipped with Gatan imaging filters and K2 summit counting electron-detector cameras (Gatan). Data were collected using the UCSF Tomo software with each tilt series ranging from −65° to 65° or (−60° to 60°) in 1 or 2° increments, an under-focus of ~10 μm, and a cumulative electron dose of ~180 e/A^2 or less for each tilt series.

Length measurements

The IMOD software package was used to calculate three-dimensional (3D) reconstructions of tilt series (160). Alternatively, the images were aligned and contrast transfer function corrected using IMOD software package before producing SIRT reconstructions using the TOMO3D program (163). CdiA structures on cell envelopes were located by visual inspection. Using the IMOD software package, a stack of 10 slices displaying the best view for each structure was used to measure lengths (by eye) from the center of the outer membrane to the tip of the filament. All filaments were measured separately by three individuals. The mean lengths within each particular dataset (as

determined by the three individuals) did not differ with statistical significance (*p*-values > 0.05 in all instances). In contrast, the mean lengths of unbound CdiA versus BamA(micelle)-bound CdiA and unbound versus BamA(vesicle)-bound measurements were significantly different (*p*-values < 0.00001 in both case for all three individuals).

Protease protection, SDS-PAGE and immunoblotting

E. coli CH14016 cells carrying plasmid pCH13604 were diluted to OD_{600} ~ 0.05 in LB medium supplemented with Amp and cultured with shaking at 37 °C. Once in mid-log phase, cultures were treated with Spc for 20 min to block protein synthesis. Cells were harvested by centrifugation and re-suspended in 1× phosphate buffered saline (PBS) supplemented with 1 mM $MgSO_4$ (PBS-Mg). Proteases were added to 20 μg/mL, and the cell suspensions incubated at ambient temperature for 20 min. Cells were collected by centrifugation and washed four times with PBS-Mg supplemented with 6 mM 2-mercaptoethanol (2-ME), 2 mM phenylmethanesulfonyl fluoride. Cell pellets were re-suspended in urea-lysis buffer [50% urea, 150 mM NaCl, 20 mM Tris-HCl (pH 8.0)] and subjected a freeze-thaw cycle to extract proteins for SDS-PAGE and immunoblotting.

Urea-soluble protein samples (5 μL) were analyzed by SDS-PAGE on Tris-tricine 6% polyacrylamide gels run at 100 V (constant) for 3 h. Gels were soaked for 15 min in 25 mM Tris, 192 mM glycine (pH 8.6), 10% methanol, then electroblotted to low-fluorescence PVDF membranes using a semi-dry transfer apparatus at 17 V (constant) for 1 h. Membranes were blocked with 4% non-fat milk in PBS for 1 h at room temperature, and incubated with primary antibodies in 0.1% non-fat milk, PBS overnight at 4 °C. Rabbit polyclonal antisera (Coca lico Biologicals, Stevens, PA) to the N-terminal TPS domain was used at a 1:10,000

dilution and anti-PT/CdiA-CT antisera was used at a 1:3,000 dilution. Blots were incubated with 800CW-conjugated goat anti-rabbit IgG (1:40,000 dilution, LICOR) in 0.1% non-fat milk in PBS. Immunoblots were visualized with a LI-COR Odyssey infrared imager.

To analyze culture supernatants for released $CdiA^{STECO31}$ chains, cells were grown to mid-log phase in LB media supplemented with Amp. Protein synthesis was then blocked with Spc and the culture incubated with shaking for 20 min at 37 °C. Cells were collected by centrifugation at 3,000 × *g* for 5 min, and 900 μL of the supernatant was added to 100 μL of trichloroacetic acid. Proteins were collected by centrifugation at 18,000 × *g*for 30 min at 4 °C. Precipitates were washed thrice with 1.0 ml of cold acetone. Air-dried pellets were dissolved in 45 μL of urea-lysis buffer, and 5 μL of each sample analyzed by SDS-PAGE and immunoblotting.

Maleimide-dye labeling to map surface topology

E. coli CH14016 cells carrying $CdiA^{STECO31}$ expression plasmids were diluted to OD_{600} ~ 0.05 in Amp supplemented LB media and grown to mid-log phase at 37 °C. Cultures were then treated with Spc for 20 m in to block protein synthesis. Cells were harvested by centrifugation and re-suspended at OD_{600} ~ 0.3 in 1.0 mL of: i) PBS-Mg to probe intact cells; ii) PBS-Mg with 100 μg/mL polymyxin B to probe permeabilized cells; or iii) PBS-Mg supplemented with 100 μg/mL polymyxin B, 100 μg/mL lysozyme, 250 U/mL benzonase to probe lysed cells. IRDye680LT-maleimide (LI-COR) was added to a final concentration of 40 μM for intact cells and 120 μM for permeabilized/lysed cells. Labeling reactions were incubated in the dark at room temperature for 15 min, then quenched with 6 mM 2-ME. Cells were collected by centrifugation and washed with PBS-Mg supplemented with 6 mM 2-ME.

Cell pellets were re-suspended in 50 μL of urea-lysis buffer and subjected to one freeze-thaw cycle to extract proteins. Urea-soluble proteins (5 μL) were resolved by SDS-PAGE and analyzed by immunoblotting using anti-TPS domain antisera. 680LT (dye-maleimide) and 800CW (secondary antibody) fluorescence was visualized using a LI-COR Odyssey infrared imager. His_6-tagged MBP was purified from urea-solubilized lysates by Ni^{2+}-affinity chromatography prior to analysis by SDS-PAGE and blotting.

The same general procedure was used to monitor changes in $CdiA^{STECO31}$ topology in response to target bacteria. *E. coli* CH14016 inhibitors that express $CdiA^{STECO31}$ variants were mixed with *E. coli* CH14016 target cells that carry pCH450 (Δ*tsx*) or pCH13603 (*tsx*$^+$) at a 1:2 ratio in fresh, pre-warmed LB media supplemented with Spc to block new protein synthesis. After 20 min with shaking, the cell mixtures were collected by centrifugation and re-suspended at OD_{600} ~ 0.3 in 1.0 mL of PBS-Mg for labeling with 40 μM IRDye680LT-maleimide. Labeling reactions were quenched and proteins extracted for analysis as described above.

Cell mixtures were washed once in PBS-Mg and resuspended in 0.5 mL PBS-Mg. Maleimide dye was added to 40 μM, followed by the addition of proteinase K at 20 μg/mL. Suspensions were incubated at ambient temperature in the dark for 20 min, then quenched with 15 mM 2-ME and 2 mM PMSF. Cells were washed thrice with PBS-Mg supplemented with 15 mM 2-ME, 2 mM PMSF, followed by one wash with PBS-Mg. Cells pellets were resuspended in urea lysis buffer for SDS-PAGE and immunoblot analyses. For sucrose-gradient fractionation, the proteinase K treated cells were resuspended in 1.0 mL PBS-Mg supplemented with 200 μg/mL lysozyme, 50 U/mL benzonase and HALT protease inhibitor cocktail (Thermo-Fisher). Suspensions were subjected to one freeze-thaw, then broken with

three French press passages. Lysates were incubated at ambient temperature in the dark for 10 min, then 400 μL was layered onto a 3.6 mL linear 10 – 60% sucrose gradient. Samples were centrifuged at ~150,000 × *g* for 1 h, and 12 fractions were collected by drip from a puncture in the bottom of the centrifuge tube. Proteins were precipitated by adjusting each fraction to 90% (vol/vol) ethanol. Precipitates were dissolved in urea lysis buffer for SDS-PAGE and immunoblot analyses.

Competition co-cultures

E. coli CH14016 (Δ*wzb* Δ*tsx*) and CH14017 (Δ*wzb* Δ*tsx* Δ*ompT*) that harbor $CdiA^{STECO31}$ expression plasmids were used as inhibitor cells in shaking broth co-cultures. *E. coli* CH14016 and CH14017 strains that carry pCH10145 (Δ*tsx*) or pZR428 (tsx^+) were used as target cells. Cells were grown in LB media at 37 °C to mid-log ph ase, adjusted to OD_{600} ~ 0.3 in fresh pre-warmed LB media without antibiotics, mixed at a 1:1 ratio (5 mL total volume) and incubated with shaking for 3 h at 37 °C. Culture aliquots were taken at the beginn ing of co-culture and after 3 h to quantify viable inhibitor and target cells as colony forming units per milliliter (CFU mL^{-1}). For solid media growth competitions, *E. coli* CH14017 cells (Δ*wzb* Δ*tsx* Δ*ompT*) that carry pCH10145 (Δ*tsx*) or pZR428 (tsx^+) were used as target bacteria. Inhibitor and target cells were grown in LB media at 37 °C to mid-log phase, adjusted to OD_{600} ~ 1 in 1× M9 salts, and mixed at a 1:1 ratio (100 μL total volume). Samples of the mixed-cell suspensions (10 μL) were spotted onto LB-agar and incubated at 37 °C. After 3 h, cells were harvested using polyester-tipped applicators and resuspended in 500 μL of 1× M9 salts. For all competitions, cell suspensions were serially diluted into 1× M9 salts and plated onto LB-agar supplemented with Amp to enumerate inhibitor cells, and

LB-agar supplemented with Kan to enumerate target cells. Competitive indices were calculated as the ratio of target to inhibitor cells at 3 h divided by the initial target to inhibitor cell ratio.

BamA purification

BamA from *E. coli* was over-produced in *E. coli* strain CH2016 carrying plasmid pCH9216 (105). Cells were grown at 37 °C in LB media supplemented with Amp and BamA production induces with 1.5 mM IPTG for 3 h. Cells were harvested by centrifugation at 6,000 × *g* for 10 min, then re-suspended in 5 mL of BugBuster reagent and broken by three passages through a French press. The lysate was diluted with 25 mL deionized water and vortexed vigorously. Inclusion bodies were collected by centrifugation at 15,000 × *g* for 20 min and washed thrice with 5 mL of 0.1 × BugBuster solution. The washed inclusion bodies were dissolved in 0.5 mL of urea-lysis buffer supplemented with 0.05% Triton X-100, then diluted into 50 mL 10 mM Tris-HCl (pH 8.0), 0.5% Triton X-100 to a final concentration of 140 μM. Diluted protein stocks were incubated on a rotisserie for three days at ambient temperature to refold. The refolding reaction was then stored at 4 °C. Greater than 95% of BamA was refolded as determined by heat-modifiable gel mobility as previously described (164).

Cell-cell adhesion by flow cytometry

Tsx-binding studies were conducted using *E. coli* strain DL4259, which expresses *gfp-mut3* from the *papBA* promoter (113). *E. coli* DL4259 cells were transformed with pCH450-derived CdiA^{STECO31} expression plasmids and the resulting strains grown at

37 °C in LB media supplemented with Tet until the cells became fluorescent. *E. coli* ZR373 cells carrying plasmid pDsRedExpress2 were used as targets. Targets were also provided with plasmid pCH450 (Δ*tsx*) or pCH13603 (*tsx*$^{+}$). Target cells were grown overnight in LB supplemented with Tet, Amp, 0.4% L-arabinose and 1 mM IPTG to induce expression of Tsx and DsRed prior to mixing with inhibitors. GFP-labeled inhibitor cells were mixed at a 5:1 ratio with DsRed-labeled target bacteria at a final OD_{600} ~ 0.2. Cell suspensions were shaken at 30 °C for 2 0 min, diluted into 1× PBS, vortexed briefly, then analyzed on an Accuri C6 flow cytometer using FL1 (533/30nm, GFP) and FL2 (585/40nm, DsRed) fluorophore filters. The fraction of target bacteria bound to inhibitor cells was calculated as the number of dual green/red fluorescent events divided by the total number of red fluorescent events. Three independent experiments were performed on separate days, and >2,000 red fluorescent events were scored for each cell mixture per experiment.

CdiA domain analyses

CdiA^{STECO31} homologs were identified by BLAST using residues Asn1637 – Asn1902 as a query to search enterobacterial genera. The query sequence includes the FHA-1 peptide immediately adjacent to the RBD and extends through the periplasmic FHA-1 repeats (pFR). 142 full-length CdiA proteins ranging from 2,963 to 6,442 residues were identified for analysis (Table S2). The number of residues comprising each RBD was plotted as a function of the length of the FHA-1 region. The number of residues comprising each FHA-2 domain was determined from automated annotations on the NCBI website (Table S2) and plotted as a function of FHA-1 length. The FHA-2 domain of CdiA^{STECO31} (residues Leu1941 to

Met2560) was submitted to the I-TASSER server for protein structure and function predictions (144).

E. Figures and tables

Movies, Table S1, and Table S2 for this publication could not be adapted in this dissertation but they can be viewed at: https://doi.org/10.1016/j.cell.2018.10.033

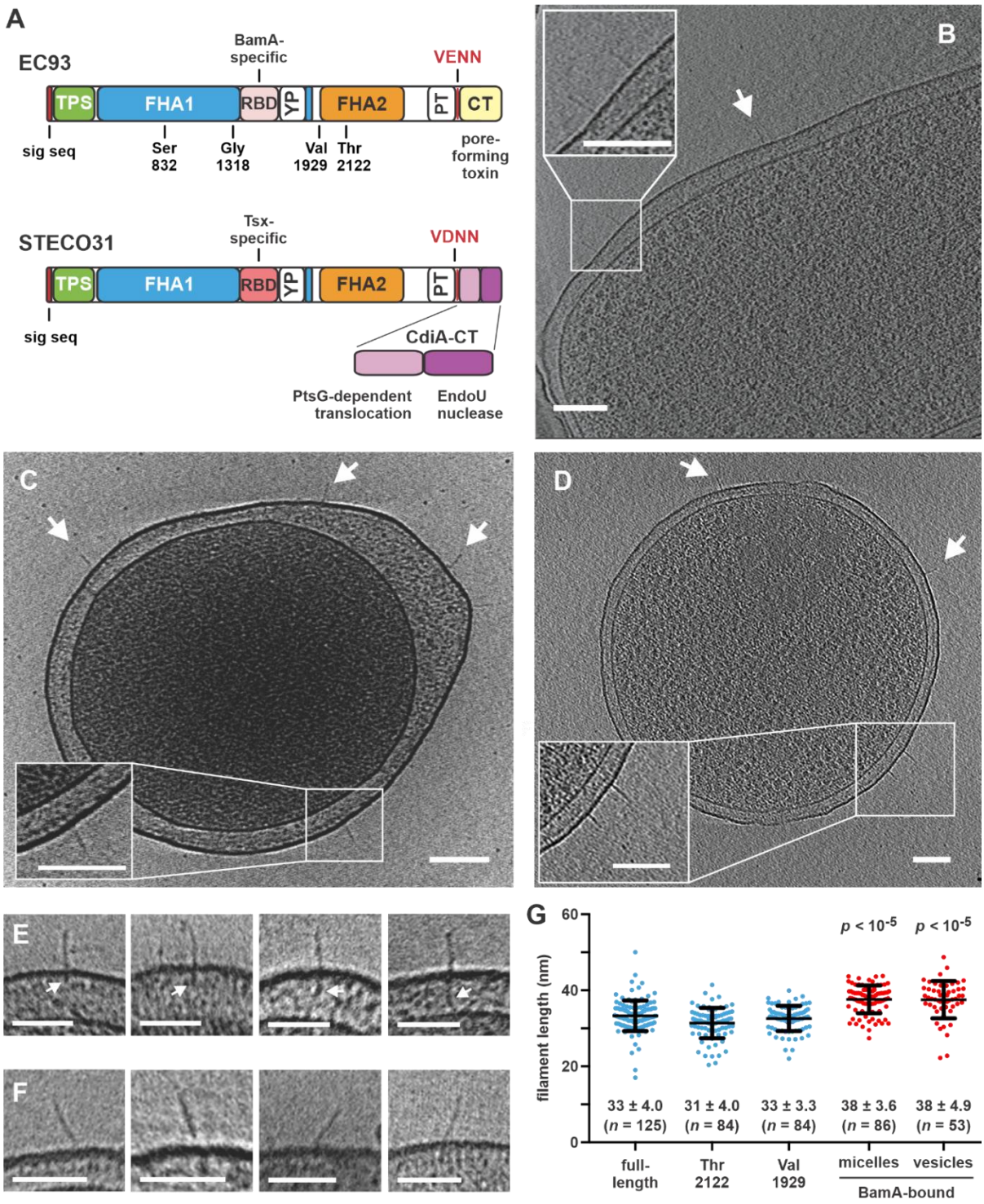

Figure 1 See next page for the legends

Figure 1. CdiA forms a filament on the cell surface. A) CdiA domain architecture. VENN/VDNN motifs demarcating the CdiA-CT regions are indicated. The YP domain is not annotated in current databases. See Figure S3. B) $CdiA^{EC93}$ on the cell surface. See Figure S1B & Movie S1. C) $CdiA^{EC93}$ on an *E. coli* minicell. See Figure S1C & Movie S2. D) $CdiA^{STECO31}$ on an *E. coli* minicell. See Movie S3. Arrows indicate individual CdiA proteins, and scale bars = 100 nm for A, B & C. E) Periplasmic densities associated with filaments. F) Angled filaments. Scale bars = 50 nm for E & F. G) Lengths of CdiAEC93 filaments. Data are presented with mean ± SD for each condition. The p values are from two tailed t-test comparisons with full-length CdiAEC93.

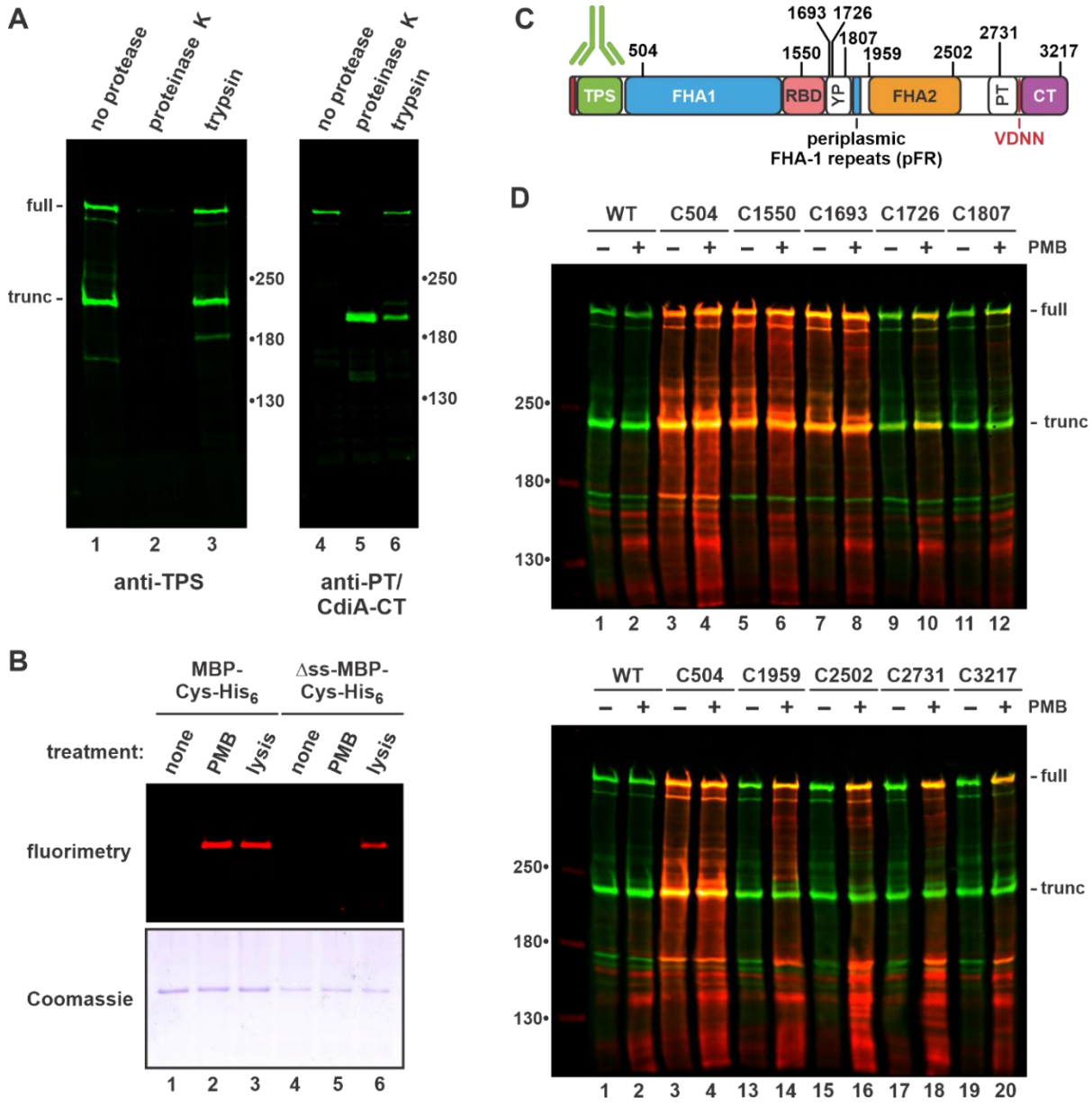
A
no protease
proteinase K
trypsin
full
trunc
•250
•180
•130
1 2 3
anti-TPS
4 5 6
anti-PT/
CdiA-CT
B
MBP-
Cys-His6
Δss-MBP-
Cys-His6
treatment:
none
PMB
lysis
fluorimetry
Coomassie
1 2 3 4 5 6
C
504
1550
1693 1726
1807
1959
2502
2731
3217
TPS
FHA1
RBD
YP
FHA2
PT
CT
periplasmic
FHA-1 repeats (pFR)
VDNN
D
WT C504 C1550 C1693 C1726 C1807
– + – + – + – + – + – + PMB
250•
180•
130•
full
trunc
1 2 3 4 5 6 7 8 9 10 11 12
WT C504 C1959 C2502 C2731 C3217
– + – + – + – + – + – + PMB
250•
180•
130•
full
trunc
1 2 3 4 13 14 15 16 17 18 19 20

Figure 2. CdiA surface topology. A) Protease protection assays. Immunoblot analysis with antisera the TPS and PT/CdiA-CT domains of $CdiA^{STECO31}$. B) Polymyxin B (PMB) permeabilizes the outer membrane. Cells expressing periplasmic or cytoplasmic (Δss) maltose-binding protein (MBP) were incubated with maleimide-dye and permeabilized with PMB or lysed as indicated. Purified MBP was analyzed by fluorimaging (top) and SDS-PAGE (bottom). C) Cys substitutions in $CdiA^{STECO31}$. The periplasmic FHA-1 repeat (pFR) cluster and major domains are indicated. See Figure S2. D) Immunoblot analysis of dye-labeled CdiA. CdiA expressing cells were incubated with maleimide-dye and permeabilized with PMB where indicated. CdiA was analyzed by immunoblotting with TPS antisera. Dye fluorescence (red) is superimposed onto antibody fluorescence (green).

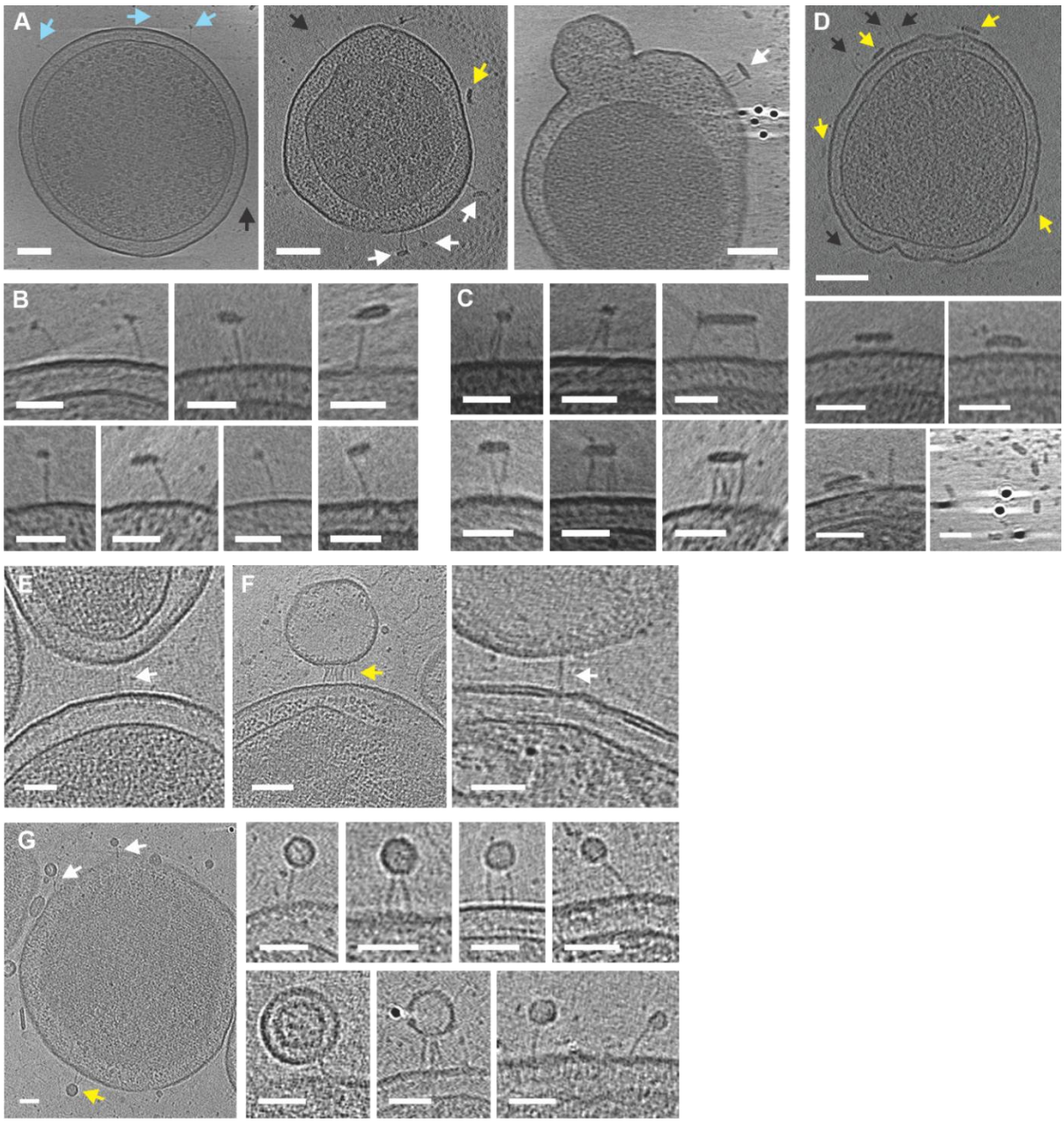

Figure 3. CdiA-receptor binding interactions. A) CdiA^{EC93} bound to solubilized BamA in globular (blue arrows) and flattened micelles (white arrows). See Movie S5. Some filaments (black arrows) and micelles (yellow arrows) do not interact. B) Enlarged views of BamA-bound filaments. C) Micelles bound to multiple filaments. D) CdiA^{EC93} expressing minicell incubated with detergent in buffer. E) CdiA^{EC93} filament bridging minicells. F) Filaments bound to vesicles from BamA-expressing minicells. G) Filaments bound to small vesicles from BamA minicells. Scale bars 100 nm for minicell views and 50 nm for close-up views.

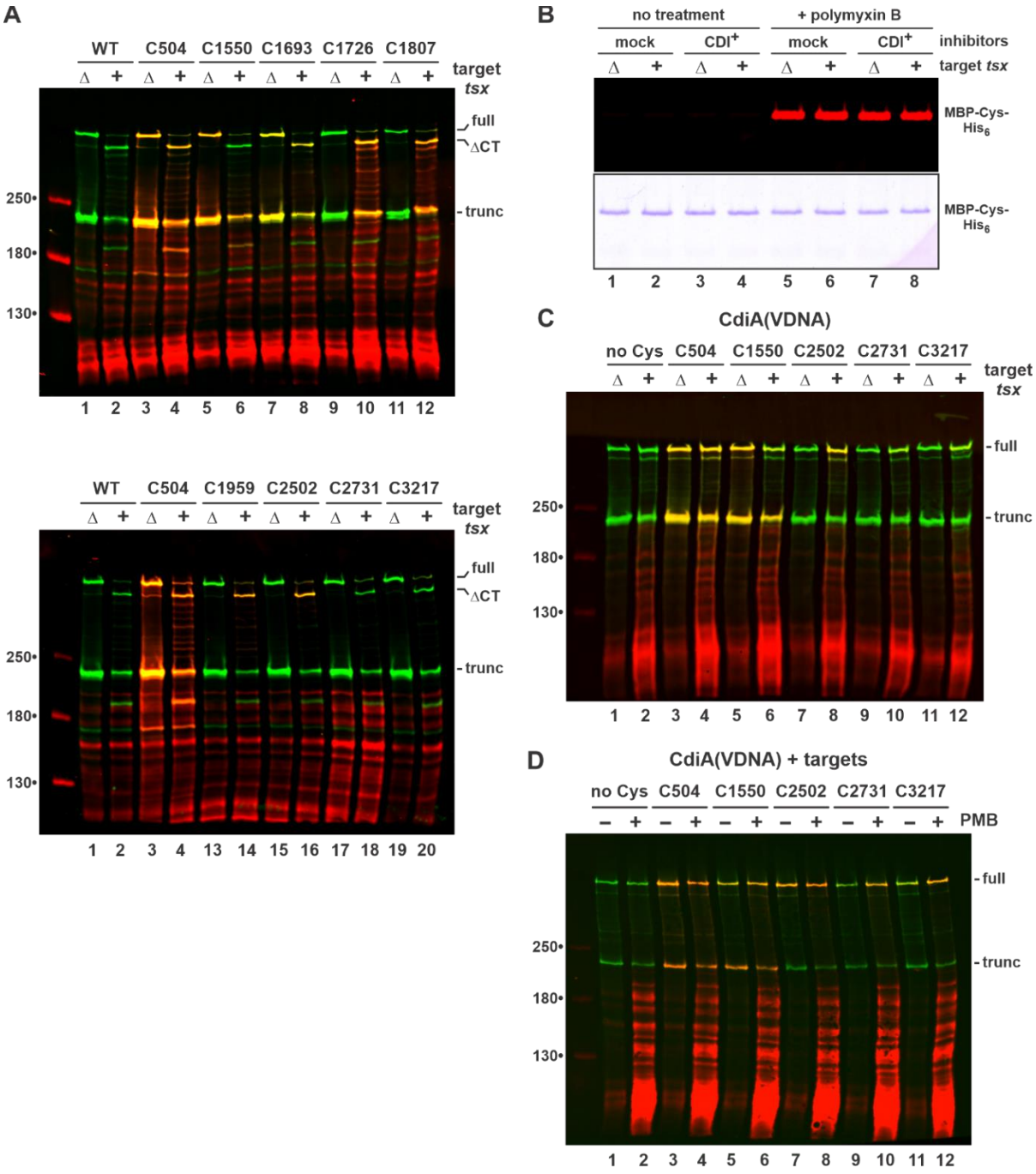

Figure 4. See next page for the legends

Figure 4. CdiA export resumes upon binding receptor. A) Topology of receptor-bound CdiA^{STECO31}. CdiA expressing cells were mixed with *tsx*$^{+}$ or Δ*tsx* targets and incubated with maleimide-dye. CdiA was analyzed by immunoblotting with anti-TPS antibodies. Full-length, CdiA-CT processed (ΔCT) and truncated proteins are indicated. **B**) Inhibitors co-expressing MBP-Cys-His$_6$ were mixed with targets and incubated with maleimide-dye. Purified MBP was analyzed by fluorimetry (top panel) and SDS-PAGE (bottom panel). **C**) CdiA(VDNA) expressing cells were mixed with targets and analyzed as in panel A. **D**) CdiA(VDNA) expressing cells were mixed with *tsx*$^{+}$ targets and incubated with maleimide-dye. Mixed cell suspensions were treated with PMB where indicated.

Figure 5. The YP domain is required for cell-surface presentation. A) CdiA^{STECO31} deletion constructs. See Figures S2. B) Target cell adhesion. GFP-labeled inhibitors were mixed with DsRed-labeled targets and analyzed by flow cytometry to quantify the fraction of target cells bound to inhibitors. Data are presented as mean ± SEM. C) Competition co-cultures. Inhibitors were mixed at a 1:1 ratio with targets and co-cultured on LB-agar. Competitive indices equal the final ratio of targets to inhibitors divided by the initial ratio. Data are presented as mean ± SEM. D) Inhibitors were mixed with targets and CdiA analyzed by anti-TPS immunoblotting. E) ΔpFR and ΔFHA-2 inhibitors were mixed with target cells, and CdiA analyzed by anti-TPS immunoblotting. Inhibitor and target cells carried Δ*ompT* mutations where indicated. White carets indicate aberrantly processed CdiA. See Figure S5.

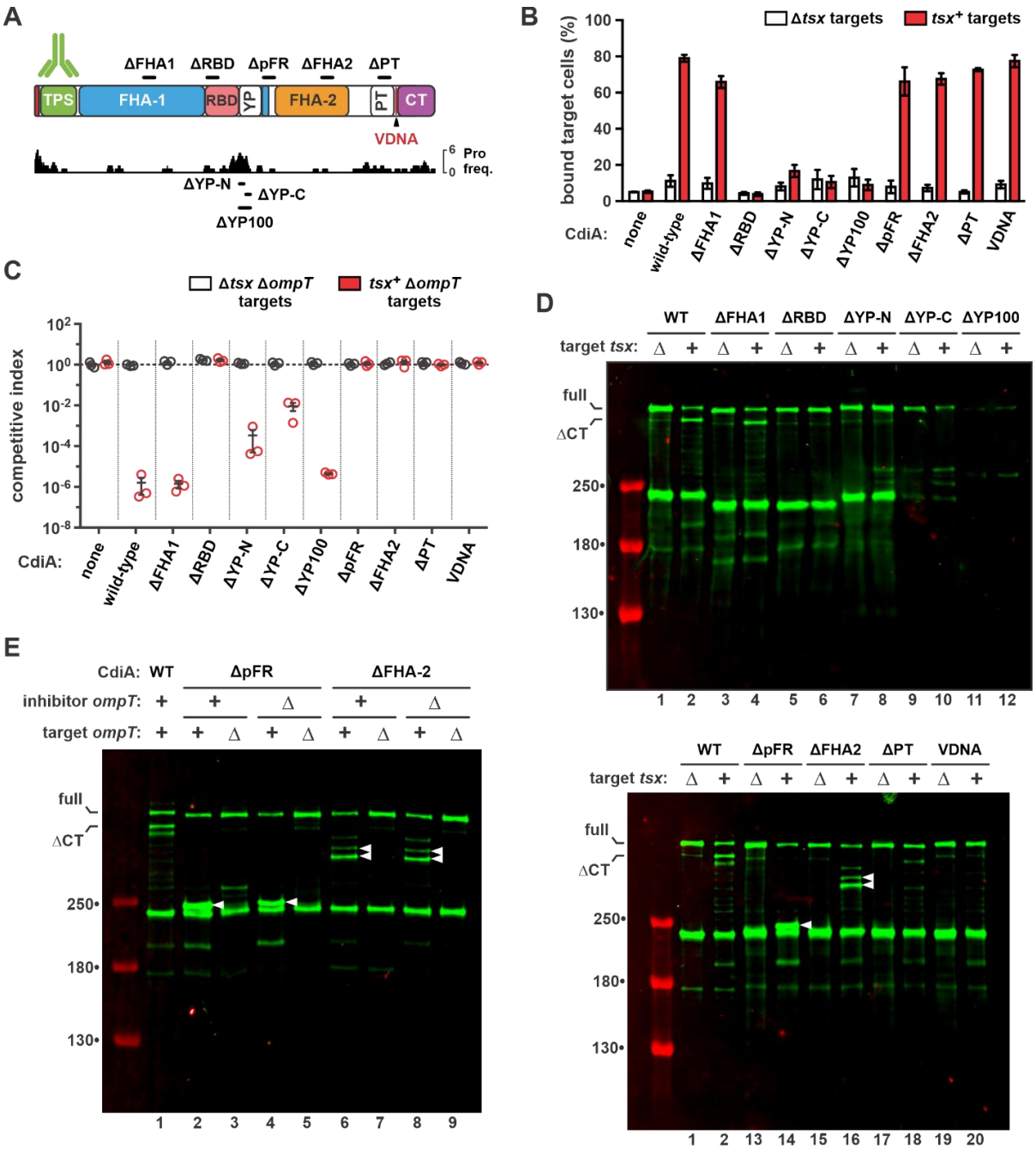

Figure 5. See the previous page for the legends

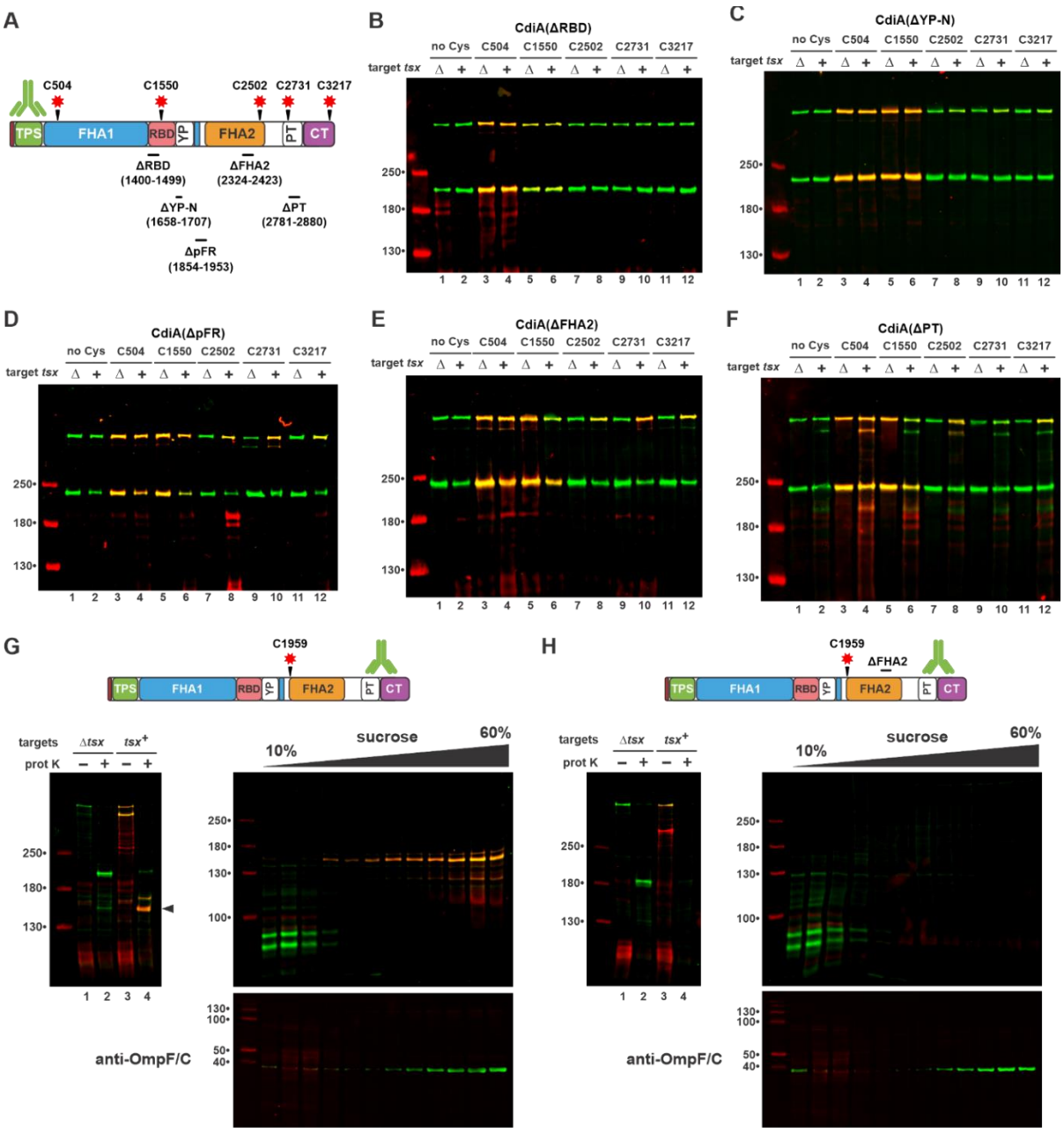

Figure 6. The FHA-2 domain is required for toxin delivery. A) CdiA deletions and Cys substitutions. Deleted residues are indicated below domain identifiers. B - F) Cells expressing the indicated CdiA effectors were mixed with targets and incubated with maleimide-dye. CdiA proteins were analyzed by anti-TPS immunoblotting. G) FHA-2 localizes to the outer membrane after export. Cells expressing Cys1959 CdiA were mixed with *tsx*$^{+}$ targets, then treated with dye and proteinase K. The sample from lane 4 was run on a sucrose gradient, and fractions analyzed by anti-TPS and anti-OmpF/C immunoblotting. H) Cells expressing Cys1959 ΔFHA2 were treated and analyzed as in panel G.

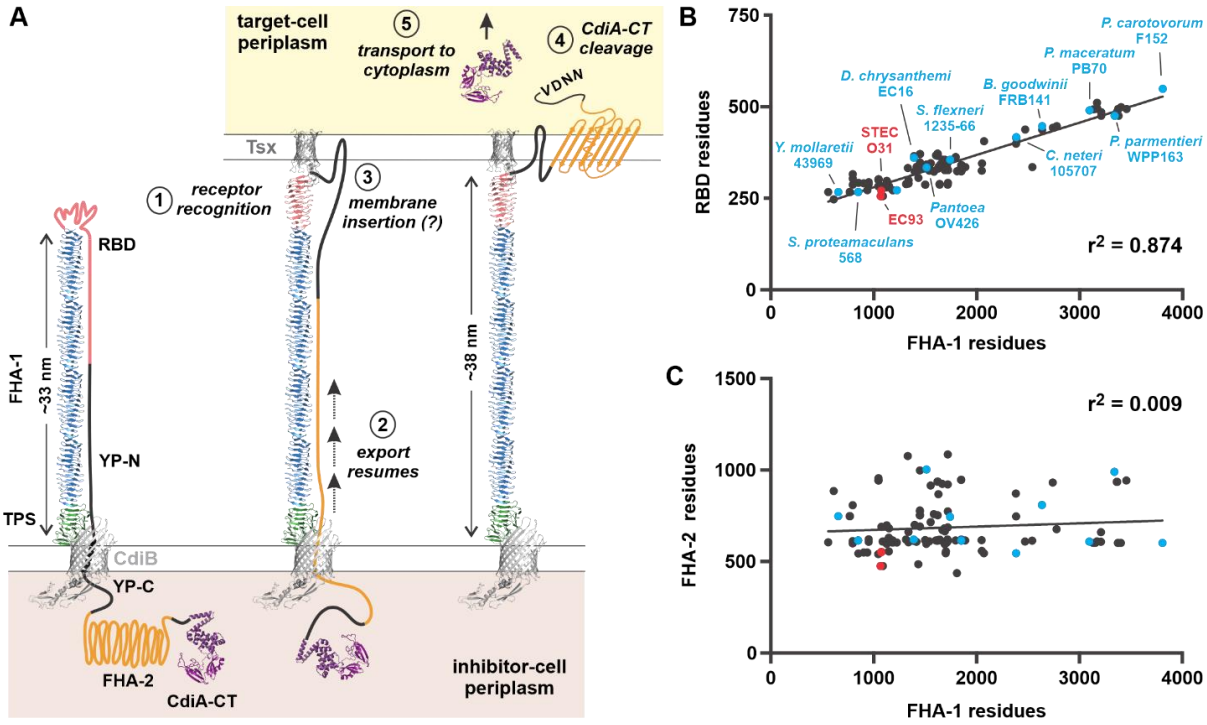

Figure 7. Model for CdiA surface topology and receptor-triggered toxin delivery. A) Model of CdiA surface topology. Receptor recognition (1) triggers export of the C-terminal half of CdiA (2). The FHA-2 domain interacts with the target-cell outer membrane (3), perhaps forming a β-barrel translocon. Once transferred into the target-cell periplasm, the CdiA-CT region is cleaved (4) for transport into the cytoplasm (5). B) RBD size is proportional to filament length. RBD residues are plotted as a function of FHA-1 residues. See Figure S3 & Table S2. C) Plot of FHA-2 versus FHA-1 residues for the effectors in panel B. See Table S2.

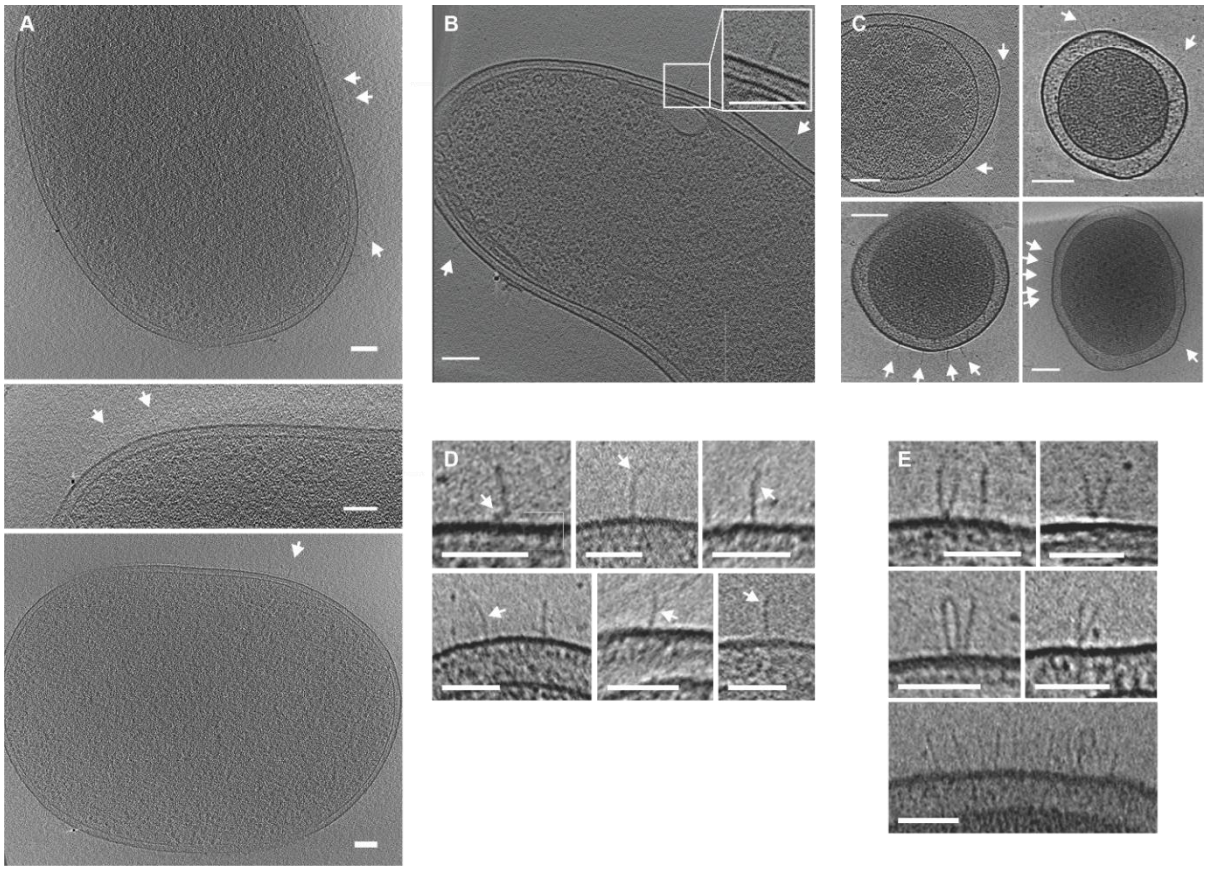

Figure S1. ECT imaging of CdiA. A) Filaments (white arrows) on the surface of *E. coli* EC93 cells. B) $CdiA^{EC93}$ filaments on the surface of an *E. coli* K-12 cell. C) $CdiA^{EC93}$ filaments on the surface of an *E. coli* K-12 minicell. Scale bars = 100 nm for A, B & C. D) Bent $CdiA^{EC93}$ filaments. E) Twinned and clustered filaments. Scale bars = 50 nm for D & E

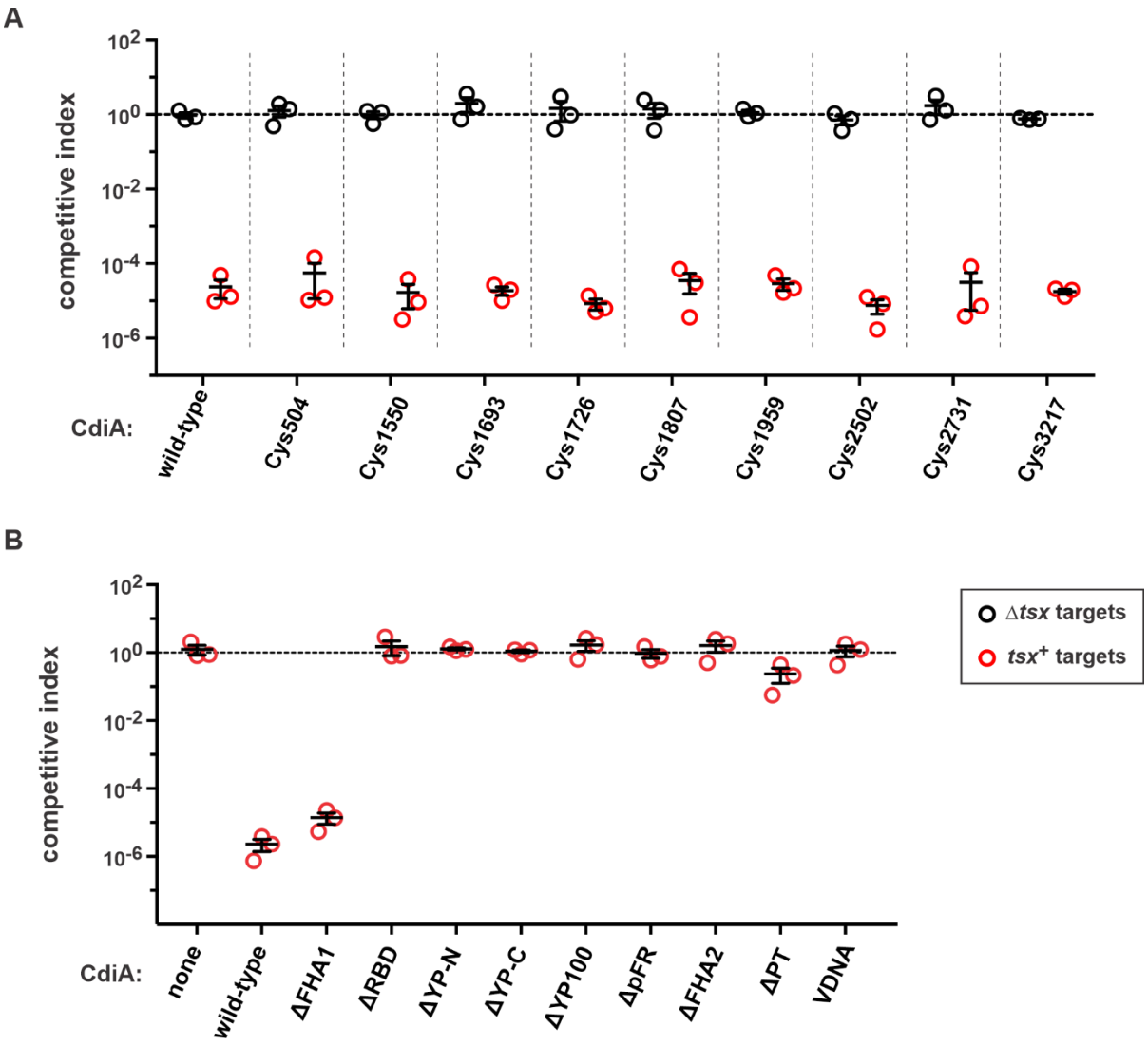

Figure S2. Competition co-cultures. A and **B**) Inhibitors were mixed at a 1:1 ratio with *tsx*⁺ or Δ*tsx* targets and incubated in shaking LB media. Competitive indices equal the final ratio of targets to inhibitors divided by the initial ratio. Data are presented as mean ± SEM for three independent experiments.

Figure S2. See next page for the legends

Figure S3. Alignment of receptor-binding and YP domains. CdiA sequences were aligned using Clustal Omega. FHA-1 sequences are in blue bold-face. $CdiA^{STECO31}$ and $CdiA^{EC93}$ RBD sequences are shown in salmon and pink, respectively. The YP domain is shown in black bold-face for $CdiA^{STECO31}$ and $CdiA^{EC93}$, beginning with the YPLP peptide motif and extending to the periplasmic FHA-1 repeats (pFR). Cys-substituted positions (Ser1550, Ser1693, Gly1726 and Ala1807) in $CdiA^{STECO31}$ are underlined and highlighted in yellow. CdiA sequences are from *Pectobacterium carotovorum* F152 (NCBI accession: PPE64673.1), *Pectobacterium parmentieri* WPP163 (ACX88282.1), *Pectobacterium maceratum* PB70 (POY59994.1), *Brenneria goodwinii* RBB141 (WP_095834043.1), *Cedecea neteri* NBRC 105707 (WP_061277518.1), *Enterobacter cloacae* MGH 54 (WP_084832630.1), *Shigella flexneri* 1235-66 (EIQ74285.1), *Pantoea* sp. OV426 (SFN23123.1), *Dickeya chrysanthemi* EC16 (AAN38708.1), *Escherichia coli* STEC_O31 (WP_001385946.1), *Escherichia coli* EC93 (AAZ57198.1), *Serratia proteamaculans* 568 (WP_012147097.1), and *Yersinia mollaretii* ATCC 43969 (WP_0r04876812.1).

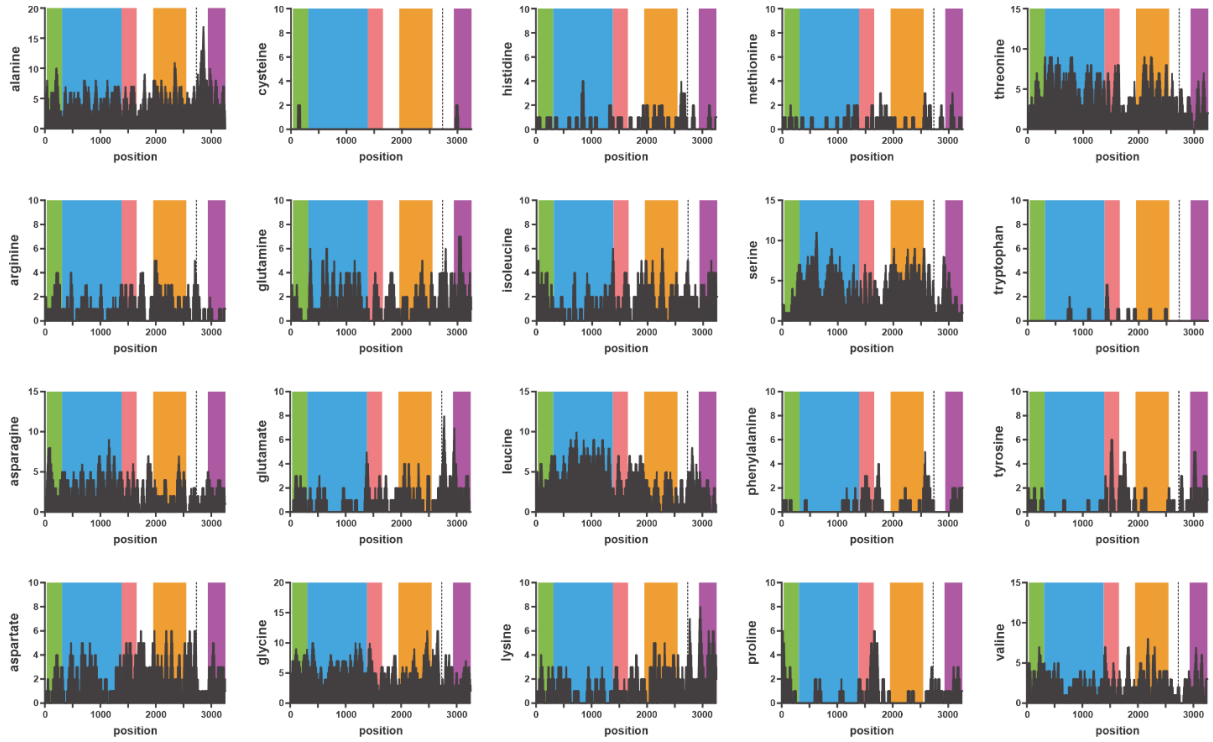

Figure S4. CdiA^{STECO31} amino acid residue frequency. Amino acid residues were counted within a sliding 40-residue window along the length of CdiA^{STECO31}. Domains are color-coded: TPS transport (green), FHA-1 (blue), RBD (maroon), FHA-2 (orange), and CdiA-CT (purple).The PT domain corresponds to the region between the dotted line and the CdiA-CT.

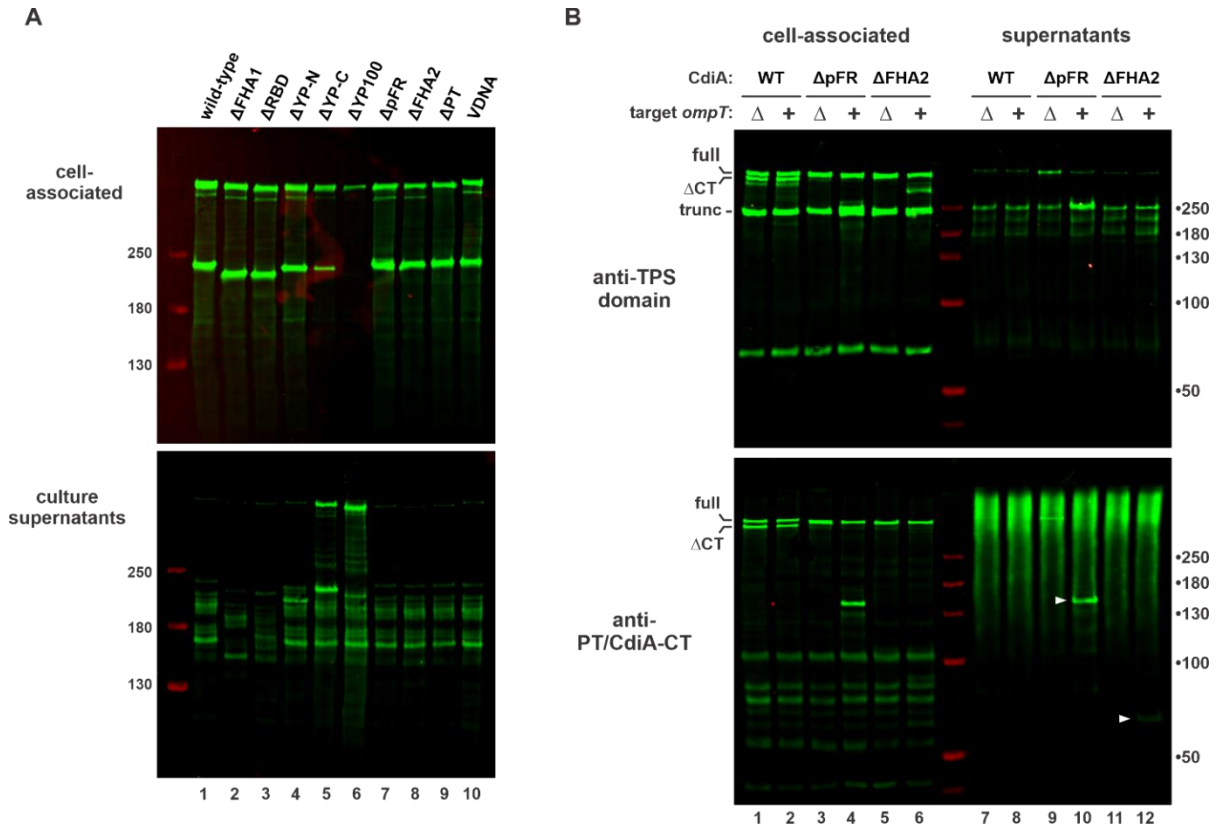

Figure S5. OmpT cleaved CdiA fragments are released from the cell. CdiA expressing cells were mixed with *tsx*$^{+}$ *ompT*$^{+}$ or *tsx*$^{+}$ Δ*ompT* targets. Cell pellets and culture supernatants were analyzed by immunoblotting with antibodies to the TPS domain and the PT/CdiA-CT region of CdiA^{STECO31}. White carets indicate C-terminal CdiA^{STECO31} fragments.

Table 1. Strains used in this study.

Strain	Reference
E. coli K-12 sub-strain MG1655	*E. coli* Genetic Stock Center
E. coli K-12 sub-strain EPI100	Epicentre/Lucigen
E. coli: DS612: BW25113 Δ*yhdE::cat mreB-A125V*	(154)
E. coli: CH2016: X90 (DE3) Δ*rna* Δ*slyD::kan*	(158)
E. coli: CH7286: MG1655 Δ*wzb::kan*	This paper
E. coli: CH7367: MG1655 Δ*wzb*	This paper
E. coli: CH9591: EPI100 Δ*bamA::cat* pZS21-*bamA*^{ECL}	(104)
E. coli: CH9604: EPI100 Δ*bamA::cat* pZS21-*bamA*$^{+}$	(104)
E. coli: CH10060: EC93 *bamA*^{LT2}	(127)
E. coli: CH10093: EC93 *ΔcdiA*	(127)
E. coli: CH14016: MG1655 Δ*wzb* Δ*tsx*	This paper
E. coli: CH14017: MG1655 Δ*wzb* Δ*tsx* Δ*ompT*	This paper
E. coli: ZR82: EPI100 Δ*bamA::cat* Δ*yhdE mreB-A125V* pZS21-*bamA*^{ECL}	This paper
E. coli: ZR83: EPI100 Δ*bamA::cat* Δ*yhdE mreB-A125V* pZS21-*bamA*$^{+}$	This paper
E. coli: DL4259: MC4100 λ640-13 P*papIB-gfp-mut3*	(113)
E. coli: ZR373: EPI100 Δ*wzb* Δ*tsx*	This paper

Table 2. Plasmids used in this study.

Plasmids	Reference
pBluescript II SK+	Agilent/Stratagene
pDsRedExpress2	Clontech
pET21b	Novagen
pCP20	(155)
pZS21-*bamA*$^{+}$	(104)
pZS21-*bamA*^{ECL}	(104)
pDAL660	(70)
pCH253	This paper
pCH450	(157)
pCH649	This paper
pCH7277	(158)
pCH9674	(105)

pCH9216	(105)
pCH9231	(105)
pCH10145	(106)
pCH12705	(70)
pCH12706	(70)
pCH12707	(70)
pCH13602	(105)
pCH13603	(105)
pCH13604	(105)
pCH13658	This paper
pCH13709	This paper
pCH14028	This paper
pCH14029	This paper
pCH14030	This paper
pCH14031	This paper
pCH14032	This paper
pCH14033	This paper
pCH14034	This paper
pCH14035	This paper
pCH14036	This paper
pCH14047	This paper
pCH14092	This paper
pCH14093	This paper
pCH14094	This paper
pCH14095	This paper
pCH14096	This paper
pCH14102	This paper
pCH14103	This paper
pCH14104	This paper
pCH14105	This paper
pCH14106	This paper
pCH14107	This paper
pCH14108	This paper
pCH14109	This paper
pCH14110	This paper
pCH14111	This paper
pCH14112	This paper
pCH14113	This paper
pCH14114	This paper
pCH14115	This paper
pCH14116	This paper
pCH14117	This paper
pCH14118	This paper

pCH14119	This paper
pCH14120	This paper
pCH14121	This paper
pCH14202	This paper
pCH14203	This paper
pCH14204	This paper
pCH14205	This paper
pCH14206	This paper
pCH14213	This paper
pCH14214	This paper
pCH14215	This paper
pCH14216	This paper
pCH14217	This paper
pCH14218	This paper
pCH14219	This paper
pCH14220	This paper
pCH14221	This paper
pZR108	This paper
pZR113	(70)
pZR420	This paper
pZR432	This paper
pZR433	This paper
pZR434	This paper
pZR435	This paper
pZR437	This paper
pZR439	This paper
pZR441	This paper
pZR442	This paper
pZR444	This paper
pZR462	This paper
pZR463	This paper

Table 3. Oligonucleotides used in this study.

Primer	**Name**	**Sequences**
CH403	T7-BglII	5´ - AAA AGA TCT TAA TAC GAC TCA CTA TAG GAA TTG TGA GCG GAT AAC
CH2770	minE-Nco-for	5´ - TTT CCA TGG CAT TAC TCG ATT TCT TTC TCT C
CH2771	minE-Bam-rev	5´ - TTT GGA TCC GGC TA TTT CAG CTC TTC TG
CH4239	STEC-Kpn-for	5´' - CAG CGG TAC CCT CTC CG
CH4240	STEC-L899-Xho-rev	5´ - TTT CTC GAG CAG AGT GAT GTT CTG CCC C

CH4241	STEC-R1000-Xho-for	5´ - AAA CTC GAG AGA GAC ATC AGC AAT AGT GGG C
CH4243	STEC-E1399-Xho-rev	5´ - TTT CTC GAG CTC AAC CGG AAT GTA TGA TTT TGT C
CH4244	STEC-G1500-Xho-for	5´ - AAA CTC GAG GGT TCA CAA CTG AAT AAT CAG TCC TTC
CH4245	STEC-A1853-Nco/Xho-rev	5´ - TTT CTC GAG CCA TGG CTG CCA GGT GAA CAT TCT GAC
CH4247	STEC-V2323-Afl/Not-rev	5´ - TTT GCG GCC GCC TTA AGG ACC GCA TTA TTG ATG GCA CTG
CH4282	STEC-Afl/Sph-for	5´ - TTT GCA TGC TTA AGG CCG GTG GTA ACA C
CH4283	STEC-S2917-Nhe/Xho-rev	5´ - TTT CTC GAG GCT AGC GCT GCT GTT TCC GG
CH4371	STEC(3)-Nhe/Afl-for	5´ - AAA GCT AGC CTT AAG GCC GGT GGT AAC AC
CH4372	STEC(3)-T2780-Sac-rev	5´ - TTT GAG CTC CGT ATC ACG CAG TTT CGC AAG
CH4373	STEC(3)-L2881-Sac-for	5´ - AAA GAG CTC CTG TAT CCG GGC GTG AAA C
CH4374	STEC(3)-Xho-rev	5´ - TTT CTC GAG TGG CCG GAA TCT
CH4381	STEC(3)-Y1657-Xho-rev	5´ - TTT CTC GAG ATA GTT CCC CTC CAC GAT GC
CH4382	STEC(3)-G1708-Xho-for	5´ - AAA CTC GAG GGG CAG GCA CCA CG
CH4383	STEC(3)-P1707-Xho-rev	5´ - TTT CTC GAG GGG GTG CAT CCT GAG C
CH4384	STEC(3)-Y1758-Xho-for	5´ - AAA CTC GAG TAT ATG CTG AAC CAG ATC GGG G
CH4412	STEC(3)-N2934A-for	5´ - AGA GCG GGA AGA ATG CTG TTG ATA ATG CCT ACC TGA GCG TG
CH4413	STEC(3)-A2918-Nhe-for	5´ - AGC GCT AGC GCA GCA GTG GGC GCA CAG AGC GGG AAG AAT GC
ZR256	tsx-Not-for	5´ - TTT GCG GCC GCG AAT TCG GGA TTT TCA AAC AGT GGC ATA C
ZR257	tsx-Xho-rev	5´ - TTT CTC GAG TCT AGA AAA TCC CGG CAT TTT CAT AAT CAG
ZR260	J2M139 CDI-Not-for	5´ - TTT GCG GCC GCA ATG TCT GGT TGT GGC AGG
ZR261	J2M139 CDI-Xho-rev	5´ - TTT CTC GAG TGG CCG GAA TCT TTA CTC AG
ZR267	cdiA(S504C) (STEC)-Kpn-rev	5´ - GAG GGT ACC GCA GTT GTT TAT CTG CGT GGC AC

ZR268	STEC-A498-Kpn-for	5´ - GCC ACG CAG ATA AAC AAC AGC
ZR269	STEC-cdiA(E512)-rev	5´ - GTT CCT TTG CCC CGG AG
ZR271	cdiA(S1550C) (STEC)-Sac-rev	5´ - CCG GAG CTC CAC AGA GAG TAA AGG TAA CGC GAT CAT C
ZR274	STEC-D1692-Sal-rev	5´ - GCT GTC GAC CTT TCC GAG ACC ATC CAG
ZR275	STEC-S1693C-Sal-for	5´ - AAG GTC GAC TGT AGT CTG TTT GCC GGA CTG TAT GAC
ZR277	STEC-G1726C-Xba-rev	5´ - CCG GTC TAG AAA ATA CGA TGA ACA CGG GAA TTG TTT TTC ATC AGT ATA CG
ZR281	STEC-L1731-Xba-for	5´ - TTT TCT AGA CCG GCT CGG GCT GAA AC
ZR280	STEC-cdiA(A1807C)-Sex-for	5´ - CAG ACC AGG TGG CGT GTC TTG ACC AAA GTA TTC TGT GGT ATA AAG
ZR285	STEC-cdiA(D1959)-rev	5´ - GTC CAG ACT ATC CAT GGC AC
ZR286	cdiA(D1959C) (STEC)-Nco-for	5´ - GTG CCA TGG ATA GTC TGT GCA TCC GGG CAG ATA AAA ACA TTT CG
ZR287	STEC-R1961-Not-rev	5´ - TTT GCG GCC GCG GAT GTC CAG ACT ATC CAT GG
ZR288	STEC-T2502C-Eco-rev	5´ - ACC AGA ATT CAG GGT GAC ACA TTT ACC GCT GTC TGT TGT GG
ZR290	STEC-N2506-Eco-for	5´ - ACC CTG AAT TCT GGT CGG GAT ACG GTA CTG
ZR293	STEC-G2648-Spe-for	5´ - TTT ACT AGT GGC AGC TTC GGG GAT AAA TTT C
ZR294	cdiA(S3217C) (STEC)-Mfe-for	5´ - CGG CAA TTG GTT ATT GCA ATG CAA TAA AAA ATG GAT TAC AGG C
ZR295	malE-Not-for	5´ - TTT GCG GCC GCC AAC AAG GAC CAT AGA TTA TG
ZR296	malE-dSS-Not-for	5´ - TTT GCG GCC GCA AGG ACC ATA GAT TAT GAA AAT CGA AGA AGG TAA ACT GG
ZR297	malE-CysHis6-Xho-rev	5´ - TTT CTC GAG CTA GTG ATG GTG ATG GTG ATG AGA TCC ACC ACA CTT GGT GAT ACG AGT CTG
ZR347	cdiA(A1954) (STEC)-Not-for	5´ - TTT GCG GCC GCC ATG GAT AGT CTG GAC ATC C

ZR348	cdiA(S2731C) (STEC)-Bam-rev	5´ - TTT GGA TCC TAT GTC GCA GAT AAG CCC CAC TGT CTG C
349	cdiA(G2734) (STEC)-Bam-for	5´ - TTT GGA TCC CAG GTG GCG GAT ATC GCG

Chapter III. The YP domain requires cognate CdiB to arrest secretion of C-terminal half of CdiA

This work has not been published yet. All data presented in this chapter are mine.

A. Introduction

Contact-dependent growth inhibition (CDI) is a competitive system widely found in proteobacteria (73,74). Cells carrying the CDI operon *cdiBAI* inhibits growth of their neighbors by delivering toxin effectors in a contact dependent manner (70). CDI activity is carried out by CdiB/CdiA two-partner secretion system (TPS) in which CdiB forms an outer membrane β-barrel transporter to secret CdiA effector protein carrying the C-terminal toxin domain (CdiA-CT) (70). Like many TPS cargo proteins, CdiA is a large (>350kD) filamentous protein extending 33nm from the surface of the CDI+ inhibitor cell (165),(100).

TPS secretion is used to export diverse filamentous effectors by many pathogenic Gram-negative bacteria (67,94). The fate and orientation of the TPS cargo (TpsA) varies greatly. A well-characterized filamentous hemagglutinin FhaB from *Bordetella pertussis* exports the N-terminal half which forms a β-helical filament as residues are exported and stacked from NT to CT fashion (68). Subsequent peptidase cleavage of the C-terminal half of FhaB (prodomain) results in mature FhaB which then gets released (68). However, HMW1 adhesin, a TpsA cargo from *Haemophilus influenzae* has a C-terminal peptide loop which prevents release from its transporter partner, HMW1B (69). Resulting adhesin filament is cell bound while its N-terminal tip is facing away from the cell surface (69).

Recent study of the CdiA topology has revealed a unique mode of CdiA secretion and mechanism (165). The N-terminal half of CdiA is exported by CdiB to form the filament, but

the secretion is stopped to retain the C-terminal half of CdiA, including the toxic CdiA-CT, in the periplasm (165). Unlike FhaB, secretion of the periplasmic half resumes when the receptor-binding domain of CdiA at the tip of the filament binds to a receptor on target cell surface (165)(71)(105)(104). Then the exported periplasmic CdiA is inserted into the target outer membrane to deliver CdiA-CT which inhibits the growth (165)(71). The region of CdiA between the extracellular N-terminal half and periplasmic C-terminal half is enriched with tyrosines and prolines, and named YP domain (165). This YP domain is crucial for secretion arrest. Deletions of the domain abolished secretion arrest causing the CdiA filament to prematurely export the periplasmic half and fall off the cell surface (165). This fully secreted CdiA filament fails to deliver CdiA-CT reliably unless an immobile target cell is already in close contact (165). Therefore, secretion arrest of CdiA is required for stable presentation of the CdiA filament and efficient delivery of CdiA-CT when cell-cell contact is transient. But the mechanisms by which the YP domain executes secretion arrest and how receptor-binding releases this mechanism remain unknown.

In this chapter, I have further evaluated the YP domain by making a series of deletions and sequence replacements. The YP domain is a well-conserved 185-resdues stretch located where CdiA makes a topological shift from outside to periplasm. YP residues 75-100 appeared most crucial for secretion arrest as deletion and sequence replacement of this region disrupted stable anchoring of the CdiA filament on surface. Yet the YP domain as a whole robustly arrests secretion of CdiA because some periplasmic residues can be pulled out without compromising secretion arrest. The YP domain also tolerated considerable permutations of the region. Furthermore, I report that the YP domain alone is insufficient to arrest secretion of a TpsA protein, rather it requires a cognate CdiB transporter. Execution of

secretion arrest is previously unknown feature of the TpsB transporters. Based on these findings, I propose that the secretion arrest and receptor-dependent restart is a widely conserved feature of other TPS systems.

B. Results

Conserved features of the secretion arrest domain

The YP domain is named due to its enrichment in tyrosines and prolines (165). This stretch of 185 residues was defined as the secretion arrest domain important for displaying the CdiA filament stable on cell surface (165). The YP domain is conserved among CdiA molecules and other TPS cargo proteins (Chapter II Figure S2)(165). The YP domain is also found in non-CdiA TpsA proteins as well. BLAST against protein database using the YP domain returns TPS proteins from diverse Gram-negative bacteria, including well-studied FhaB from *Bordetella pertussis* (Figure S1). This suggests that secretion arrest may not be a unique feature in CdiA alone.

Secondary structure prediction by Phyre 2.0 predicts several α-helices in the YP domain (Figure 1A). This is interesting because most of the CdiA protein is composed of predicted β-strands including the β-helical FHA1 domain which makes up most of the 33nm filament and the FHA2 domain which is predicted to form a translocon in the target cell's outer membrane. C-terminal toxin domain has many α-helical features but otherwise the CdiA is devoid of α-helices except for the YP domain. To explore the importance of these structural features, I analyzed another *E. coli* CdiA from STEC4 (not shown) and homolog from *Bordetella pertussis* FhaB using Phyre 2 (Figure 1B). Similar structural features were

conserved in the homologs suggesting they could be playing an important role in secretion arrest (Figure 1).

The YP-C is required for secretion arrest

In the CdiA deletion analysis study (Chapter II)(165), I have shown that deletion of the YP domain (ΔYP100) fails to arrest secretion and the entire effector is secreted to the supernatant (Chapter II, Figure 5). Periplasmic YP domain (YP-C) was most crucial for secretion arrest as this smaller 50-residue deletion (ΔYP-C) phenocopies the full 100-residue deletion (Figure 2)(165). Remaining 84 residues C-terminal to YP-C has not been studied yet. These residues were deleted to make ΔYP84 (ΔY1758-N1841) mutant (Figure 2A). Secretion arrest remained robust despite the deletion and ΔYP84 was stably cell bound (Figure 2B). When ΔYP84 was combined with ΔYP-C to make a larger 134-residue deletion, ΔYP-C/84 (ΔG1708-N1841), the secretion arrest was disrupted, and the mutant filament was released into the supernatant (Figure 2B). The level of ΔYP-C/84 filament in supernatant was comparable to ΔYP-C (Figure 2B). Any deletions which include removal of the YP-C domains (ΔYP100, ΔYP-C, and ΔYP-C/84) had defects in CdiA surface presentation suggesting YP-C is the most critical portion of the YP domain for secretion arrest.

In competition co-culture, ΔYP84 and ΔYP-C84 showed severe defects to inhibit *tsx+* target cells (Figure 2C, liquid). Secreted ΔYP100 and ΔYP-C mutants can still deliver CdiA-CT to adjacent targets when cells are mix on solid media (Figure 2C). However, ΔYP84 and ΔYP-C/84 both had reduced activity even on solid media (Figure 2C). Although ΔYP84 does not abrogate secretion arrest, YP84 may play a role in downstream process of toxin delivery.

Sequence of the YP domain is crucial for secretion arrest

To investigate the importance of the primary sequence of the YP-C domain, the 50 residues of the YP-C (G1708-N1757) were replaced with a random coil sequence from a small acid-soluble spore protein, SspC from *Bacillus subtilis* (residues A2-V52). SspC is a DNA-binding protein known to be intrinsically unstructured in its unbound state (166,167). In the periplasm, SspC should serve as an unstructured polypeptide chain to replace the YP domain while keeping the overall protein length constant. To further pinpoint the secretion arrest mechanism, YP-C was divided into 25-residue halves (YP-C 1st; G1708-D1732 and YP-C 2nd; R1733-N1757) and each halves were replaced with 25-residues of SspC (residues A2-Q26).

The 50-residue replacement of YP-C (YP-C/sspC) and the latter 25 residue replacement (YP-C 2nd/sspC(25)) failed to stably cell bound and were lost to the supernatant (Figure 3A). Protein level of YP-C/sspC in supernatant was comparable to the deletion mutant of the same region (ΔYP-C) (Figure 2A). Loss of YP-C 2nd/sspC(25) to supernatant was not as severe (Figure 2A). YP-C 1st/sspC(25) had no notable defects in secretion arrest (Figure 2A).

In competition co-culture, YP-C/sspC and YP-C 2nd/sspC(25) showed almost no inhibitory activity against *tsx+* target cells (Figure 3B). In contrast, YP-C 1st/sspC(25) successfully inhibited target growth (Figure 3C). CdiA immunoblot after target cell mixing confirmed that the first 25 residue replacement retained wild-type level of activity (Figure 3C). Maleimide-labeling of periplasmic 1726Cys reports receptor-dependent export of C-terminal half. And CdiA cleavage showed adequate CdiA-CT delivery (Figure 3C).

However, very little effector is detected in YP-C/sspC as this filament is lost to the supernatant (Figure 3C). More of these mutants are lost in cell mixing experiments because the effectors are binding to the target cells and the cells are washed more vigorously during maleimide-dye labeling. The latter replacement, YP-C 2nd/sspC(25) has enough effectors cell bound during target cell mixing and successfully export its C-terminal half upon receptor-binding (Figure 3C). However, the aberrant CdiA processing receptor-binding suggests that subsequent assembly into target outer membrane is defective. This cleavage is most likely to be OmpT-dependent based on previous findings (165).

These data suggest that the sequence of YP domain is important and previous identified defects in secretion arrest is not simply due to shortening of an extended region. The latter half of the YP-C domain (R1733-N1757) seems most important for the secretion arrest mechanism.

V1837G mutant enhances disruptions in the YP-C domain

While cloning the YP-C 2nd/sspC(25) replacement, I made two clones with the correct sequence replacement but drastically different stability on cell surface (Figure 4A). One clone picked up a spontaneous point mutation, V1837G, which greatly compounded defective secretion arrest (Figure 4A). When V1837G was combined with other sequence replacements, the point mutation greatly enhanced the mutant phenotype. V1837G greatly deteriorated the defective secretion arrest in YP-C/sspC50 and YP-C 2nd/sspC25, indicated by increased level of secretion to supernatant and loss of the major processed band (Figure 4B). V1837G alone does not cause any defect in secretion arrest, and V1837G had no effect on YP-C 1st/sspC25 (Figure 4B). This additive effect was specific to Val to Gly mutation.

When Val1837 was mutated to a Cys, supernatant levels of the mutants were comparable to the wild-type Val1837 clones (Figure 4C).

The sequence replacement experiment showed that residues R1733-N1757 are most crucial to retain CdiA stably cell-bound. However, V1837G is a mutation in downstream YP84 which can be completely removed without a significant defect in secretion arrest (Figure 2B). It is interesting that a point mutation in YP84 can profoundly impact the secretion arrest mechanism when combined with the sequence replacement of R1733-N1757.

Secretion arrest is robust

Residue 1726 is periplasmic, and I have often used Cys1726 mutation to visualize the export of periplasmic CdiA using maleimide-dye. To probe the robustness of secretion arrest, I combined Cys1726 with the deletions at around the residue: ΔYP-N (ΔP1658-P1707), ΔRBD/YP-N (ΔQ1385-P1707), and ΔYP84 (ΔY1758-N1841) (Figure 5A). YP-C is undisrupted and secretion arrest is intact in these mutants. Surprisingly, Cys1726 in all three deletions were dye-labelled without outer membrane permeabilization (Figure 5C). The first two mutants, ΔYP-N and ΔRBD/YP-N, have shortened extensions upstream of the Cys1726 so the periplasmic residue could have been pulled out as a result. ΔYP84 is a C-terminal deletion downstream of Cys1726 but the deletion still caused the periplasmic residue 1726 to spill out, possibly due to a disruption in the local secondary structure. So, the core mechanism of secretion arrest by YP-C domain seems robust and can tolerate spilling out of a few periplasmic residues.

Next, I set out to remove the predicted α-helices in the YP-C to pin down a secondary structure responsible for secretion arrest (Figure 1A). There are a few stretches of predicted

α-helices in the YP-C but since residue 1726 can be yanked out while secretion arrest is intact, I focused on the last predicted α-helix (A1748-I1763) and made a deletion of this stretch (ΔA1748-I1763) (Figure 1A). This structural prediction is also conserved in corresponding region of FhaB (N2400-L2415) (Figure 1B). There is also a predicted β-strand just upstream of this α-helix (Figure 1A). I made another deletion, ΔD1741-I1763, remove both predicted β-strand and α-helix.

Surprisingly, both deletions of predicted secondary structures did not disrupt secretion arrest. CdiA immunoblot showed the effectors are stably cell-bound (Figure 6A). However, they were defective in growth inhibition of targets (Figure 6B). When *tsx*+ cells are mixed in, both ΔA1748-I1763 and ΔD1741-I1763 mutants had minimal CdiA-CT delivery comparable to ΔYP84 because all three mutants stayed mostly full-length (Figure 6C). The normally periplasmic Cys1726 was extracellular in these mutants, further supporting the data that disruption of the YP domain C-terminal to 1726 can cause the residue to spill out.

The defect in CdiA-CT is likely due to failure to assemble into target outer membrane. Such phenotype results in aberrant cleavage like in YP-C 2nd/sspC(25) (Figure 3C). However these deletion mutants were expressed in Δ*ompT* cells. To figure out the exact defect of these structural deletions, I combined the deletions with Cys1959 and Cys2731, and monitored receptor-dependent export and target cell insertion. Position 1959 is periplasmic and exports upon receptor-binding (165). Position 2731 assembles inside the outer membrane of target cells after receptor-dependent export (165). After co-incubating with *tsx*+ target cells, periplasmic Cys1959 exported as expected (Figure 6C). However, the Cys2731 residues were dye-labelled in the mutants suggesting insertion into target outer-membrane is

impaired and the FHA2 domain lingers in the extracellular space (Figure 7D). In *ompT*+ cells, this will result in similar cleavage patterns seen in Figure 3C.

So far, the YP-C domain, specifically the second half of it (R1733-N1757) seems to play the most important role in secretion arrest. Other deletions including deletions of the predicted structures in YP-C successfully displayed the CdiA effectors on cell surface. Disruptions of the local secondary structure can compromise some periplasmic residues, but secretion arrest is intact as long as the YP-C domain remains.

The YP domain requires cognate CdiB for secretion arrest

It is tempting to speculate that the YP domain interacts with CdiB in order to arrest the secretion of C-terminal half of CdiA. YP-C which is critical for secretion arrest is likely to be in close proximity with CdiB, specifically with the periplasmic POTRA domain which initiates CdiA export.

CdiB can be tricked into secreting a non-canonical cargo by fusing the TPS domain from CdiA to the cargo protein. I replaced the signal sequence of hemolysin, HpmA with the signal sequence and the TPS domain from $CdiA_{STEC3}$. When co-expressed with CdiB, the fusion hemolysin gets exported and lyses the blood cells on sheep blood agar plate (Figure 7A, second row first column). This is a useful plate-based assay to report full secretion of the TpsA cargo across the outer membrane. Exported HpmA is free to diffuse away and can be Coomassie stained from the supernatant fraction (Figure 7B, second row first column). In these *E. coli* cells, HpmA is the largest protein (>160kD) and no immunoblot is required.

Then I fused YP domains from $CdiA^{STEC3}$, *Bordetella pertussis* FhaB, and *E. coli* $CdiA^{STEC4}$ at the end of the HpmA sequence (Figure S1). The YP domain is determined by the 185 residues following the RBD of $CdiA^{STEC3}$. This sequence was aligned with

Bordetella pertussis FhaB, and *E. coli* CdiA^{STEC4} to get 185 residues of their equivalent YP domain (Figure S1). I also added a C-terminal FLAG tag to visualize full construct expression using anti-FLAG immunoblot. The four fusion *hpmA* constructs (including HpmA without a YP domain) were combined with four transporters-TPS pairs: HpmB (native TpsB transporter for HpmA), *E. coli* CdiB^{STEC3}, *Bordetella pertussis* FhaC, and *E. coli* CdiB^{STEC4}.

Coomassie blots of the cell and supernatant fractions showed that the HpmA-YP domain fusions remain cell bound only when they are exported via cognate transporter (Figure 7B). Presumably, the YP domain interacts with the cognate transporter to arrest the HpmA anchored on cell surface while the N-terminus of hemolysin is facing away from the cell surface. Since secretion arrest of hemolysin prevents free diffusion away from cell, the clearing around the colonies expressing cognate transporter-YP domain pair were visibly smaller (Figure 7A).

Anti-FLAG immunoblot generally agrees with the Coomassie blots but the FLAG-tag C-terminal to FhaB YP domain was unstable and cleaved (not shown). The 185 residues of the FhaB sequence I grabbed based on alignment may not be a structurally stable domain. Some C-terminal residues have been nibbled but the Coomassie stain showed that most of the FhaB YP domain is intact judging by the express of a fusion protein larger than HpmA without any YP domain (not shown).

C. Discussion

Secretion arrest is crucial for timely toxin delivery of CdiA (165). Premature release of the secretion arrest wastes the CdiA filament to the supernatant and the released effector quickly deems ineffective unless a receptor+ target cell happens to be nearby (165). The

conserved YP domain is responsible for the secretion arrest. This 185-residue stretch is thought to extend from the RBD at the distal tip of the CdiA filament to the periplasm traveling through the lumen of CdiB (165). Given its cellular localization and proximity to CdiB, the YP domain is the prime candidate to hold the mechanism of secretion arrest. Deletion of the YP-C disrupted secretion arrest (165). Here, I have shown that the 25-residue of the YP-C identified as YP-C-2nd (R1733-N1757) is most important for secretion arrest as sequence replacement of this region was the smallest perturbance sufficient to disrupt the secretion arrest (Figure 3). Sequence replacement of the YP-C releases the effector to the supernatant. This suggests that the failed secretion arrest in the deletions are not simply due to shorting of the extended region and further confirms that the YP-C carries the mechanism to arrest CdiA export.

The mechanism of secretion arrest seems robust than initially expected. When the extended region is shortened in ΔRBD and ΔRBD/YP-N, the periplasmic residue 1726Cys is extracellular while the C-terminal half CdiA still remains in the periplasm. Residue 1726 is within the YP-C domain. It is surprising that part of this domain can be yanked out by deletions N-terminal of this position, yet secretion arrest remains intact (Figure 5B). Interestingly 1726Cys is also extracellular when combined with ΔYP84, a deletion C-terminal to the YP-C (Figure 5B). In this construct, the overall structure of the YP domain could be disrupted causing some periplasmic residues to spill out prematurely. Overall, data suggest that the YP domain can take significant disturbance around the YP-C domain to maintain secretion arrest.

Secretion arrest also tolerated deletions of predicted secondary structures in the YP-C. Since 1726Cys can be extracellular without compromising secretion arrest, the most

interesting structural feature remaining was the β-strand followed by an α-helix in D1741-I1763. This feature is also predicted in FhaB (Figure 1B). When this region is removed, C-terminal CdiA had insufficient assembly into the outer-membrane of target cells yet secretion arrest and restart were undisturbed. Secretion arrest by the YP-domain is a robust phenotype that can tolerate deletions around the YP-C and some smaller deletions in the YP-C.

It appears that the overall structure of the YP-C is important for the secretion arrest. The fact that V1837G has an additive effect with the sequence replacement mutants suggest that the entire YP domain contributes to the mechanism (Figure 4). It is possible that the structural deletions in the YP-C was not enough to disrupt this overall YP domain structure. Alternatively, there could be redundant mechanisms for secretion arrest in the YP-C and YP84. Regardless, the 25-residue stretch of YP-C 2nd seems to play the most important role in secretion arrest specific folding. Disruption of secretion arrest correlates with the severity of interruptions to the YP-C. Larger deletions or sequence replacements caused more CdiA to the supernatant. Deletions caused more CdiA release than sequence replacements.

Whatever structure the YP-C folds into, it is insufficient to arrest secretion alone. The YP domains from *E. coli* CdiA^{STEC3}, CdiA^{STEC4}, and *Bordetella pertussis* FhaB all failed to limit full export of HpmA when secreted through non-cognate transporters (Figure 7). This suggests that CdiA secretion arrest is fundamentally different from that of the HMW1 adhesin (69). In HMW1, C-terminal cysteine pair induced peptide loop to anchor the adhesion on cell surface (69). CdiA YP lacks any cysteines and unlike HMW1, YP alone is insufficient to arrest secretion. However, when cognate transporter and the YP domain were paired, together they arrested the export of otherwise fully secreted HpmA and anchored it onto the cell surface (Figure 7). TpsB transporters recognize the cognate cargo using the

periplasmic POTRA domain. Similarly, the YP domain could be interacting with the POTRA domain of the CdiB to stop the export of the C-terminal CdiA. Structural analysis of a well-studied TpsB transporter, FhaC, suggests a N-terminal α-helix of POTRA domain could plug the lumen of CdiB before TPS binding (89). The predicted α-helix of the YP-C was an attractive alternative to this plug model, but deletion of the predicted α-helix did not have any effect on secretion arrest. Instead, the YP domain could be interacting with the POTRA domain to indirectly "turn off" the CdiB transporter by an unknown pathway.

I have tried to make POTRA and β-barrel swaps within CdiB to narrow down possible sites of YP-interaction. Unfortunately, POTRA/β-barrel swaps between $CdiB^{STEC3}$ and FhaC were not functional for CdiA export and these chimeric transporters could not be tested (results not shown). The only reported case of POTRA and β-barrel swap in TPS system was done between two closely related transporters from the same strain of *Neisseria* (168). TpsB proteins require the β-barrel assembly machine channel BamA for membrane insertion (71). Interestingly, cross-species POTRA/β-barrel swaps of BamA are functional (169). However, β-barrel of TpsB transporters could not functionally replace the β-barrel of BamA, possibly because TpsB has evolved to export cargos across the outer membrane while BamA β-barrel specializes in insertion of new β-barrel proteins in the outer membrane (169). It is possible that POTRA/β-barrel swaps of TpsB is not functional because TpsB has higher specificity for its TpsA substrate than BamA with its outer membrane protein substrate.

Although it is yet to be discovered how CdiB interacts with the YP domain to arrest export, my data proposes a novel function of the TPS transporters. It is well-known that POTRA of transporters interacts with TPS domain of the cargo to initiate secretion (92,93).

Here I propose a more sophisticated function of the TPS transporters that cargo secretion can be stalled at the YP domain and resumes after the receptor-binding.

Lastly, my results further support the hypothesis that secretion arrest and restart is a conserved feature among other TPS cargos including FhaB. We proposed that the FhaB resembles the general mechanism of CdiA (165). Here, I present data showing the FhaB domain corresponding to the YP domain can arrest secretion of a TPS cargo when paired with FhaC transporter. The YP-domain is a distinguishable feature conserved in some other TPS homologues. It is likely that the secretion arrest is conserved in these systems.

D. Materials and methods

Bacterial growth conditions.

Bacterial strains were derivatives of E. coli K-12 strains MG1655. Bacteria were cultured in lysogeny broth (LB) or on LB agar at 37 °C. Unless indicated otherwise, media were supplemented with antibiotics at the following concentrations: 150 μg/mL ampicillin (Amp), 50 μg/mL kanamycin (Kan), 25 μg/mL tetracycline (Tet), and 200 μg/mL spectinomycin (Spc).

Plasmid construction

In-frame deletions of C-terminal YP domain were generated by PCR using pZR435 (165) as template to include G1726C mutation. The fragments from primer pairs CH4816/CH4231 and CH4244/CH4817 were cloned sequentially into pDUET using NcoI/BamHI-HF and BamHI-HF/SacI, respectively. The SacI/NcoI fragment was then subcloned to pCH14563 to generate pCH2828 (ΔYP84: ΔY1758-N1841). The fragments

from primer pairs CH4816/CH4231 and CH4244/CH4818 were cloned sequentially into pDUET using NcoI/BamHI-HF and BamHI-HF/SacI, respectively. The SacI/NcoI fragment was then subcloned to pCH14563 to generate pCH2829 (ΔYP-C/84: ΔG1708-N1841).

Sequence encoding *Bacillus subtilis* SspC was amplified from pCH10 (pSspC-Ala) while fragments from cdiA was amplified from pCH14563. A set of primers were designed with 20 bp long overlapping regions to allow Gibson assembly. PCR products amplified with CH5029/5030, CH4978/5025, and CH5028/4979 were assembled then SacI/NcoI cloned to p4006 generate pCH4917 (YP-C/sspC-50 with 1959Cys). PCR products amplified with CH5029/5033, CH4978/5025, and CH5027/4979 were assembled then SacI/NcoI cloned to p4006 generate pCH4918 (YP-C 1st/sspC-25 with 1959Cys). PCR products amplified with CH5031/5032, CH4978/5026, and CH5028/4979 were assembled then SacI/NcoI cloned to p4006 generate pCH4918 (YP-C 2nd/sspC-25 with 1959Cys). While cloning p4918, I acquired a spontaneous clone which also has V1837G mutation. This clone failed to promote auto-aggregation in receptor+ cloning background (MC1061) which suggested that CdiA presentation on surface was defective.

V1837G and V1837C mutations were made using mega-primers and introduced to plasmid pCH14563. The megaprimers were amplified using primer pairs CH5064/ZR287 and CH5065/ZR287. Second PCR was amplified using CH4244 and the two megaprimers and SacI/NcoI cloned to generate pCH5513 (V1837G) and pCH5537 (V1837C), respectively. These point mutations were combined with YP-C/SspC sequence replacements by repeating the same megaprimer PCR using pCH4917, pCH4918, and pCH4919 as templates then SacI/NcoI cloning to pCH14563.

To combine G1726C with ΔYP-N (ΔP1658-P1707), PCR fragment was amplified using primer pair CH4382/CH4242 using pZR435 (165) as template and XhoI/NcoI cloned to the pBluescript II SK+ vector carrying ZR268/CH4383 fragment which was previously used to generate pCH14030 (ΔYP-N: ΔPro1658-Pro1707) (165). Then the stitched fragment was KpnI/NcoI subcloned to pCH14563 to generate pCH5408 (ΔYP-N, ΔP1658-P1707, with G1726C). PCR was used to generate ΔRBD-YP1 with G1726C. Fragment with primer pair CH4906/4242 was amplified from pZR435 then BamHI/NcoI cloned to pCH2207 (complete ΔRBD with EcoRI/BamHI sites) to finally generate pCH14029. pCH2207 was generated by PCR. The fragments from primer pairs CH4239/CH4752 and CH4753/CH4242 were sequentially cloned to pCH14563 using KpnI/SacI and SacI/NcoI, respectively.

The structural deletions were generated by PCR and introduced to plasmid pCH14563. Fragments were amplified with primer pair CH4950/CH4264 from both WT (pCH14563) and 1726C (pZR435) templates and SacI/NheI cloned to pCH14563. Then fragment from primer pair CH4244/CH4948 was SacI/BamHI cloned to generate pCH4005 (ΔA1748-I1763) and pCH3903 (ΔA1748-I1763 with 1726C). Fragment from primer pair CH4244/CH4949 was SacI/BamHI cloned to generate pCH4008 (ΔD1741-I1763) and pCH3904 (ΔD1741-I1763 with 1726C). Cysteines at 1959 and 2731 were combined with the structural deletions by PCR. Fragments were amplified using CH4816/CH4264 from either pZR439 or pZR442 to grab 1959C and 2731C, respectively, and NcoI/NheI cloned to pCH4005 or pCH4008 to combine both structural deletions with either cysteine mutations.

TpsB and YP pairs were cloned to hpmA chassis using Gibson assembly. PCR fragments were amplified from pCH429 to make a new hpmA chassis removing internal restriction enzyme sites (XbaI, XhoI, and NheI). Fragment with primer pair CH5224/CH5225

was reamplified with CH5224/CH5226 to add a C-terminal FLAG. This extended fragment was assembled with fragments made with CH5218/CH5219, CH5220/CH5221, and CH5222/CH5223. The stitched fragment was EcoRI/HindIII cloned to pTrc99a to generate p CH6885. Transporter to TPS sequences were cloned to this chassis by EcoRI/NheI cloning. YP domain sequences were cloned to this chassis by XhoI/XbaI cloning. HpmB-TPS^{HpmA} was amplified with CH5227/CH5228. FhaC-TPS^{FhaB} was amplified with CH5252/CH5253 from pCH1981. CdiB-TPS^{STEC3} was amplified with CH4307/CH5229 from pCH14563. CdiB-TPS^{STEC4} was amplified with CH5257/CH5258 from pCH1055. YP^{STEC3} was amplified with CH5230/CH5231. YP^{STEC4} was amplified with CH5259/CH5260. YP^{FhaB} was first amplified with CH5254/CH5255 then this fragment was used as a megaprimer and amplified again with CH5256 to remove an internal XhoI site.

Protein analysis in cell and supernatant

E. coli CH14017 cells carrying CDI plasmid were diluted to OD600 ~ 0.05 in LB medium supplemented with Amp and cultured with shaking at 37 °C. Once in mid-log phase, cultures were treated with Spc for 20 min to block protein synthesis. 1ml of culture were harvested by centrifugation (3,000 X g for 5 min) while keeping 900 µL of the supernatant for TCA-precipitation. Collected cell fraction was washed in 1X phosphate buffered saline (PBS) supplemented with 1 mM MgSO4 (PBS-Mg). Cells were collected by centrifugation and pellets were re-suspended in urea-lysis buffer [50% urea, 150 mM NaCl, 20 mM Tris-HCl (pH 8.0)] and subjected a freeze-thaw cycle to extract proteins. 5 µL of each sample analyzed by SDS-PAGE and immunoblotting.

To analyze culture supernatants for released CdiA mutants, retained 900 µL of the supernatant was added to 100 µL of trichloroacetic acid. Proteins were collected by centrifugation at 18,000 X g for 30 min at 4 °C. Precipitates were washed thrice with 1.0 ml of cold acetone. Air-dried pellets were dissolved in 45 µL of urea-lysis buffer, and 5 µL of each sample analyzed by SDS-PAGE and immunoblotting.

Urea-soluble protein samples (5 µL) were analyzed by SDS-PAGE on Tris-tricine 6% polyacrylamide gels run at 100 V (constant) for 1 h to 3.5 h, depends how well resolved the samples need to be. Gels were soaked for 15 min in 25 mM Tris, 192 mM glycine (pH 8.6), 10% methanol, then electroblotted to low-fluorescence PVDF membranes using a semi-dry transfer apparatus at 17 V (constant) for 1 h. Membranes were blocked with 4% non-fat milk in PBS for 1 h at room temperature, and incubated with primary antibodies in 0.1% non-fat milk, PBS overnight at 4 °C. Rabbit polyclonal antisera (Cocalico Biologicals, Stevens, PA) to the N-terminal TPS domain was used at a 1:10,000 dilution. Blots were incubated with 800CW-conjugated goat anti-rabbit IgG (1:40,000 dilution, LICOR) in 0.1% non-fat milk in PBS. Immunoblots were visualized with a LI-COR Odyssey infrared imager.

Maleimide-dye labeling to map surface topology.

E. coli CH14016 or CH14017 cells carrying CdiA^{STECO31} expression plasmids were diluted to OD600 ~ 0.05 in Amp supplemented LB media and grown to mid-log phase at 37 °C. Cultures were then treated with Spc for 20 min to block protein synthesis. Cells were harvested by centrifugation and re-suspended at OD600 ~ 0.3 in 1.0 mL of PBS-Mg to probe intact cells or PBS-Mg with 100 µg/mL polymyxin B to probe permeabilized cells. IRDye680LT-maleimide (LI-COR) was added to a final concentration of 40 µM. Labeling

reactions were incubated in the dark at room temperature for 15 min, then quenched with 6 mM 2-ME. Cells were collected by centrifugation and washed with PBS-Mg supplemented with 6 mM 2-mercaptoethanol (2-ME). Cell pellets were re-suspended in 50 µL of urea-lysis buffer and subjected to one freeze-thaw cycle to extract proteins. Urea-soluble proteins (5 µL) were resolved by SDS-PAGE and analyzed by immunoblotting using anti-TPS domain antisera.

Competition co-cultures.

E. coli CH14016 (for sequence replacements) and CH14017 (for deletions) that harbor CdiA^{STECO31} expression plasmids were used as inhibitor cells in shaking broth co-cultures. *E. coli* CH14016 (for sequence replacements) and CH14017 (for deletions) strains that carry pCH14046 (Δtsx) or pCH14047 (tsx+) were used as target cells. Cells were grown in LB media at 37 °C to mid-log phase, adjusted to OD600 ~ 0.3 and mixed at a 1:1 ratio (5 mL total volume) and incubated with shaking for 3 h at 37 °C. Culture aliquots were taken at the beginning of co-culture and after 3 h to quantify viable inhibitor and target cells as colony forming units per milliliter (CFU mL-1). For solid media growth competitions, *E. coli* CH14017 cells (Δwzb Δtsx ΔompT) that carry pCH14046 (Δtsx) or pCH14047 (tsx+) were used as target bacteria. Inhibitor and target cells were grown in LB media at 37 °C to mid-log phase, adjusted to OD600 ~ 1 in 1X M9 salts, and mixed at a 1:1 ratio (100 µL total volume). Samples of the mixed-cell suspensions (10 µL) were spotted onto LB-agar and incubated at 37 °C. After 3 h, cells were harvested using polyester-tipped applicators and resuspended in 500 µL of 1X M9 salts.

For all competitions, cell suspensions were serially diluted into 1X M9 salts and plated onto LB-agar supplemented with Amp to enumerate inhibitor cells, and LB-agar supplemented with Kan to enumerate target cells. Competitive indices were calculated as the ratio of inhibitor to target cells at 3 h divided by the initial inhibitor to target to cell ratio.

Protein analysis of hpmA clones

E. coli CH14017 cells carrying hpmA plasmids were cultured then cell/supernatant fractions were collected as described above. However, all clones except those carrying the native HpmB had to be induced with 1.5mM IPTG at mid-log for 1hr to maximize protein yield. Urea-soluble protein samples (10 µL) were analyzed by SDS-PAGE on Tris-tricine 6% polyacrylamide gels run at 100 V (constant) for 1 h and Coomassie stained.

Blood agar plate analysis.

E. coli CH14017 cells carrying hpmA plasmids were streaked on LB-agar plate supplemented with Amp. A colony was scooped up and resuspended in 990 µL 1X M9 salts. From this resuspension 1:10 dilution was made in 1X M9 salts down to 10^{-4}. 10 µL of dilutions were spotted on sheep blood agar plate and incubated ON at 37 °C.

E. Figures and tables

Figure 1 (Next page). Conserved features of the secretion arrest domain. Secondary structure prediction by Phyre2.0 **A)** Predicted secondary structure of CdiA^{STEC3} YP domain (185 residues). Important residues are marked. **B)** Secondary structure prediction by Phyre2.0 **A)** Predicted secondary structure of FhaB YP domain (185 residues). Important residues are marked.

A

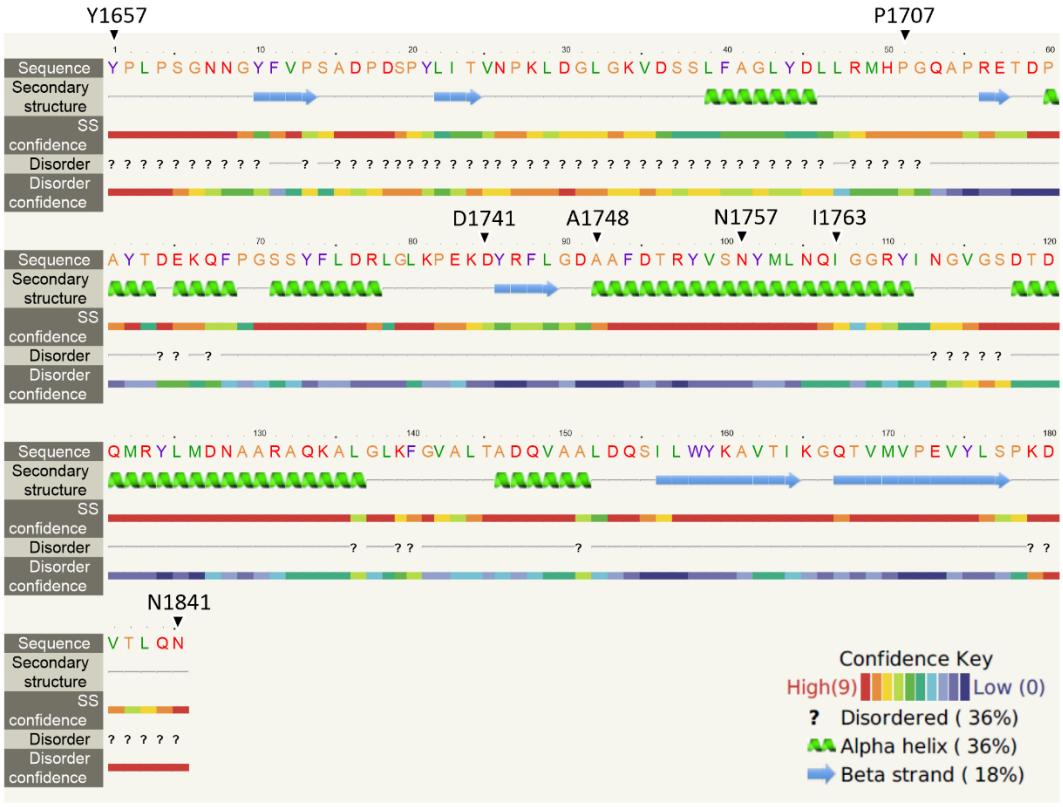
Y1657
P1707
D1741
A1748
N1757
I1763
N1841
Sequence
Secondary structure
SS confidence
Disorder
Disorder confidence
Confidence Key
High(9)
Low (0)
? Disordered (36%)
Alpha helix (36%)
Beta strand (18%)

B

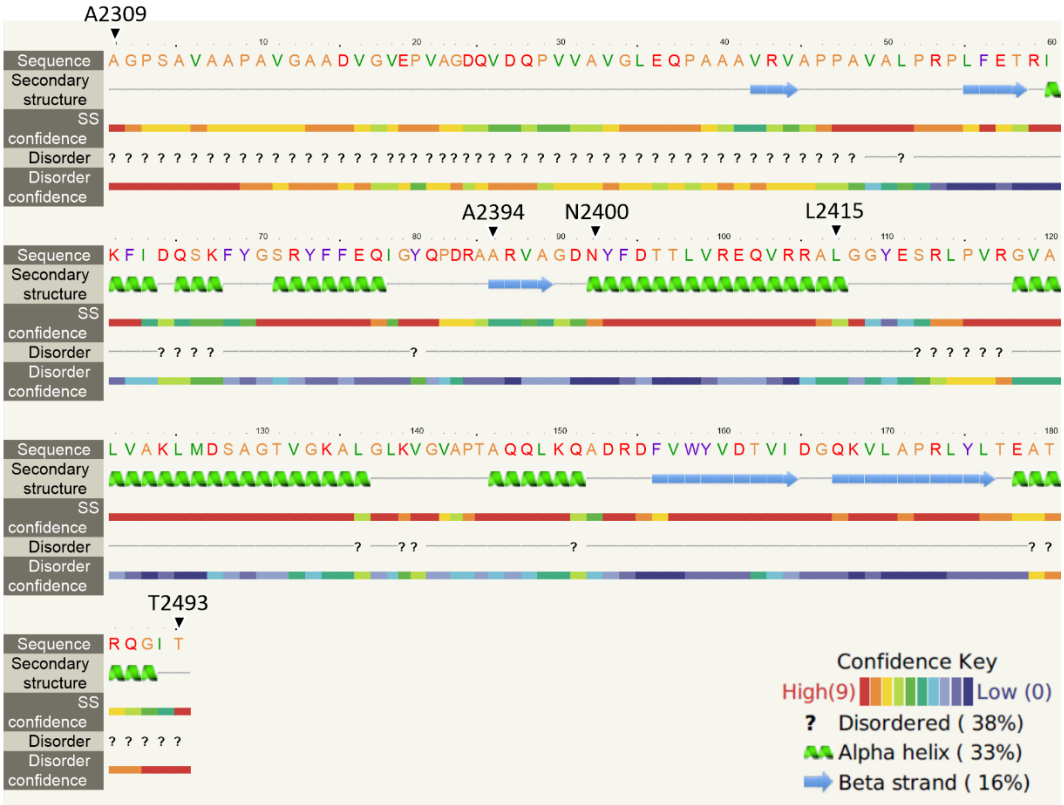
A2309
A2394
N2400
L2415
T2493
Sequence
Secondary structure
SS confidence
Disorder
Disorder confidence
Confidence Key
High(9)
Low (0)
? Disordered (38%)
Alpha helix (33%)
Beta strand (16%)

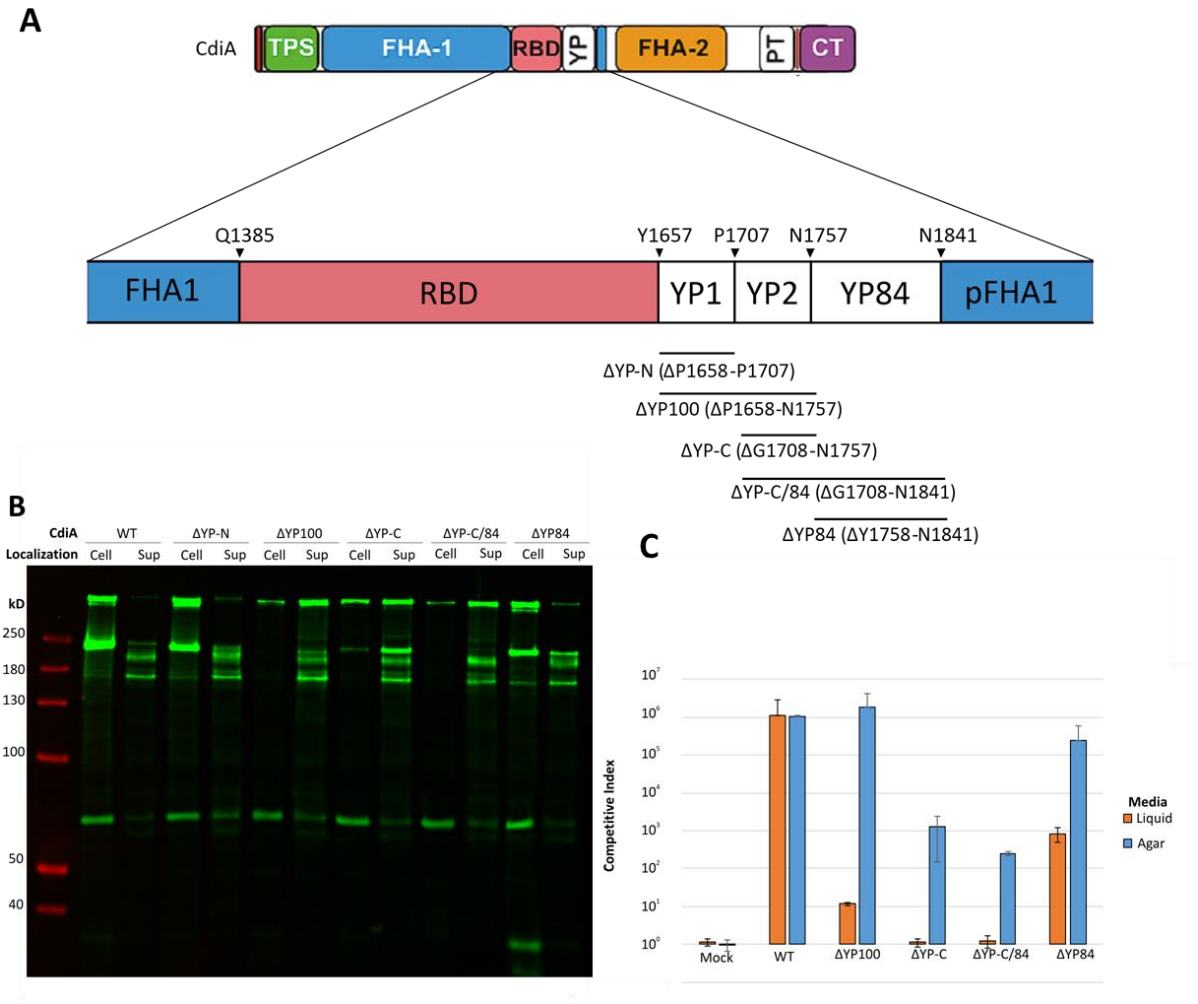

Figure 2. The YP-C is required for secretion arrest. A) CdiA domains (top) and closeup of the transition between extracellular N-terminal half and periplasmic C-terminal half (bottom). In-frame deletions made to narrow down the mechanism of secretion arrest is mapped. **B)** CdiA immunoblot in cell/sup. When deletions remove the YP-C, secretion arrest is disrupted, and effectors is lost to the supernatant. **C)** Competition co-culture both in liquid and on solid agar. Deletion of YP84 affects CdiA-CT delivery rather than secretion arrest.

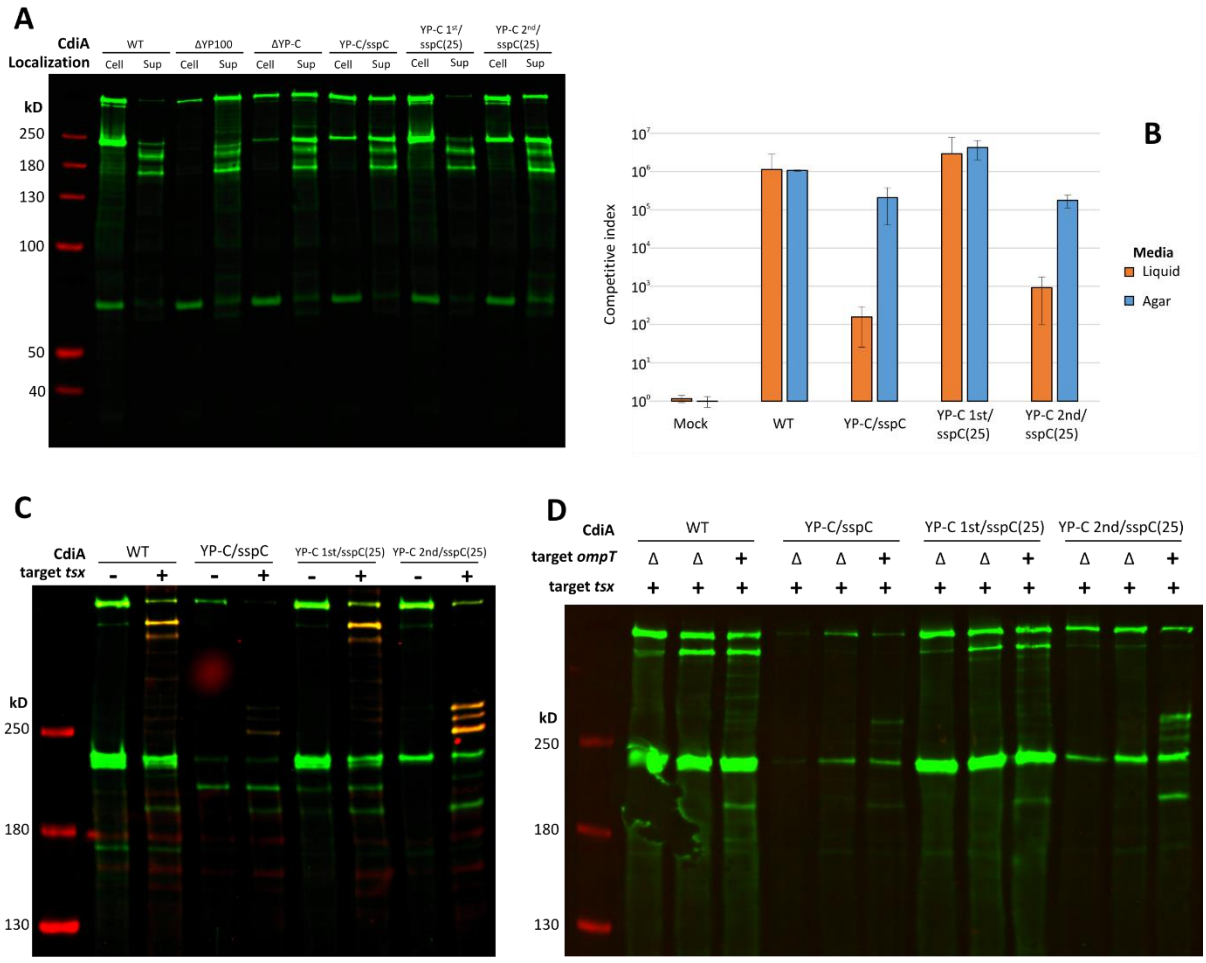

Figure 3. Sequence of the YP domain is crucial for secretion arrest. A) CdiA immunoblot in cell/sup of cells expressing YP-C sequence replacements. Sequence replacement mutant (YP-C/sspC) mimics the deletion mutant (ΔYP-C); both mutants are lost in supernatant. Replacing the latter 25 residues of YP-C [YP-C 2nd/sspC(25)] begins to disrupt secretion arrest. **B)** Competition co-culture in liquid. When YP-C is replaced with SspC, the mutant lost CDI activity. The 2nd half of the YP-C sequence replacement mimics the full 50 residue YP-C sequence replacement. **C)** CdiA immunoblot after target cell mixing. Receptor-dependent export is visualized by maleimide-labeling of 1726Cys.

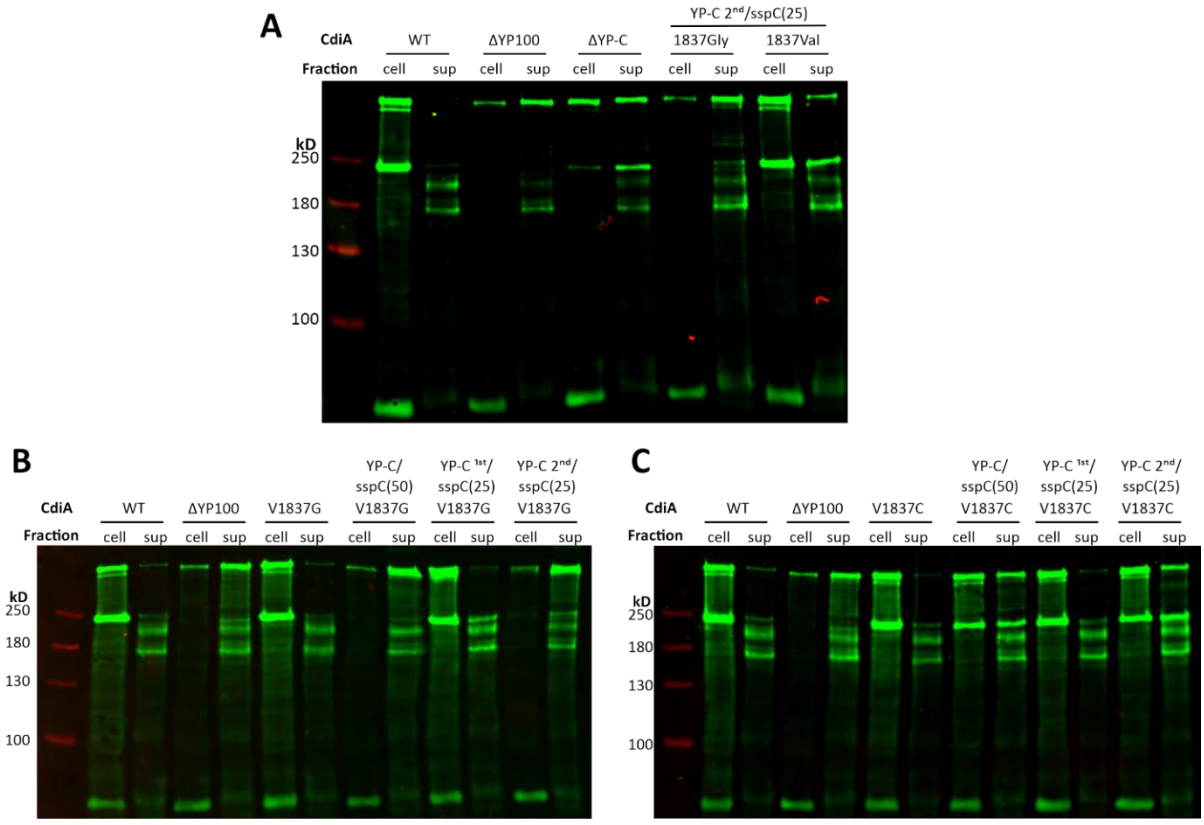

Figure 4. V1837G mutant enhances disruptions in the YP-C domain. CdiA immunoblots in cell/sup of strains expressing YP-C/sspC replacements. WT CdiA and ΔYP100 are used as positive and negative controls for secretion arrest, respectively **A)** Spontaneous mutation in 1837 to Gly enhanced mutant phenotype of YP-C 2nd/sspC(25). **B and C)** Sequence replacement mutants combined with V1837G (B) and V1837C (C).

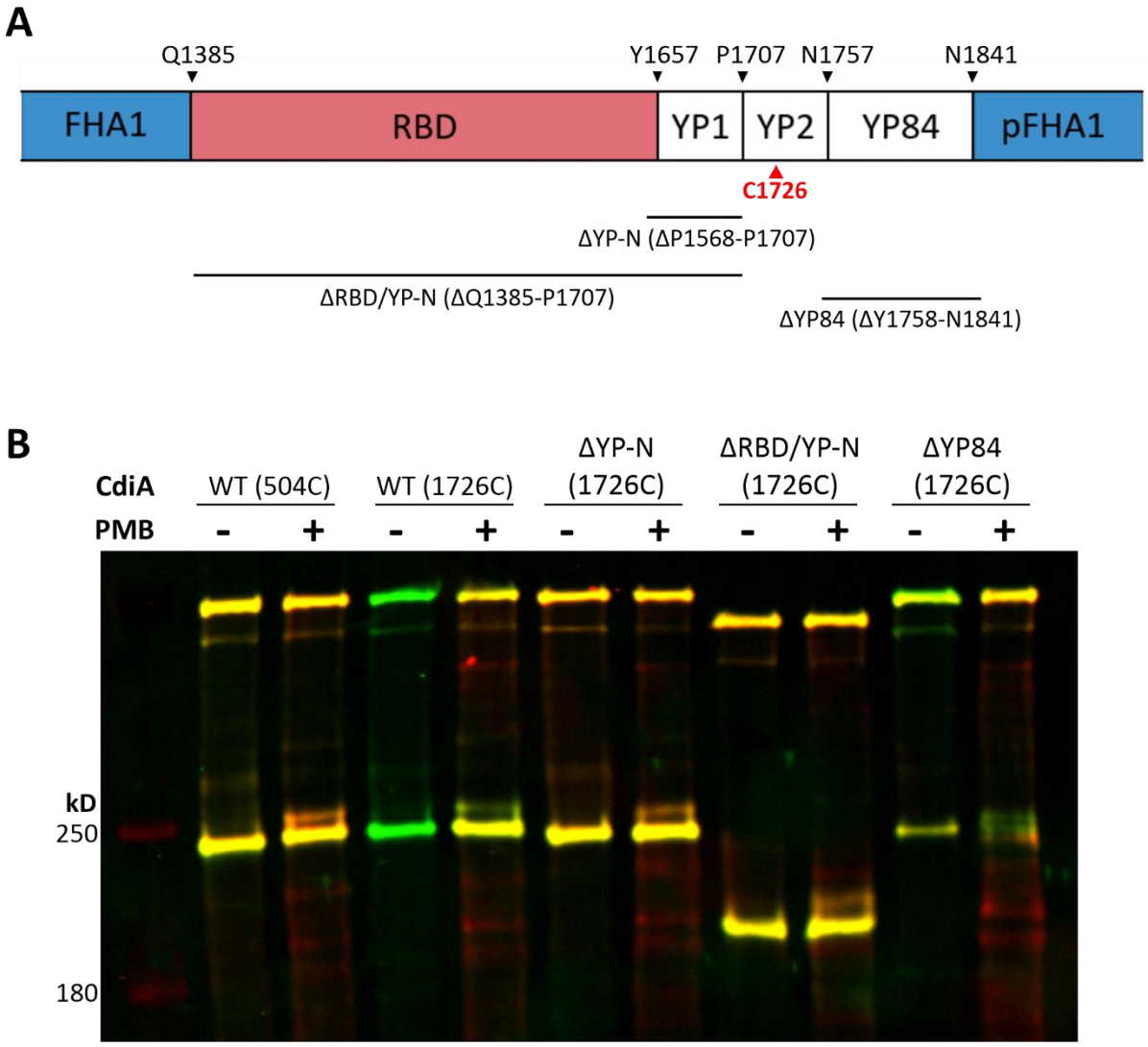

Figure 5. Normally periplasmic residue 1726 are forced out by adjacent deletions. A) Map of in-frame deletions around the periplasmic residue 1726. **B)** CdiA immunoblot after maleimide-dye labeling with or without PMB. Dye labeling probed localization of 1726Cys.

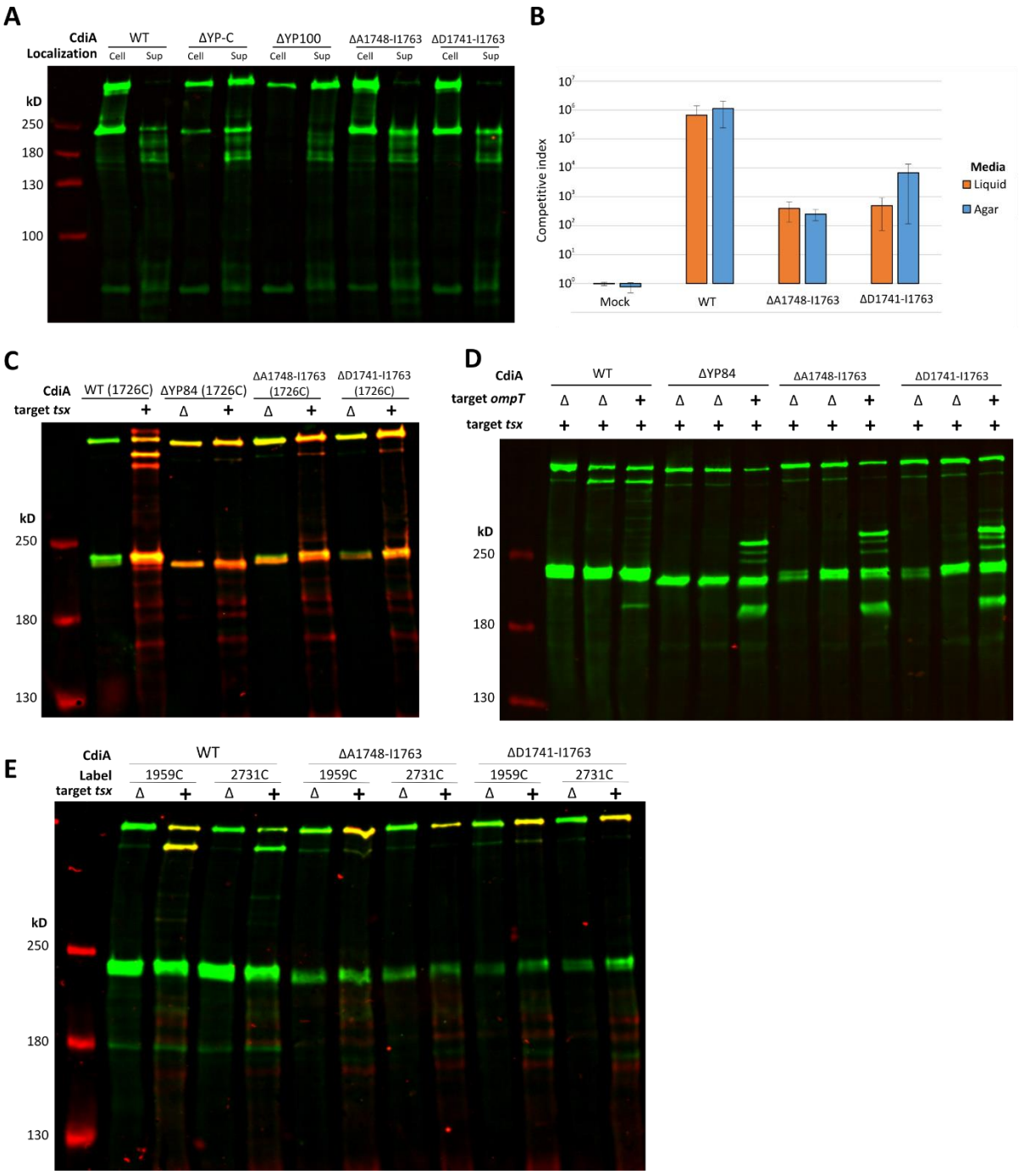

Figure 6. See next page for the legends.

Figure 6. Deletions of predicted secondary structures in YP-C have defects in toxin delivery. A) CdiA immunoblots in cell/sup of strains expressing structural deletions. WT CdiA and ΔYP100 are used as positive and negative controls for secretion arrest, respectively **B)** Competition co-culture in liquid. Mean value of N=3; error bar shows ±SEM. **C)** CdiA immunoblot after target cell mixing. Maleimide-dye labeling of residue 1726C (actual residue number differs in deletions) intended to probe export of the C-terminal half. **D)** CdiA immunoblot after target cell mixing. Maleimide-dye labeling of residue 1956C probes C-terminal export. Maleimide-dye labeling of residue 2731C probes

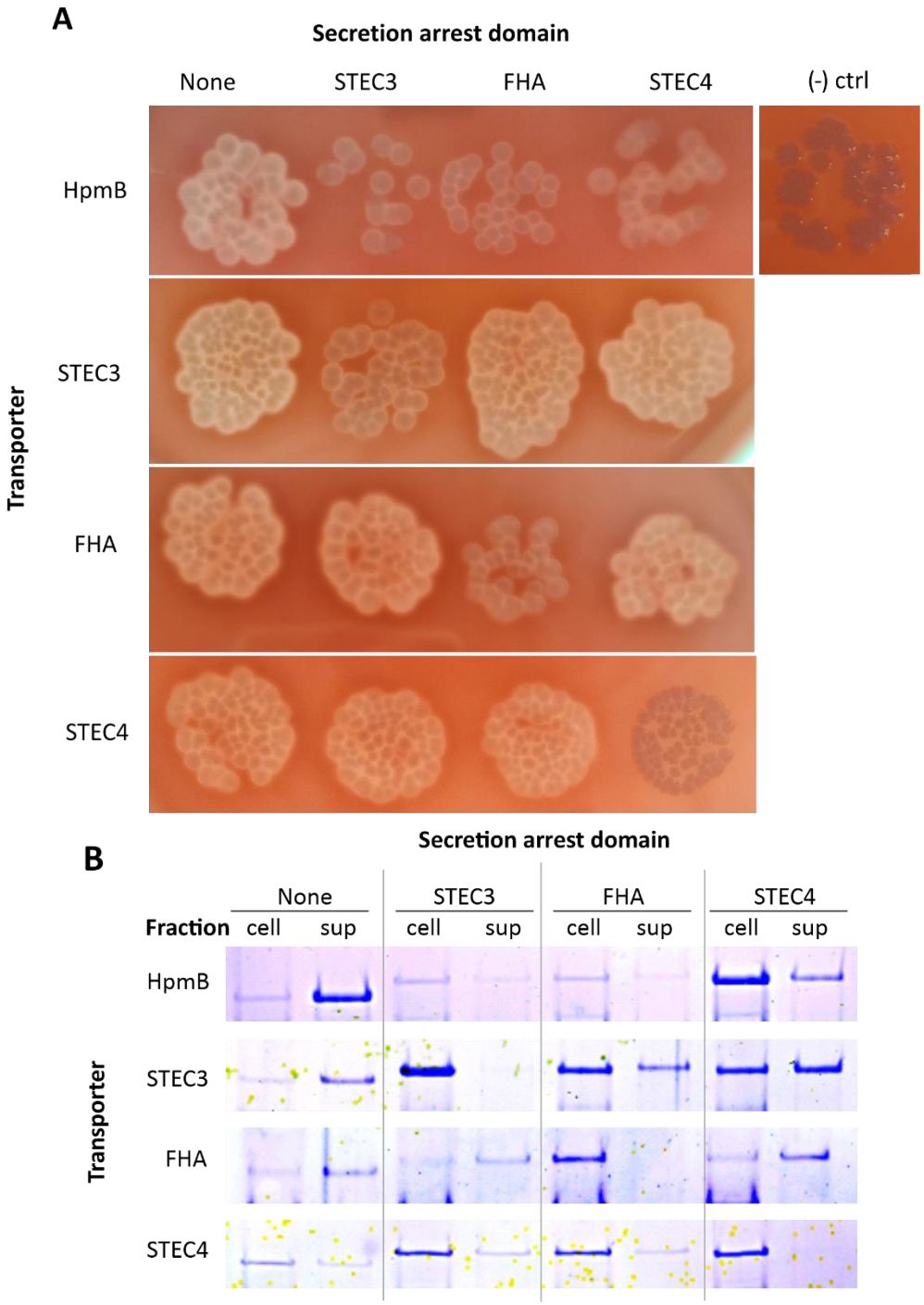

Figure 7. The YP domain requires cognate CdiB for secretion arrest. TpsB-YP pairs are tested in HpmA chassis. **A)** *E. coli* cells expressing HpmA constructs on blood agar plate. Cognate transporter and YP pairs prevent full secretion of HpmA. Resulting zone of clearing is smaller. **B)** Coomassie stain of urea soluble HpmA in cell and supernatant. Transporters export HpmA to supernatant. Cognate transporter and YP pairs prevent full

A

SA(STEC3) Y1657-N1841	SA(STEC4) G1545-A1729	SA(FhaB) A2309-T2483
YPLPSGNNGYFVPSADPDSP	GEPVILLPGQQFEVSAPQGS	AGPSAVAAPAVGAADVGVEP
YLITVNPKLDGLGKVDSSLF	IHVAGPDTRLPDSSLFKTNP	VAGDQVDQPVVAVGLEQPAA
AGLYDLLRMHPGQAPRETDP	AVNVPYLVETDPRFTNQKTW	AVRVAPPAVALPRPLFETRI
AYTDEKQFPGSSYFLDRLGL	LGSDYMQKAFSQNGDNMLKR	KFIDQSKFYGSRYFFEQIGY
KPEKDYRFLGDAAFDTRYVS	LGDGFYEQRLIREQVVALTG	QPDRAARVAGDNYFDTTLVR
NYMLNQIGGRYINGVGSDTD	QRYLDGYSNDEEQFKALMDA	EQVRRALGGYESRLPVRGVA
QMRYLMDNAARAQKALGLKF	GIAFGKQYNLTPGVALTAEQ	LVAKLMDSAGTVGKALGLKV
GVALTADQVAALDQSILWYK	MALLTGDIVWLVNTTVTLPD	GVAPTAQQLKQADRDFVWYV
AVTIKGQTVMVPEVYLSPKD	GSTQTVQVPQVYARVKPGDV	DTVIDGQKVLAPRLYLTEAT
VTLQN**SR**DYKDDDDK	NSAGA**SR**DYKDDDDK	RQGIT**SR**DYKDDDDK

B

```
CLUSTAL O(1.2.4) multiple sequence alignment


STEC4       -----GEPVILLPGQQ----FEVSA---------PQGSIHVAGPDTRLPDSSLFKTNPAV 42
STEC3       YPLPSGNNGYFVPSADPDSPYLITVNPKLDGLGKVDSSL-FAGL--Y---DLLRMHP--- 51
FhaB        ----AGPSAVAAPAVGAA---DVGVEPVA-G-DQVDQPVVAVGL--EQPAAAVRVAPPAV 49
                 *      *.       : .          :  :  .*        :

STEC4       N-VPYLVETDPRFTNQKTWLGSDYMQKAFSQNGDNMLKRLGDGFYEQRLIREQVVALTGQ 101
STEC3       --GQAPRETDPAYTDEKQFPGSSYFLDRLGLKPEKDYRFLGDAAFDTRYVSNYMLNQIGG 109
FhaB        ALPRPLFETRIKFIDQSKFYGSRYFFEQIGYQPDRAARVAGDNYFDTTLVREQVRRALGG 109
                   **   : ::. : ** *: . :. : :.  :  **  ::   : : :    *

STEC4       RYLDGYSNDEEQFKALMDAGIAFGKQYNLTPGVALTAEQMALLTGDIVWLVNTTVTLPDG 161
STEC3       RYINGVGSDTDQMRYLMDNAARAQKALGLKFGVALTADQVAALDQSILWYKAVTIK---- 165
FhaB        YESRLPVRGVALVAKLMDSAGTVGKALGLKVGVAPTAQQLKQADRDFVWYVDTVID---- 165
                  .   .  *** .    *  .*. *** **:*:     .::*   ..:

STEC4       STQTVQVPQVYARVKPGDVNSAGA     185
STEC3       -GQTVMVPEVYLSPKDVTLQN---     185
FhaB        -GQKVLAPRLYLTEATRQGIT---     185
              *.* .*.:*         .
```

Figure S1. The YP domains CdiA^{STEC3}, CdiA^{STEC4,} and FhaB. A) 185 residues of the YP domain from *E. coli* CdiA^{STEC3} were used to define corresponding regions in CdiA^{STEC4} and *Bordetella pertussis* FhaB. **B)** Multiple sequence alignment of the three YP domains.

Table 1. Strain used in this study.

Strain	Reference
E. coli: CH14016: MG1655 Δ*wzb* Δ*tsx*	(165)
E. coli: CH14017: MG1655 Δ*wzb* Δ*tsx* Δ*ompT*	(165)

Table 2. Plasmids used in this study.

Strains	Plasmid	Reference
CH14563	pET21b-cdiBAI (STEC_O31 J2M139) (MCS-) 2918Nhe, Amp^r	(165)
CH2828	pET21b-cdiBAI (STEC3) (MCS-) ΔY1758-N1841 (1726C), Amp^r	This study
CH2829	pET21b-cdiBAI (STEC3) ΔG1708-N1841 (1726C), Amp^r	This study
pZR435	pET21b::cdiBA(G1726C)I (STEC_O31 J2M139), Amp^r	(165)
CH10	pET11d::pSspC-Ala, Amp^r	Chris Hayes
CH4917	pET21b-cdiBAI (STEC3) G1708-sspC(50)-N1757 (1959C), Amp^r	This study
CH4918	pET21b-cdiBAI (STEC3) G1708-sspC(25)-D1732 (1959C), Amp^r	This study
CH4919	pET21b-cdiBAI (STEC3) R1733-sspC(25)-N1757 (1959C), Amp^r	This study
CH4006	pET21b-cdiBAI (STEC3) d1748-1763 (1959C) MCS-, Amp^r	This study
CH5513	pET21b-cdiBAI (STEC3) MCS- V1837G, Amp^r	This study
CH5537	pET21b-cdiBAI (STEC3) MCS- V1837C, Amp^r	This study
CH5514	pET21b-cdiBAI (STEC3) MCS- G1708-sspC-N1757 (V1837G), Amp^r	This study
CH5515	pET21b-cdiBAI (STEC3) G1708-sspC(25)-D1732 (V1837G), Amp^r	This study
CH5516	pET21b-cdiBAI (STEC3) R1733-sspC(25)-N1757 (V1837G), Amp^r	This study
CH5539	pET21b-cdiBAI (STEC3) MCS- G1708-sspC-N1757 (V1837C), Amp^r	This study
CH5540	pET21b-cdiBAI (STEC3) G1708-sspC(25)-D1732 (V1837C), Amp^r	This study
CH5541	pET21b-cdiBAI (STEC3) R1733-sspC(25)-N1757 (V1837C), Amp^r	This study
CH5408	pET21b-cdiBAI (STEC3) MCS- ΔYP1 (ΔP1658-P1707) G1726C, Amp^r	This study
CH5401	pET21b-cdiBAI (STEC3) (MCS-) ΔRBD-YP1 (ΔQ1385-P1707)(1726C), Amp^r	This study
CH14029	pET21b-cdiBAI (STEC3) (MCS-) ΔRBD(ΔN1400-S)(1726C), Amp^r	This study

CH2207	pET21b-cdiBAI (STEC3) (MCS-) ΔRBD EcoBam (1726C), Amp^r	This study
CH3903	pET21b-cdiBAI (STEC3) ΔA1748-I1763 (1726C), Amp^r	This study
CH3904	pET21b-cdiBAI (STEC3) ΔD1741-I1763 (1726C), Amp^r	This study
CH4005	pET21b::cdiBAI(STEC3) ΔA1748-I1763, Amp^r	This study
CH4006	pET21b::cdiBAI(STEC3) ΔA1748-I1763 (1959C), Amp^r	This study
CH4007	pET21b::cdiBAI(STEC3) ΔA1748-I1763 (2731C), Amp^r	This study
CH4008	pET21b::cdiBAI(STEC3) ΔD1741-I1763, Amp^r	This study
CH4009	pET21b::cdiBAI(STEC3) ΔD1741-I1763 (1959C), Amp^r	This study
CH4010	pET21b::cdiBAI(STEC3) ΔD1741-I1763 (2731C), Amp^r	This study
pZR439	pET21b::cdiBAI(STEC3) D1959C, Amp^r	(165)
pZR442	pET21b::cdiBAI(STEC3) S2731C, Amp^r	(165)
CH429	pCH450::hpmBA (S456C), Amp^r	Chris Hayes
CH53	pTrc99a, Amp^r	Chris Hayes
CH6885	pTrc99A-hpmBA chassis (S456C), Amp^r	This study
CH6886	pTrc99A-hpmBA-YP(STEC3), Amp^r	This study
CH7231	pTrc99A-hpmBA-SA(FhaB), Amp^r	This study
CH7232	pTrc99A-hpmBA-SA(STEC4), Amp^r	This study
CH6887	pTrc99A-cdiB-TPS(STEC3)-hpmApTrc99A, Amp^r	This study
CH6888	pTrc99A-cdiB-TPS(STEC3)-hpmA-YP(STEC3), Amp^r	This study
CH7233	pTrc99A-cdiB-TPS(STEC3)-hpmA-SA(FhaB), Amp^r	This study
CH7234	pTrc99A-cdiB-TPS(STEC3)-hpmA-SA(STEC4), Amp^r	This study
CH7235	pTrc99A-fhaC-TPS(fhaB)-hpmA, Amp^r	This study
CH7236	pTrc99A-fhaC-TPS(fhaB)-hpmA-YP(STEC3), Amp^r	This study
CH7237	pTrc99A-fhaC-TPS(fhaB)-hpmA-SA(fhaB), Amp^r	This study
CH7238	pTrc99A-fhaC-TPS(fhaB)-hpmA-SA(STEC4), Amp^r	This study
CH7239	pTrc99A-cdiB-TPS(STEC4)-hpmA, Amp^r	This study
CH7240	pTrc99A-cdiB-TPS(STEC4)-hpmA-YP(STEC3), Amp^r	This study
CH7241	pTrc99A-cdiB-TPS(STEC4)-hpmA-SA(FhaB), Amp^r	This study
CH7242	pTrc99A-cdiB-TPS(STEC4)-hpmA-SA(STEC4), Amp^r	This study
pCH14046	pZS21, Kan^r	(165)
pCH14047	pZS21::tsx, Kan^r	(165)
CH1981	pCH450::STEC4(M1-P77)-fhaB, Tet^r	Chris Hayes
CH1055	pET21(MCS-)::cdiBCAI (STEC4), Amp^r	Chris Hayes

Table 3. Oligonucleotides used in this study.

Primer	Name	Sequence	Reference
CH4818	STEC3-P1707-Bam-rev	5' - TTT GGA TCC GGG GTG CAT CCT GAG CAG - 3'	This study
CH4817	STEC3-N1757-Bam-rev	5' - AAA GGA TCC TAT ATG CTG AAC CAG ATC GGG G - 3'	This study
CH4816	STEC3-G1842-Bam-for	5' - AAA GGA TCC GGC AGT ATT ATC AGC GGT CAG - 3'	This study
CH4244	STEC-G1500-Xho-for	5' - AAA CTC GAG GGT TCA CAA CTG AAT AAT CAG TCC TTC - 3'	(165)
CH4231	STEC_O31(L2189P)-rev	5' - CAT GGT TAC CCG CCG CCG GTG ACA CAT CCC GGT CAG CC	This study
CH5025	STEC3-P1707-rev	5' - GGG GTG CAT CCT GAG C - 3'	This study
CH5026	STEC3-D1732-rev	5' - GTC AAG AAA ATA CGA TGA GCC CG - 3'	This study
CH5027	STEC3-R1733-for	5' - CGG CTC GGG CTG AAA C - 3'	This study
CH5028	STEC3-Y1758-for	5' - TAT ATG CTG AAC CAG ATC GGG G - 3'	This study
CH5029	sspC-P1707-for	5' - ACC TGC TCA GGA TGC ACC CCG CTC AAC AAA GTA GAT CAA GAT CAA AC - 3'	This study
CH5030	sspC(50)-Y1758-rev	5' - CCG ATC TGG TTC AGC ATA TAA ACT GAA CCG TTT GCA CGA G -3'	This study
CH5031	sspC(25)-D1732-for	5' - GCT CAT CGT ATT TTC TTG ACG CTC AAC AAA GTA GAT CAA GAT CAA AC - 3'	This study
CH5032	sspC(25)-Y1758-rev	5' - CCG ATC TGG TTC AGC ATA TAT TGT TCA ATA GCT GAA GCT GC - 3'	This study
CH5033	sspC(25)-R1733-rev	5' - TCC GGT TTC AGC CCG AGC CGT TGT TCA ATA GCT GAA GCT GC - 3'	This study
CH4978	STEC3-V1545-for	5' - GTT ACC TTT ACT CTC TCC GGA GC - 3'	This study
CH4979	STEC3-I1960-rev	5' - GGA TGT CCA GAC TAT CCA TGG C - 3'	This study
CH5064	STEC3-V1837G-for	5' - CCG AAA GAT GGG ACG CTG CAG AAC GG -3'	This study
CH5065	STEC3-V1837C-for	5'- TCA CCG AAA GAT TGT ACG CTG CAG AAC GG -3'	This study
ZR287	STEC-R1961-Not-rev	5' - TTT GCG GCC GCG GAT GTC CAG ACT ATC CAT GG	This study
CH4382	STEC(3)-G1708-Xho-for	5' - AAA CTC GAG GGG CAG GCA CCA CG - 3'	(165)
CH4242	STEC-Nco/Not-rev	5' - TTT GCG GCC GCC CAT GGC ACT GAC AGA GG - 3'	(165)
ZR268	STEC-A498-Kpn-for	5' - GCC ACG CAG ATA AAC AAC AGC	(165)

CH4383	STEC(3)-P1707-Xho-rev	5' - TTT CTC GAG GGG GTG CAT CCT GAG C - 3'	(165)
CH4906	STEC3-G1708-Bam-for	5' - AAA GGA TCC GGG CAG GCA CCA CG -3'	This study
CH4239	STEC-Kpn-for	5' - CAG CGG TAC CCT CTC CG - 3'	(165)
CH4752	STEC(3)-Q1386-Eco/Sac-rev	5' - TAT GAG CTC CCG CGA ATT CAG TAA ATG TCC GGT TC - 3'	This study
CH4753	STEC(3)-S1661-Sac/Bam-for	5' - CCC GAG CTC GGA TCC AAC AAT GGT TAT TTT GTC CC - 3'	This study
CH4948	STEC3-K1740-Bam/Nco-rev	5' - TTT CCA TGG GGA TCC TTT TTC CGG TTT CAG CCC G - 3'	This study
CH4949	STEC3-D1747-Bam/Nco-rev	5' - TTT CCA TGG GGA TCC ATC CCC CAG GAA GCG ATA A - 3'	This study
CH4950	STEC3-G1764-Sac/Bam-for	5' - AAA GAG CTC GGA TCC GGG GGG CGC TAT ATC AAC - 3'	This study
CH4264	STEC-S2917-Nhe-rev	5' - TTT GCT AGC GCT GCT GTT TCC GG - 3'	(165)
CH5218	hpmA(G167)-pTrc-GA-for	5' - ACA CAG GAA ACA GAC CAT GGA ATT CAA AGC TAG CGG TCA GCT AAA AGG CTA TAG CAC - 3'	This study
CH5219	hpmA(T451)-GA-rev	5' - ACA TTC TAA TCT CGA AGT ATG ATT ACG TTT ATT GCC ATT TTC AC - 3'	This study
CH5220	hpmA(R453)-GA-for	5' - ATA CTT CGA GAT TAG AAT GTG GTA GTT GGA GTA ACA G - 3'	This study
CH5221	hpmA(V1219)-GA-rev	5' - CTC GGG ATA CGC TTT TCT CAT CTT GTT TAC CAA TAG - 3'	This study
CH5222	hpmA(R1221)-GA-for	5' - TGA GAA AAG CGT ATC CCG AGA AGG AGG AAC GAT TAA TAA CTC - 3'	This study
CH5223	hpmA(I1360)-GA-rev	5' - CTT TTT GGC TCG CAA TAT TGA GTG AAC CAC CGA C - 3'	This study
CH5224	hpmA(S1362)-GA-for	5' - CAA TAT TGC GAG CCA AAA AGA GAG TGA TCG C - 3'	This study
CH5225	hpmA(K1577)-Xho/Xba-rev	5' - TCG TCT TTG TAG TCT CTA GAT TTC TCG AGT TTT TCA GAA ATA GAT GCT TTT GTA TTG ACG - 3'	This study
CH5226	FLAG-pTrc-GA-rev	5' - TCC GCC AAA ACA GCC AAG CTT ACT TGT CGT CAT CGT CTT TGT AGT CTC TAG ATT TCT CG - 3'	This study
CH5227	hpmB-Eco-for	5' - AAA GAA TTC ATG AAA AAA AAA GTT GTT TTA TTA ACA CTA TTA AGC TG - 3'	This study
CH5228	hpmA(N166)-Nhe-rev	5' - TTT GCT AGC ATT TTC AAA GAG CGG ATT ACC AAC AAC - 3'	This study

CH5252	fhaC-Eco-for	5' - AAA GAA TTC ATG ACT GAC GCA ACG AAC CG - 3'	This study
CH5253	fhaB(R342)-Nhe-rev	5' - TTT GCT AGC GCG CTG GAC CGT GGC - 3'	This study
CH5254	fhaB(A2420)-Bam/Xho-for	5' - AAA GGA TCC CTC GAG GCC GGG CCG AGC GCC G - 3'	This study
CH5255	fhaB(G2453)-rev	5' - CGG CAG GCT GCT CCA GCC CGA CCG CCA C - 3'	This study
CH5256	fhaB(T2604)-Xba-rev	5' - TTT TCT AGA CGT GAT GCC CTG GCG C - 3'	This study
CH5257	STEC4-cdiB-Eco-for	5' - AAA GAA TTC ATG TCT GTT TTA CTA TCG CCT TTA TCT C - 3'	This study
CH5258	STEC4-I329-Nhe-rev	5' - TTT GCT AGC AAT ACG TCC GTC AGC CGT C - 3'	This study
CH5259	STEC4-G1545-Bam/Xho-for	5' - AAA GGA TCC CTC GAG GGT GAA CCG GTC ATT CTG TTG - 3'	This study
CH5260	STEC4-A1729-Xba-rev	5' - TTT TCT AGA CGC ACC GGC GCT GT - 3'	This study
CH4307	STEC-cdiB-Eco/Bam-for	5' - TTT GAA TTC GGA TCC GCC AGA ATA CGG GGA GAA C - 3'	This study
CH5229	STEC3-T322-Nhe-rev	5' - TTT GCT AGC TGT CCC GGT AAC GCT GAG - 3'	This study
CH5230	STEC3-Y1657-Xho-for	5' - AAA CTC GAG TAT CCC CTG CCT TCC GG - 3'	This study
CH5231	STEC3-N1841-Xba-rev	5' - TTT TCT AGA GTT CTG CAG CGT CAC ATC TTT C - 3'	This study

Chapter IV. Receptor binding secretes C-terminal half of CdiA unfolded

This work has not been published yet. BamA purification has been done by Dr. Zach Ruhe. I used plasmids made by Nicole Chan (pCH2575) and Professor Chris Hayes (pCH1038). I produced all other data presented in this chapter.

A. Introduction

Contact-dependent growth inhibition (CDI) is a unique competitive system which delivers a toxin effector to a closely related neighbor cell upon direct cell-cell contact (70). Growth inhibition is mediated by a large (>350kD) filamentous surface protein CdiA which carries a C-terminal toxin domain (CdiA-CT) (70). Delivery of the CdiA-CT toxin is directed by receptor-binding of CdiA (71,73,74,105). During its biogenesis, CdiA exported through an outer membrane transporter, CdiB and forms a 33nm long filament extending from the surface of the cell (165). Secretion of CdiA is arrested in the middle of its primary sequence to display its central receptor-binding domain (RBD) at the tip of the filament while the remaining CdiA is retained in the periplasm (165). In the previous chapter, I have discussed in depth about this secretion arrest mechanism.

Receptor-binding induces export of the periplasmic CdiA which then delivers CdiA-CT to the target cell (165). Previous work by others have significantly advanced our understanding of the receptors which CdiA targets (71,105,106,108). So far, four classes of CdiA has been identified based on the receptor group they target. Class I to III target outer membrane proteins such as BamA (71), Tsx (104), and OmpC/OmpF heterotrimer complex (106). Class IV CdiA targets specific LPS core of the target membrane which demonstrates the adaptability of CDI system to recognize a target (108).

CdiA binds receptors of the same species (104). For example, BamA-targeting CdiA from *E. coli* strain EC93 fails to bind to *E. coli* targets cells expressing *E. cloacae* BamA (104). So, the receptor-binding is a finely tuned method of directing the toxin activity to an intended target. This narrow target specificity suggests that CDI system is used to inhibit closely related neighbors, possible as a kin selection mechanism rather than as a general competitive system to dominate a given physical space (104). CdiA exhibits impressive modularity. CdiA-CT effectors are demarcated by conserved VENN motif. Both CdiA-CT and the RBD can be swapped (105,114). In principle, artificial CdiA construct can be assembled to deliver a selected toxin effector to a target cell of desire. However, how receptor-binding releases the secretion arrest mechanism at the YP domain is unknown.

My work in Chapter III showed that both the YP region and CdiB work together for secretion arrest. Receptor-binding event somehow releases the secretion arrest mechanism at this interaction. Based on our current model, receptor-induced export of the C-terminal CdiA must occur through the lumen of CdiB (165). A model of CdiB can be predicted based on the structure of closed related FhaC, another TpsB β-barrel transporter from *Bordetella pertussis* (89). A few other TpsB proteins have been structurally solved; the lumen of these TpsB transporters are limited in its space (> 3 nm in diameter) (90,91). As with many secretion systems, secretion of cargo via the T5SS, which CDI belongs to, is thought to occur in an unfolded state (96).

In this chapter, I will show that the receptor-induced export of the periplasmic CdiA must occur unfolded using DHFR fusion at the C-terminal CdiA. DHFR is often fused to other proteins to study their stability and membrane translocation (170,171). DHFR binds tightly to a substrate homologue, methotrexate (MTX) and remains stably folded (172,173).

Folded DHFR was prevented from receptor-dependent export. Additonally, the periplasmic half of CdiA can be replaced to make enzymatic fusion which functions as a receptor-dependent switch that exports the enzymatic activity extracellularly. Lastly, I will explore possible mechanism of receptor-dependent release of the secretion arrest by inducing protein folding at the RBD and by replacing the RBD with colicin receptor-biding domains.

B. Results

CdiA binds to purified receptor to release the secretion arrest

Receptor-binding interactions releases the CdiA secretion arrest to export the periplasmic half of CdiA (165). RBD can be exchanged between CdiA genes to direct the effector specificity (105). For example, Tsx-binding RBD of $CdiA^{STEC3}$ can be replaced with BamA-binding RBD from $CdiA^{EC93}$. This chimera directs toxin delivery to BamA on target outer membrane. Toxin delivery can be visualized by pronounced increase of shorter CdiA protein (CT-less) in immunoblot (Figure 1A, lane 5). Receptor recognition is species-specific, and *E. coli* targets expressing *E. cloacae* BamA are no longer targeted by this chimeric effector (Figure 1A, lane 4).

Purified and reconstituted receptor can also initiate secretion of the periplasmic CdiA. When purified *E. coli* BamA is introduced, the periplasmic CdiA resumes export demonstrating that isolated protein can serve as a CDI receptor and releases the secretion arrest of CdiA (Figure 1B). The export of periplasmic CdiA is visualized by maleimide-dye labeling of a periplasmic cysteine. Again, receptor-binding is species-specific and ECL BamA does not serve as a receptor (Figure 1B).

Periplasmic DHFR fusion can be exported via CdiB

To test the hypothesis that the periplasmic half of CdiA unfolds during resumed secretion, I fused murine dihydrofolate reductase (DHFR) at three position of the periplasmic CdiA: D1959, K2425, and S2919. DHFR fusion at D1956 replaces most of the periplasmic CdiA. DHFR fusion at K2425 interrupts CdiA in the middle of the FHA2 domain. Fusion at S2919 retains all of the FHA2 and the PT domain, similar to a toxin effector swap. These CdiA-DHFR chimeras were also combined with ΔYP-100 (165) to force secretion to the supernatant and to probe their compatibility for export by CdiB. When the YP-100 domain is removed, all three constructs were released to the supernatant suggesting DHFR is compatible for CdiB-mediate export (Figure 2A).

Next, I used CdiA-DHFR fusion at D1956 to visualize receptor-dependent export. I predicted that DHFR domain readily unfolds without methotrexate and gets secreted through CdiB when target cells are mixed in. We should be able to visualize this export by labelling the single cysteine of DHFR with the maleimide dye as done previously (165). The native mouse cysteine in DHFR was not labelled when in the periplasm (Figure 2B, lane 8). But after mixing with tsx+ target cells, the DHFR was exported and its cysteine was labelled (Figure 2B, lane 9). This confirms that DHFR domain is compatible for RBD-triggered secretion. It should be noted that I used ΔacrB strains for MTX experiments to maximize the MTX concentration entering the cell.

C-terminal half is unfolded during resumed secretion

In folded DHFR structure, its cysteine residue is largely internal and occluded from external surface (174). The dye accessibility of this native cysteine was compared with or

without MTX after the outer membrane is permeabilized with polymyxin B (Figure 3A). Without MTX, the native cysteine readily reacted with the maleimide dye in the periplasm. However, this labelling was greatly reduced with 1mM MTX (Figure 3A). This suggests that MTX entered the periplasm and stabilized DHFR to a folded state where its cysteine was partially occluded.

To disentangle domain folding from localization, I then replaced the native cysteine of DHFR with a serine and introduced a C-terminal cysteine [D1956-DHFR(C7S)-Cys]. The dye reactivity of this cysteine in the periplasm was independent of methotrexate concentration thus can serve as a probe to report cellular localization (Figure 3B). Then tsx+ target cells were mixed in to induce periplasmic CdiA secretion. However, MTX prevented DHFR export, and the C-terminal Cys was not labelled (Figure 3C). DHFR-MTX complex must be locked in a folded state, preventing the export through CdiB. This experiment supports our hypothesis that CdiA must be able to unfold to travel through the lumen of CdiB.

CdiA-Enzyme fusions

I have fused three enzymes varying in size and stability to the periplasmic CdiA. *B. subtilis* amylase (AmyE), *D. dadantii* pectin methylesterase A (PmeA), and *D. dadantii* pectate lyase E (PelE) were fused at D1956, K2425, and S2919. Chimeric constructs were made in both WT and ΔYP-100 CdiA to access secretion compatibility (Figure 4).

AmyE is a large cytoplasmic α-amylase with a complex tertiary structure that normally do not get secreted (175,176). ΔYP CdiA-AmyE fusions were barely secreted to the supernatant possibly due to failure to unfold (Figure 4A). On the other hand, PmeA and PelE

are both secreted through Type II Secretion system (177,178). PelE was efficiently exported at all three fusions, but PmeA was only secreted when grafted at D1956 (Figure 4bB). Leaving larger portion of the periplasmic CdiA hindered PmeA export.

Export of PmeA and PelE are visible on pectin agar plate with ruthenium red dye. Pectin is large polymer impermeable to the outer membrane and can only be modified by exported PmeA or PelE. PmeA demethylates pectin which increases affinity to ruthenium red while PelE does the opposite (not shown). ΔYP CdiA(D1956)-PmeA exported PmeA and created red halos around the colonies (Figure 5). But WT CdiA(D1956)-PmeA chimera retained the enzyme in the periplasm and did not make red halos (Figure 5).

These experiments show that an enzyme can be fused to the periplasmic CdiA. If the enzyme readily unfolds and secretion compatible, CdiA serves as a receptor-dependent trigger to export the enzymatic activity outside of the cell.

RBD replaced with DHFR does not export periplasmic CdiA with MTX

The RBD was then replaced with DHFR (RBD-DHFR) to test if MTX-induced folding can mimic receptor binding and initiate periplasmic CdiA export. Two additional replacements were made each lacking 25 and 50 residues of the extended YP-N (RBD/YP25-DHFR and RBD/YP-N-DHFR, respectively) in order to introduce more “tug” when the DHFR domain folds. RBD replacements with native DHFR was used to probe the domain folding upon introducing MTX. At 10mM [MTX], cysteine in DHFR had greatly reduced reactivity to maleimide-dye because of DHFR folding (Figure 6A). However, the DHFR domain replacing both RBD and 50 residues of YP-N (RBD/YP-N-DHFR) retained considerable dye reactivity with MTX (Figure 6A). This could suggest that the DHFR

domain is too extended along the CdiA filament to adequately bind to its substrate. Alternatively, the stability of secretion arrest may have prevented DHFR to fold completely and RBD/YP-N-DHFR was the only construct short enough to show it through difference in dye-reactivity.

In any case, DHFR folding did not alleviate secretion arrest and there was no loss of cell bound CdiA (Figure 6A). To monitor localization of the periplasmic CdiA, the Cys in DHFR was again mutated to Ser then combined with a periplasmic cysteine (1959Cys or 2731Cys). None of the periplasmic residues were dye-accessible even with MTX (Figure 6B). The periplasmic residues were labelled with maleimide-dye when the outer membrane is permeabilized with PMB, confirming the residues were still in the periplasm (Figure 6B).

RBD^{colicin} cannot replace CdiA RBD

Finally, the CdiA^{STEC3} RBD was replaced with RBD from colicins, ColE5 or Col1a. However, both chimeras were aberrantly cleaved by OmpT roughly at the site of sequence replacement (Figure 7A). Resulting cleaved CdiA filaments were lost to the supernatant as expected (Figure 7A). Expression of these RBD chimeras in Δ*ompT* CH14017 prevented the cleavage (Figure 7A). So CdiA-RBD^{colicin} effectors were expressed in Δ*ompT E. coli*, yet the RBD chimeras failed to bind to target cells overexpressing cognate receptors (Figure 7B). The target cells were not made Δ*ompT*, so it is possible the effectors are cleaved by OmpT on target cells. CdiA-RBD^{ColE5} showed some specific binding but none of the CdiA-RBD^{colicin} effectors had any CDI activity in co-culture with targets (Figure 7C). Only Δ*ompT* cells were used for target co-culture competitions to preserve the CdiA-RBD^{colicin} proteins.

C. Discussion

Receptor-binding induced export of the periplasmic half is a crucial feature of CdiA which directs the toxin activity to an intended target cell in a timely and efficient manner. Receptor specificity is limited to those in the same species (104). This is likely to devote the toxin delivery to neighboring cells from the same species. Inhibition of the neighbors who may compete for the same niche of resources is an evolutionarily advantageous strategy.

The resumed export most likely occurs through the lumen of CdiB just like the export of the N-terminal half. CdiB is a member of Omp85 outer membrane β-barrel proteins which are assembled by β-barrel assembly machinery including BamA (70). BamA has been shown to open its lateral gate between its terminal transmembrane β-strands, β1 and β16, in order to release mature β-barrel proteins (81–84). It is possible that CdiB could first export N-terminal CdiA through its lumen then set aside the rest of CdiA through this lateral gate mechanism allowing export of another CdiA cargo. However, opening of the lateral gate requires specific interactions between β1 and a new β-strand of the substrate (86). The YP domain of CdiA where secretion arrest occurs does not have any β-strand long enough to mimic this interaction between β1 and β16 of CdiB (Chapter III). Therefore, there is little evidence to believe CdiB dedicates its lumen to more than one CdiA at a time.

Whether the periplasmic export occurs through CdiB lumen or through the space next to the barrel in the lipid bilayer, folded tertiary structure cannot be accommodated. The predicted lumen of CdiB is ~1.6nm in diameter. Therefore, periplasmic CdiA must be susceptible to unfolding during receptor-initiated secretion. In this chapter, folding state of the periplasmic domain was controlled by replacing it with DHFR. In ΔacrB strain, 1mM

was sufficient to lock DHFR to a folded state. As the result, the domain was prevented from export even after tsx+ target cells were mixed in (Figure 3).

Other proteins can replace the periplasmic CdiA. As long as the chimeric domain can readily unfold, it can be fused to CdiA to make a receptor-dependent molecular trigger which will export the periplasmic protein upon receptor-binding. Large proteins or stable proteins like AmyE are not compatible for export via CdiB. Readily secreted PmeA and PelE were more compatible for CdiB-mediate export. PmeA was only efficient exported when less periplasmic CdiA was left (Figure 4). However, D1956-PmeA chimera is efficiently exported via CdiB. The substrate for PmeA is pectin, a large outer membrane impermeable polymer (179,180). On a pectin agar plate with ruthenium red, the activity of PmeA is reported when the enzyme is exported though CdiB (Figure 5). This is a useful tool to set up a plate-based genetic screening to unravel the mechanism of secretion arrest. The WT-PmeA chimera can be mutagenized then any clones that secrete PmeA in tsx- strain will report defects in secretion arrest. I expect to find mutations in the YP domain and the CdiB transporter that are responsible for secretion arrest.

Furthermore, CdiA could be a useful bioengineering tool of controlling other enzymatic activity across the outer membrane, if the enzyme readily unfolds. For example, a surface modifying enzyme could be fused to CdiA and asked to specifically modify the surface of target cells which encounters CDI+ cells. Such experiments could map bacterial interactions and their distribution in a complex environment.

The mechanism of receptor-mediate secretion remains unknown. The RBD could fold upon receptor-binding which then releases the secretion arrest in the YP domain.

Alternatively, RBD could provide a contact point to securely engage to a target cell, then mechanical pulling during cell movement could overcome the secretion arrest mechanism.

To test the receptor-inducing folding model, I have replaced the RBD with DHFR and found DHFR folding is insufficient to initiate export (Figure 6). However, DHFR folding may not have provided enough folding energy in my tested constructs. The domain folding was probed by Cys occlusion in RBD-DHFR and RBD/YP25-DHFR (Figure 6A). In these constructs, the remaining extended YP domain could have served as a loosened string and mitigated the folding energy of DHFR. In RBD/YP-N-DHFR where I imagine DHFR is tightly extended across the filament, MTX did not sufficiently induce DHFR folding (Figure 6A) most likely because fully stretched DHFR would lack enough structural features to initiate MTX-binding. It is possible that the experiment is working as intended and secretion arrest is more stable interaction than folding energy of DHFR-MTX complex. However, my data is insufficient to make any confident conclusion.

CdiA-RBD^{colicin} chimeras were made to test the mechanical binding model. Unfortunately, RBDs from ColE5 and Col1a were unstable and subject to OmpT-cleavage. This cleavage occurred in monocultures (Figure 7A). It is unknown whether self OmpT or OmpT on a neighboring cell cleaved the chimeric CdiA because I did not knock out the chromosomal btuB or cirA. CdiA-RBD^{colicin} also failed to promote sufficient target cell-binding (Figure 7B). Although the effectors were expressed in Δ*ompT*, the targets were ompT+. Using Δ*ompT* targets could promote more target cell-binding. However, CdiA-RBD^{colicin} effectors had no CDI activity even when ΔompT cells were used throughout (Figure 7C). So even if target-cell binding were to improve in the adhesion assay, this

binding did not result in successful CdiA-CT delivery. Unfortunately, current data are insufficient to support either models of receptor-mediated export.

D. Materials and methods

Bacterial growth conditions

Bacterial strains were derivatives of E. coli K-12 strains MG1655, MC4100, X90 or EPI100. Bacteria were cultured in lysogeny broth (LB) or on LB agar at 37 °C. Unless indicated otherwise, media were supplemented with antibiotics at the following concentrations: 150 µg/mL ampicillin (Amp), 50 µg/mL kanamycin (Kan), 200 µg/mL spectinomycin (Spc) and 25 µg/mL tetracycline (Tet).

Strain constructions

The Δ*acrB*::kan disruption was introduced into *E. coli* MG1655 Δ*wzb* Δ*tsx* Δ*ompT* (CH14017) (165) from the Keio collection (156) by phage P1-mediated transduction. Kan resistance cassettes were removed with FLP recombinase.

Plasmid construction

Three template cdiBA^{STEC3} constructs were made for easy protein fusions to C-terminal CdiA by SpeI/XhoI cloning. Initially, amyE was chosen to replace the periplasmic CdiA and make template constructs. *Bacillus subtilis* amyE was amplified with primer pairs CH4603/CH4606, CH4604/CH4606, and CH4605/CH4606. These fragments were cloned to pCH14563 using NcoI/XhoI, AflII/XhoI, and NheI/XhoI, respectively. Final clones have

SpeI sites introduced at CdiA residues 1956, 2425, or 2919 (CH14591, CH14592, and CH14593, respectively).

Mouse DHFR sequence was amplified from pCH14736 (pET23a-tp22-DHFR) using primer pair CH4683/4684. *Dickeya dadantii* pelE was amplified using primer pair CH4692/CH4693. *Dickeya dadantii* pmeA was amplified using primer pair CH4694/CH4695. All three heterologous domains were fused to the three template constructs above by SpeI/XhoI cloning. ΔYP versions were made by NcoI/XhoI subcloning to pCH14404 (ΔYP). pCH14404 is a modified version of previously published pCH14032 (ΔYP-100: ΔP1658-N1757)(165). The internal XhoI site in the deletion of pCH14032 has been removed by SalI cloning one of the fragments. These cloning generate pCH3809 to pCH3826 which has DHFR, pelE, or pmeA fusions at D1956, K2425, or S2919 with or without the YP-100 domain.

To disentangle DHFR folding and cellular localization, the native cysteine residue of DHFR was mutated to serine. DHFR was amplified with primer pair CH4806/CH4807. 4806 is a mutagenic primer while 4807 adds a C-terminal Cys and a portion of FLAG tag. The resulting PCR was further extended with CH4806/CH4808 to add the remaining FLAG tag as well as an XhoI site. The final PCR product was SpeI/XhoI cloned to pCH3809 to generate pCH2522 [D1956-DHFR(C7S)-Cys-FLAG].

RBD replacement with DHFR was also made by PCR. Fragments using primer pair CH4906/CH4242 and CH4907/CH4242 were BamHI/NcoI cloned to pCH5397. pCH5397 is a modified version of pCH2207 which as the RBD deletion (ΔQ1385-G1662) but the Cys at 1726 is restored to WT Gly. The resulting clones make pCH5398 with RBD/YP25 deletion (ΔQ1385-N1682) and pCH5400 with longer RBD/YP-N deletion (ΔQ1385-P1707),

respectively. Then DHFR was amplified with primer pair CH4904/CH4905 and EcoRI/BamHI cloned to pCH5397, pCH5398, and pCH5400 to generate pCH5402, pCH5404, and pCH5406, respectively. Cys-less DHRF(C7S) was also amplified with primers CH4904/CH4905 and cloned with EcoRI/BamHI. Then periplasmic cysteines at 1959 and 2731 from pZR439 and pZR441, respectively, were combined by NcoI/XhoI cloning the cysteines.

RBD^{CdiA} replacements with $RBD^{colicin}$ were made by PCR. ColE5 RBD was amplified with primer pair CH4944/CH4945. Col1a RBD was amplified with primer pair CH4946/CH4947. They were EcoRI/BamHI cloned to pCH2207. Then the whole cdiBAI with RBD fusion was NotI/XhoI cloned to pCH450 over arabinose induction. To overexpress colicin receptors, btuB was amplified with primers CH5042/CH5043 and cirA was amplified with primers CH5044/CH5045. The btuB fragment was KpnI/XhoI cloned to pCH450Kpn to generate pCH4101. The cirA fragment was EcoRI/XhoI cloned to pCH450 to generate pCH4102.

BamA purification and mixing

BamA from *E. coli* or *E. cloacae* was over-produced in *E. coli* strain CH2016 carrying plasmid pCH9216 or pCH9231 (105). Cells were grown at 37 °C in LB media supplemented with Amp and BamA production induces with 1.5 mM IPTG for 3 h. Cells were harvested by centrifugation at 6,000X g for 10 min, then re-suspended in 5 mL of BugBuster reagent and broken by three passages through a French press. The lysate was diluted with 25 mL deionized water and vortexed vigorously. Inclusion bodies were collected by centrifugation at 15,000X g for 20 min and washed thrice with 5 mL of 0.1X BugBuster

solution. The washed inclusion bodies were dissolved in 0.5 mL of urea-lysis buffer supplemented with 0.05% Triton X-100, then diluted into 50 mL 10 mM Tris-HCl (pH 8.0), 0.5% Triton X-100 to a final concentration of 140 µM. Diluted protein stocks were incubated on a rotisserie for three days at ambient temperature to refold. The refolding reaction was then stored at 4 °C. Greater than 95% of BamA was refolded as determined by heat-modifiable gel mobility as previously described (164).

E. coli MG1655 *Δwzb Δtsx* (CH14016) or MC4100 rifR Δ*arfB*::kan::BamA (Δ2014-2043) carrying CdiA expression plasmids were diluted to OD600 ~ 0.05 in Amp supplemented LB media and grown to mid-log phase at 37 °C. These inhibitor cultures were mixed with *E. coli* EPI100 Δ*bamA*:cat target cells that carry pZS21::*bamA*(ECL)or pZS21::*bamA*(*E. coli*) at a 1:1 ratio with Spc to block new protein synthesis. After 20 min with shaking, 1 mL of the mixture was harvested by centrifugation. Cell pellets were re-suspended in 50 µL of urea-lysis buffer and subjected to one freeze-thaw cycle to extract proteins. Urea-soluble proteins (5 µL) were resolved by SDS-PAGE and analyzed by immunoblotting using anti-TPS domain antisera.

For purified BamA mixing, *E. coli* MG1655 *Δwzb Δtsx* (CH14016) or MC4100 rifR Δ*arfB*::kan::BamA (Δ2014-2043) carrying CdiA expression plasmids were grown as described above. 1mL of Spc-treated culture was mixed with 10 µL of purified BamA preps for 1 h at 37 °C. Cells were harvested by centrifugation and resuspended in 1.0 mL of 1X phosphate buffered saline (PBS) supplemented with 1 mM MgSO4 (PBS-Mg). IRDye680LT-maleimide (LI-COR) was added to a final concentration of 40 µM. Labeling reactions were incubated in the dark at room temperature for 15 min, then quenched with 6 mM 2-mercaptoethanol (2-ME). Cells were collected by centrifugation and washed with

PBS-Mg supplemented with 6 mM 2-mercaptoethanol (2-ME). Cell pellets were re-suspended in 50 µL of urea-lysis buffer and subjected to one freeze-thaw cycle to extract proteins. Urea-soluble proteins (5 µL) were resolved by SDS-PAGE and analyzed by immunoblotting using anti-TPS domain antisera.

Protein extraction from cell and supernatant

E. coli CH14016 or CH14017 cells carrying cdiA expression plasmid were diluted to OD600 ~ 0.05 in LB medium supplemented with Amp and cultured with shaking at 37 °C. Once in mid-log phase, cultures were treated with Spc for 20 min to block protein synthesis. 1ml of culture were harvested by centrifugation (3,000 X g for 5 min) while keeping 900 µL of the supernatant for TCA-precipitation. Collected cell fraction was washed in 1X phosphate buffered saline (PBS) supplemented with 1 mM MgSO4 (PBS-Mg). Cells were collected by centrifugation and pellets were re-suspended in urea-lysis buffer [50% urea, 150 mM NaCl, 20 mM Tris-HCl (pH 8.0)] and subjected a freeze-thaw cycle to extract proteins. 5 µL of each sample analyzed by SDS-PAGE and immunoblotting.

To analyze culture supernatants for released CdiA mutants, retained 900 µL of the supernatant was added to 100 µL of trichloroacetic acid. Proteins were collected by centrifugation at 18,000 X g for 30 min at 4 °C. Precipitates were washed thrice with 1.0 ml of cold acetone. Air-dried pellets were dissolved in 45 µL of urea-lysis buffer, and 5 µL of each sample analyzed by SDS-PAGE and immunoblotting.

MTX-induced folding

E. coli MG1655 *Δwzb ΔtsxΔompT ΔacrB* cells carrying CdiA expression plasmid were grown as described above. After Spc-treatment, 1mM final [methotrexate] was added to the cultures at RT for 10 min. 1 mL of the culture was harvested by centrifugation and resuspended either in PBS-Mg or in PBS-Mg with 100 µg/mL polymyxin B to probe permeabilized cells. IRDye680LT-maleimide (LI-COR) was added for dye-labelling as described above. Cell pellets were re-suspended in 50 µL of urea-lysis buffer and subjected to one freeze-thaw cycle to extract proteins. Urea-soluble proteins (5 µL) were resolved by SDS-PAGE and analyzed by immunoblotting using anti-TPS domain antisera.

Immunoblotting

Urea-soluble protein samples (5 µL) were analyzed by SDS-PAGE on Tris-tricine 6% polyacrylamide gels run at 100 V (constant) for 3.5 h. Gels were soaked for 15 min in 25 mM Tris, 192 mM glycine (pH 8.6), 10% methanol, then electroblotted to low-fluorescence PVDF membranes using a semi-dry transfer apparatus at 17 V (constant) for 1 h. Membranes were blocked with 4% non-fat milk in PBS for 1 h at room temperature, and incubated with primary antibodies in 0.1% non-fat milk, PBS overnight at 4 °C. Rabbit polyclonal antisera (Cocalico Biologicals, Stevens, PA) to the N-terminal TPS domain was used at a 1:10,000 dilution. Blots were incubated with 800CW-conjugated goat anti-rabbit IgG (1:40,000 dilution, LICOR) in 0.1% non-fat milk in PBS. Immunoblots were visualized with a LI-COR Odyssey infrared imager.

Pectin agar assay

LB-agar made with 0.1% m/v final concentration pectin was autoclaved to sterilize and melt the pectin. When cooled enough, antibiotics and 1% Ruthenium Red solution (0.004% m/v final) were added and poured to petri dish. *E. coli* MG1655 *Δwzb ΔtsxΔompT* (CH14017) carrying CdiA-PmeA expression plasmid were grown on LB as described above. Cultures were diluted in 1X M9 salts and spread on Pectin agar plates. Zone of ruthenium red staining is analyzed after ON growth at 37 °C.

Cell-cell adhesion by flow cytometry.

Receptor-binding studies were conducted using *E. coli* strain CH5570 (MG1655 *Δwzb ΔtsxΔompT*) which expresses gfp-mut3 from the papBA promoter (113). *E. coli* CH5570 cells were transformed with pCH450-derived CdiA-RBD^{colicin} expression plasmids and the resulting strains grown at 37 °C in LB media supplemented with Tet until the cells became fluorescent. *E. coli* ZR373 cells carrying plasmid pDsRedExpress2 were used as targets. Targets were also provided with plasmid pCH450 (control), pCH13603 (*tsx+*), pCH4101 (btuB overexpressed), or pCH4102 (cirA overexpressed). ZR373 target still carries chromosomal btuB and cirA. Target cells were grown overnight in LB supplemented with Tet, Amp, 0.4% L-arabinose and 1 mM IPTG to induce expression of Tsx and DsRed prior to mixing with inhibitors. GFP-labeled inhibitor cells were mixed at a 5:1 ratio with DsRed-labeled target bacteria at a final OD600 ~ 0.2. Cell suspensions were shaken at 30 °C for 20 min, diluted into 1X PBS, vortexed briefly, then analyzed on an Accuri C6 flow cytometer using FL1 (533/30nm, GFP) and FL2 (585/40nm, DsRed) fluorophore filters. The fraction of target bacteria bound to inhibitor cells was calculated as the number of dual green/red

fluorescent events divided by the total number of red fluorescent events. More than 2,000 red fluorescent events were scored for each cell mixture.

Competition co-cultures.

E. coli CH14017 (MG1655 Δ*wzb* Δ*tsx* Δ*ompT*) that harbor CdiA-RBD^{colicin} expression plasmids were used as inhibitor cells in shaking broth co-cultures. *E. coli* CH14017 strains that carry pCH14047 (*tsx*+) were used as target cells. Cells were grown in LB media at 37 °C to mid-log phase, adjusted to OD600 ~ 0.3 and mixed at a 1:1 ratio (5 mL total volume) and incubated with shaking for 3 h at 37 °C. Culture aliquots were taken at the beginning of co-culture and after 3 h to quantify viable inhibitor and target cells as colony forming units per milliliter (CFU mL^{-1}). Cell suspensions were serially diluted into 1X M9 salts and plated onto LB-agar supplemented with Amp to enumerate inhibitor cells, and LB-agar supplemented with Kan to enumerate target cells. Competitive indices were calculated as the ratio of target to inhibitor cells at 3 h divided by the initial target to inhibitor cell ratio.

E. Figures and tables

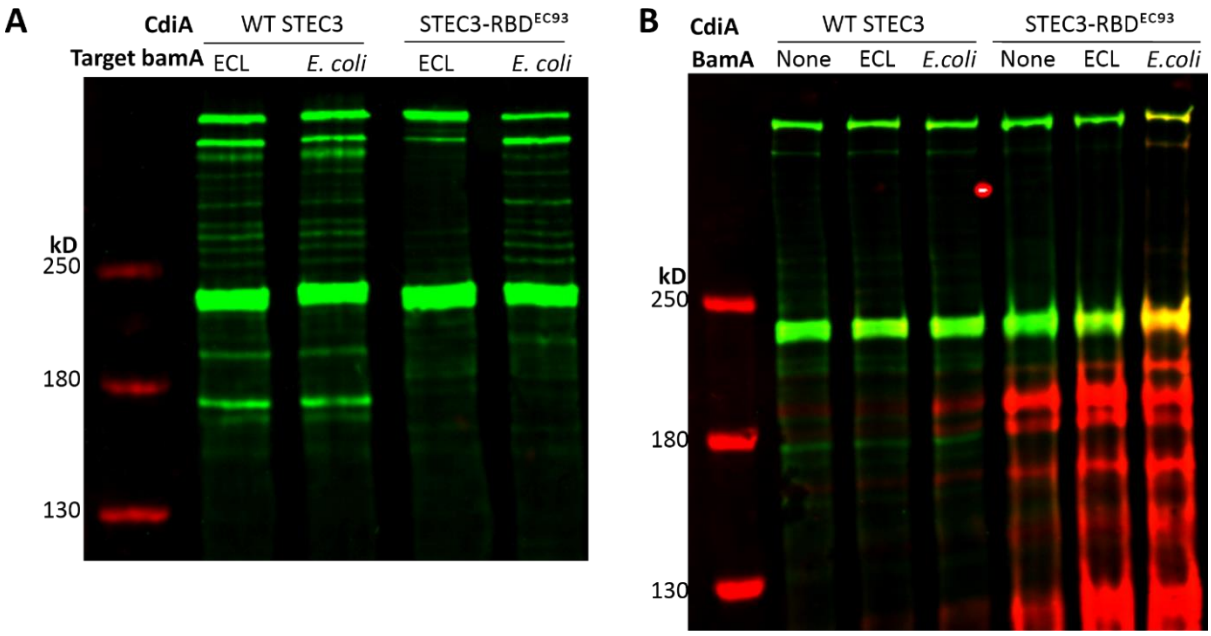

Figure 1. CdiA binds to purified receptor to release the secretion arrest. Tsx-binding RBD of CdiA^{STEC3} has been replaced with the BamA-binding RBD from CdiA^{EC93}. (A) Cell mixing with *E. coli* targets expressing either ECL BamA or *E. coli* BamA. CdiA immunoblot shows RBD^{EC93} specifically recognizes *E. coli* BamA to delivery CdiA-CT. (B) CdiA immunoblot after mixing in purified BamA. Periplasmic cysteine at 1726 is labelled with maleimide-dye to report export. BamA does not need to be on a live cell surface to serve as a CdiA receptor.

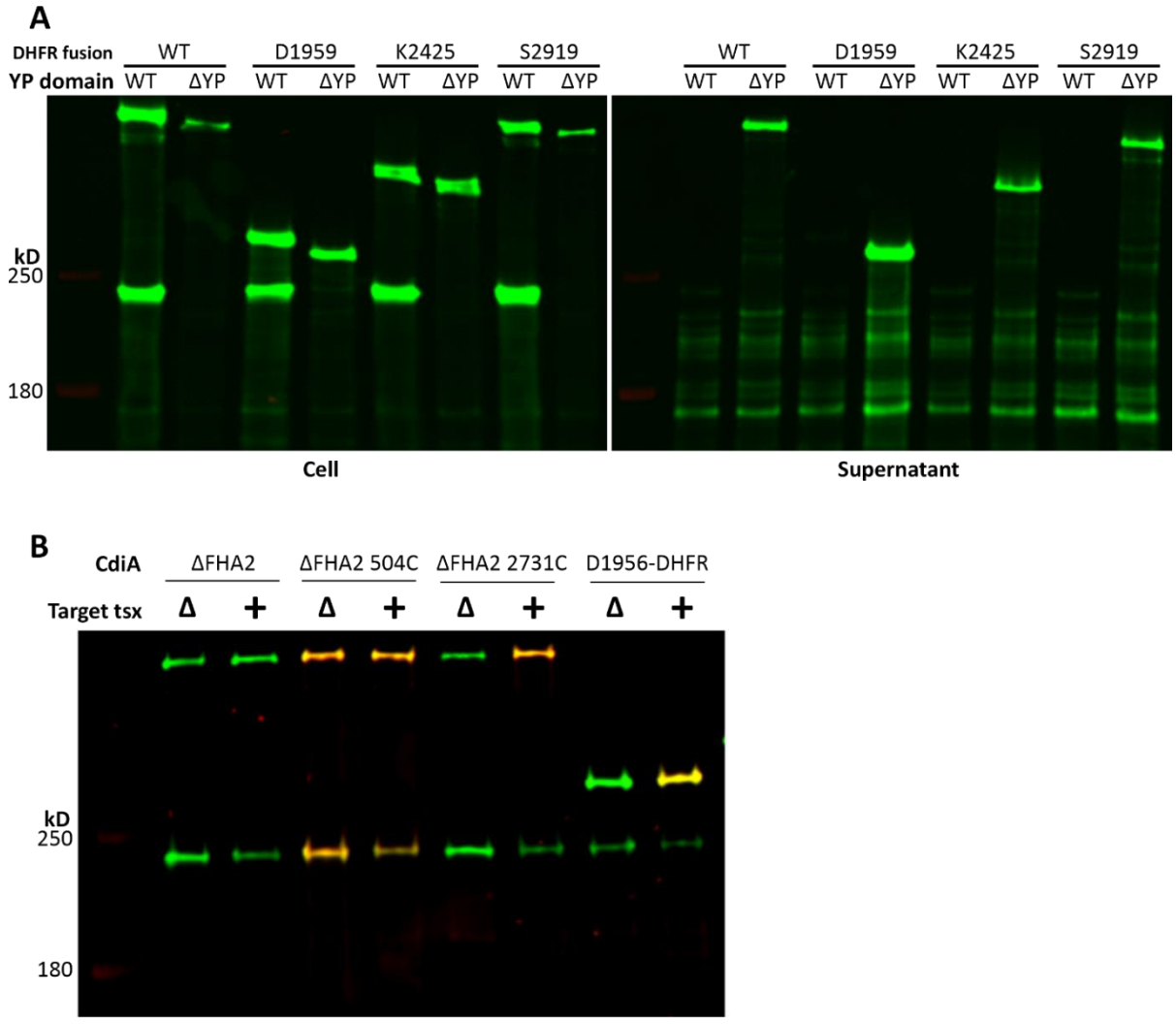

Figure 2. Periplasmic DHFR fusion can be exported via CdiB. DHFR is fused at various position of the C-terminal CdiA. (A) CdiA immunoblot of cell/sup fractions. CdiA-DHFR fusion at all three positions are exported through CdiB. Secretion of the DHFR domain is induced by deletion of the YP-100 domain. (B) CdiA immunoblot after mixing in target cells followed by maleimide labelling. Receptor-dependent export of DHFR is visualized by labeling of the native Cys. ΔFHA2 CdiA was used as a control to mimic a domain that gets exported but not fully delivered into target cells. 504Cys is an extracellular control. 2731C is a periplasmic control.

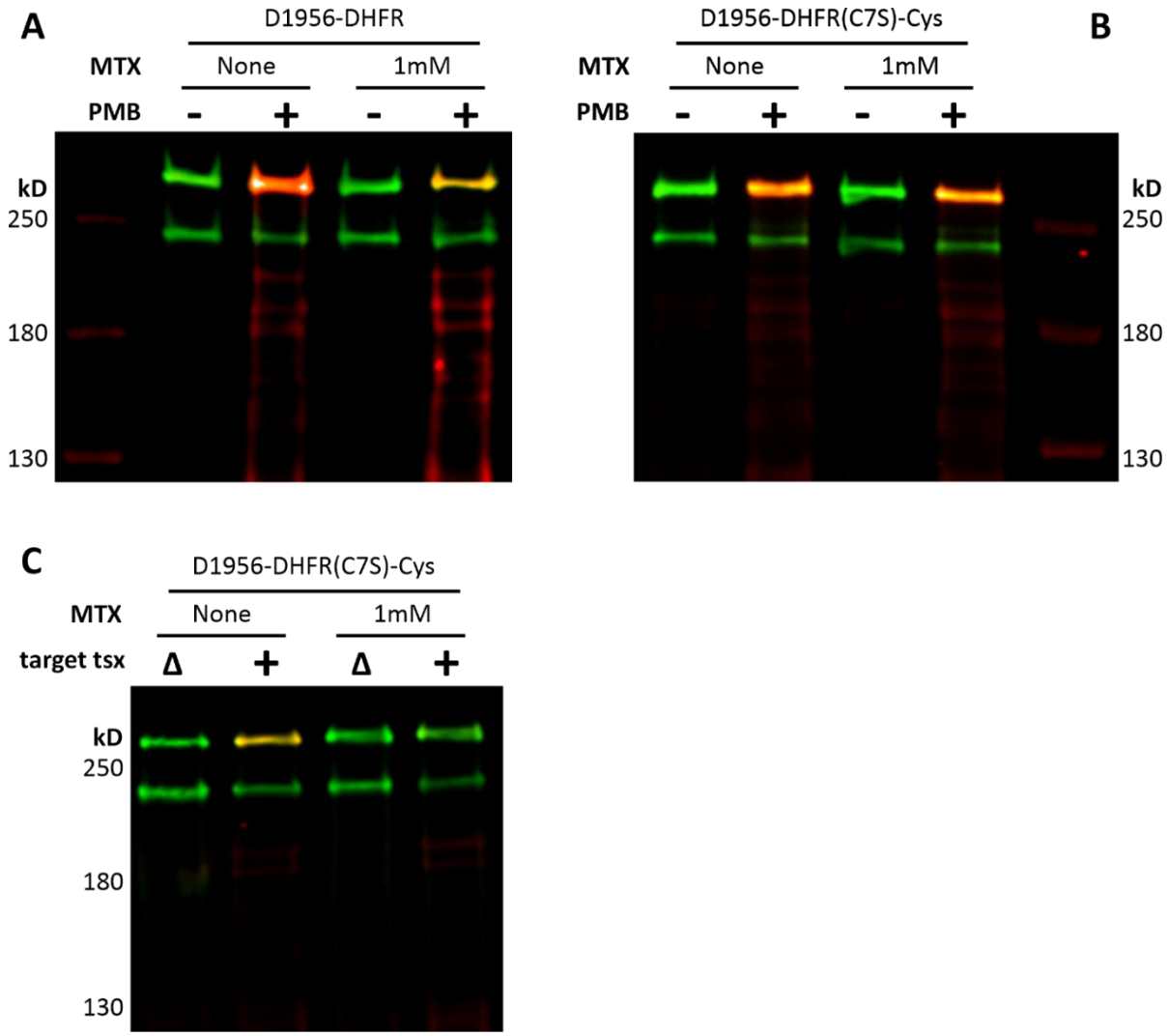

Figure 3. C-terminal half is unfolded during resumed secretion. CdiA immunoblots of DHFR fusion at CdiA(D1956) after maleimide-dye labeling. (A) Maleimide-dye reactivity in the periplasmic DHFR is probed by treating the cells with PMB. DHFR domain folds tightly when methotrexate (MTX) is introduced at 1mM. Reduced dye reactivity of the Cys in DHFR suggests folding-induced occlusion. (B) The native Cys in DHFR is mutated to a Ser. A C-terminal Cys is added which dye-reactivity does not change with DHFR folding. (C) Maleimide-dye reactivity of exported DHFR is probed by mixing in tsx+ target cells. MTX-induced folding prevents DHFR export.

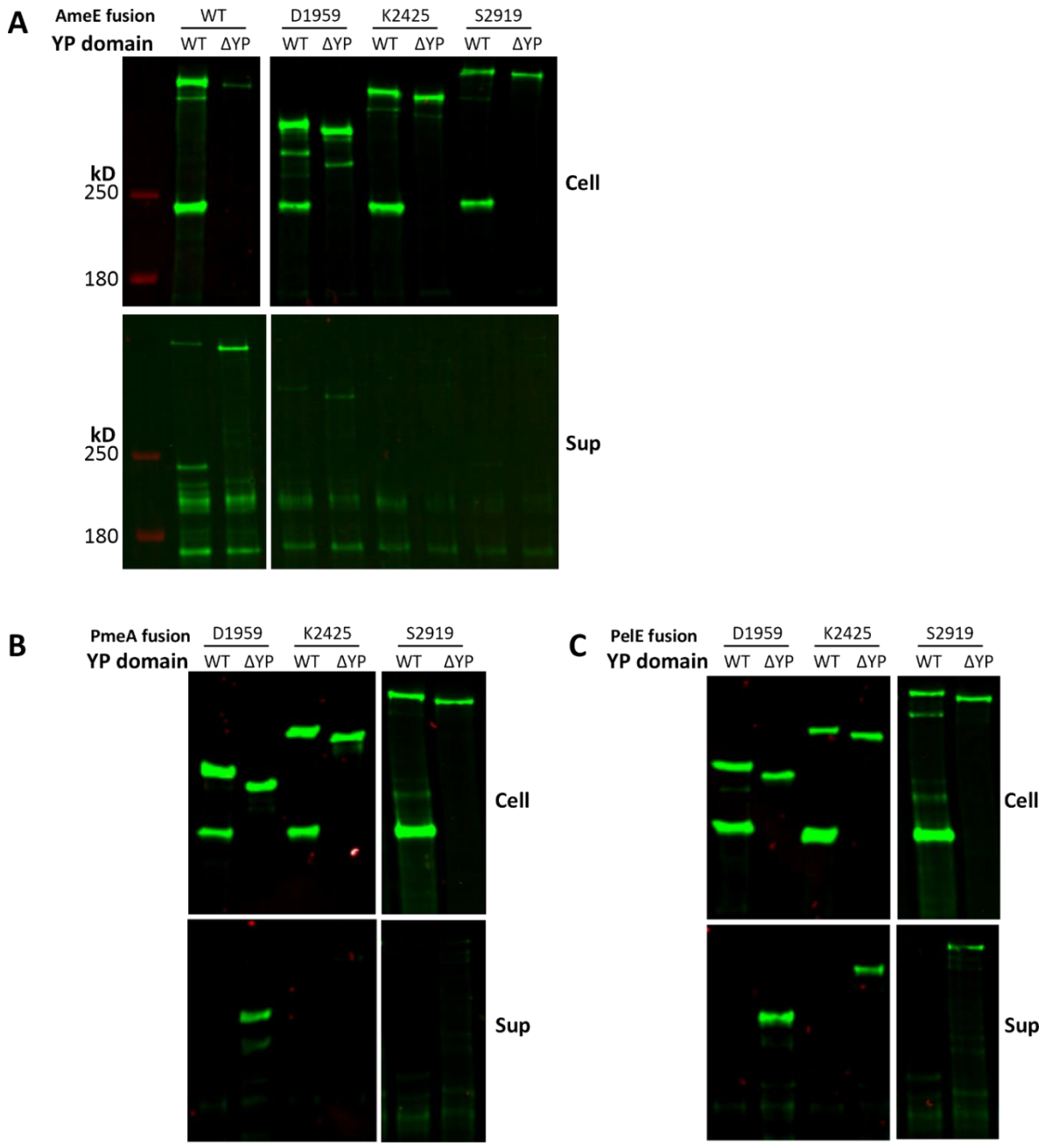

Figure 4. CdiA-Enzyme fusions. CdiA immunoblots of enzyme fusion at D1956, K2425, and S2919. after maleimide-dye labeling. Secretion of the enzymatic domains is induced by deletion of the YP-100 domain. (A) AmyE fusions at the three positions of CdiA. AmyE is not readily secreted through CdiB. (B) PmeA fusions at the three positions of CdiA. PmeA is only secreted when fused at D1956. (C) PelE fusions at the three positions of CdiA. PelE is readily secreted at all three fusions.

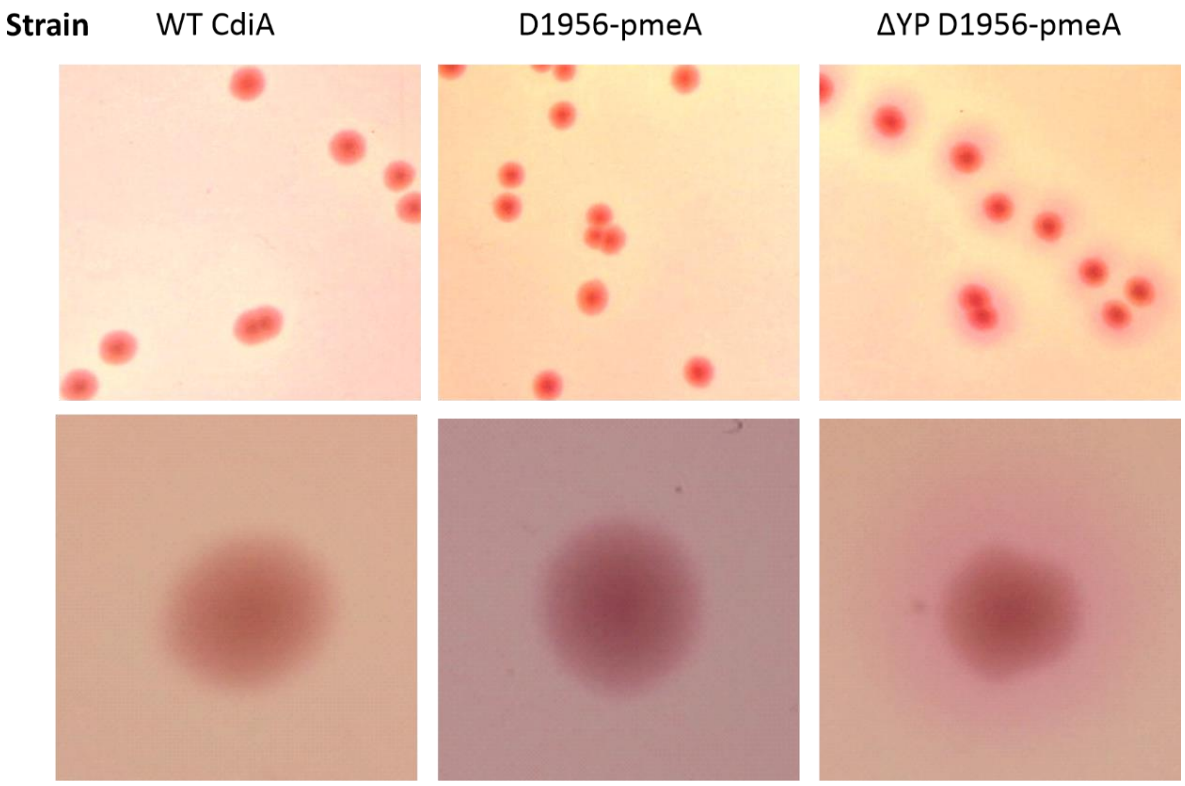

Figure 5. Export of PmeA is visualized on pectin agar plate. Top: *E. coli* cells expressing CdiA(D1956)-PmeA are plated on pectin agar with ruthenium red dye. Bottom: closeup of a colony from each plate. Deletion of the YP-100 domain forces export of PmeA which then demethylates pectin and increases affinity to ruthenium red dye (last column). These cells have red halos around the colonies.

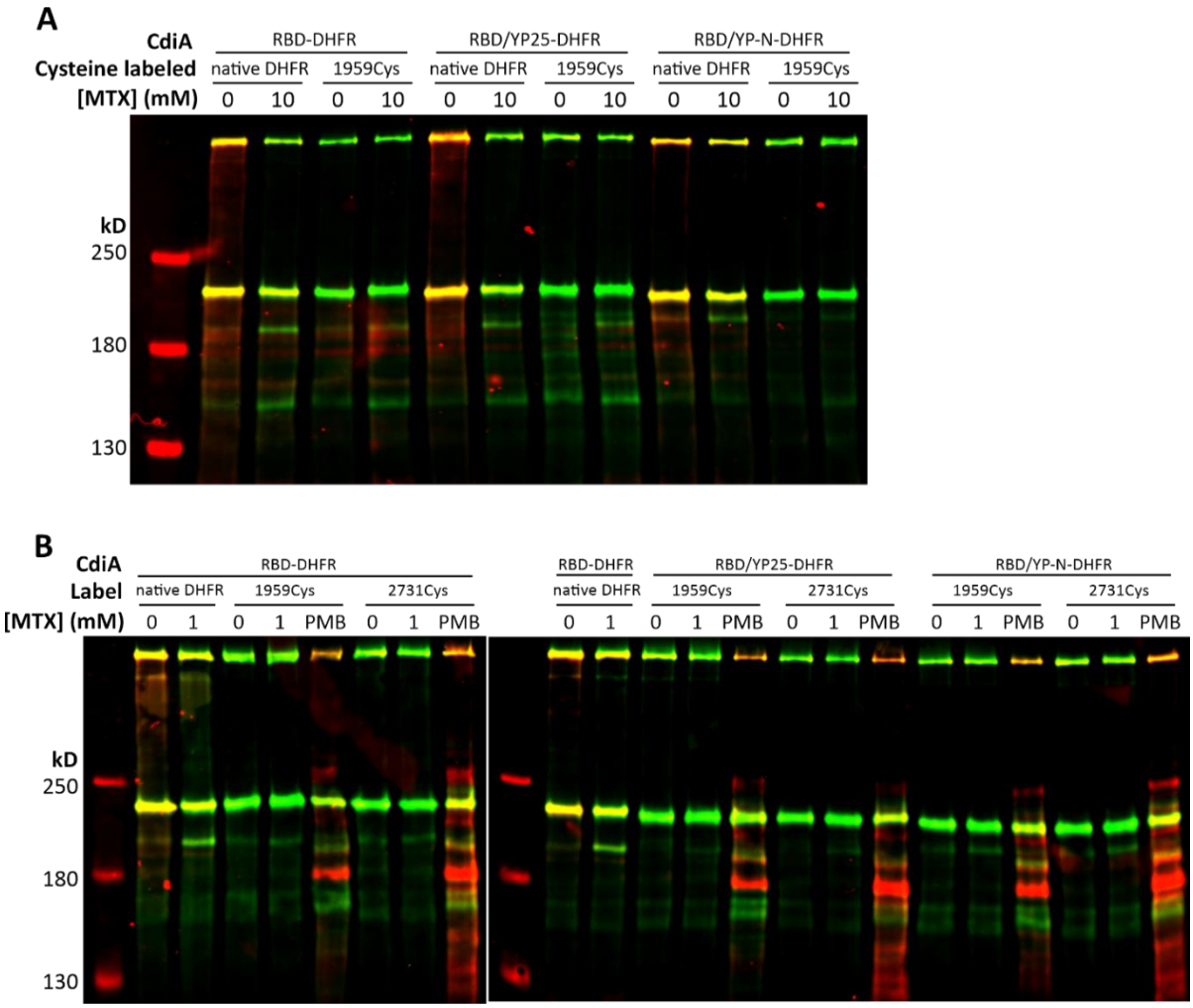

Figure 6. RBD replaced with DHFR does not export periplasmic CdiA with MTX. CdiA RBD and increasing portions of the extended YP domain is replaced with DHFR. MTX is introduced to induce DHFR folding, visualized by reduced maleimide reactivity of the native Cys. Folding-induced export of the periplasmic CdiA is visualized by maleimide labeling of periplasmic Cys. (A) 10mM MTX induces folding of DHFR replacing the RBD. But DHFR replacing RBD and YP-N still maintains significant dye reactivity, suggesting insufficient folding. (B) The C-terimnal CdiA remains in the periplasm even with 1mM MTX. Periplasmic residues are probed by PMB treatment.

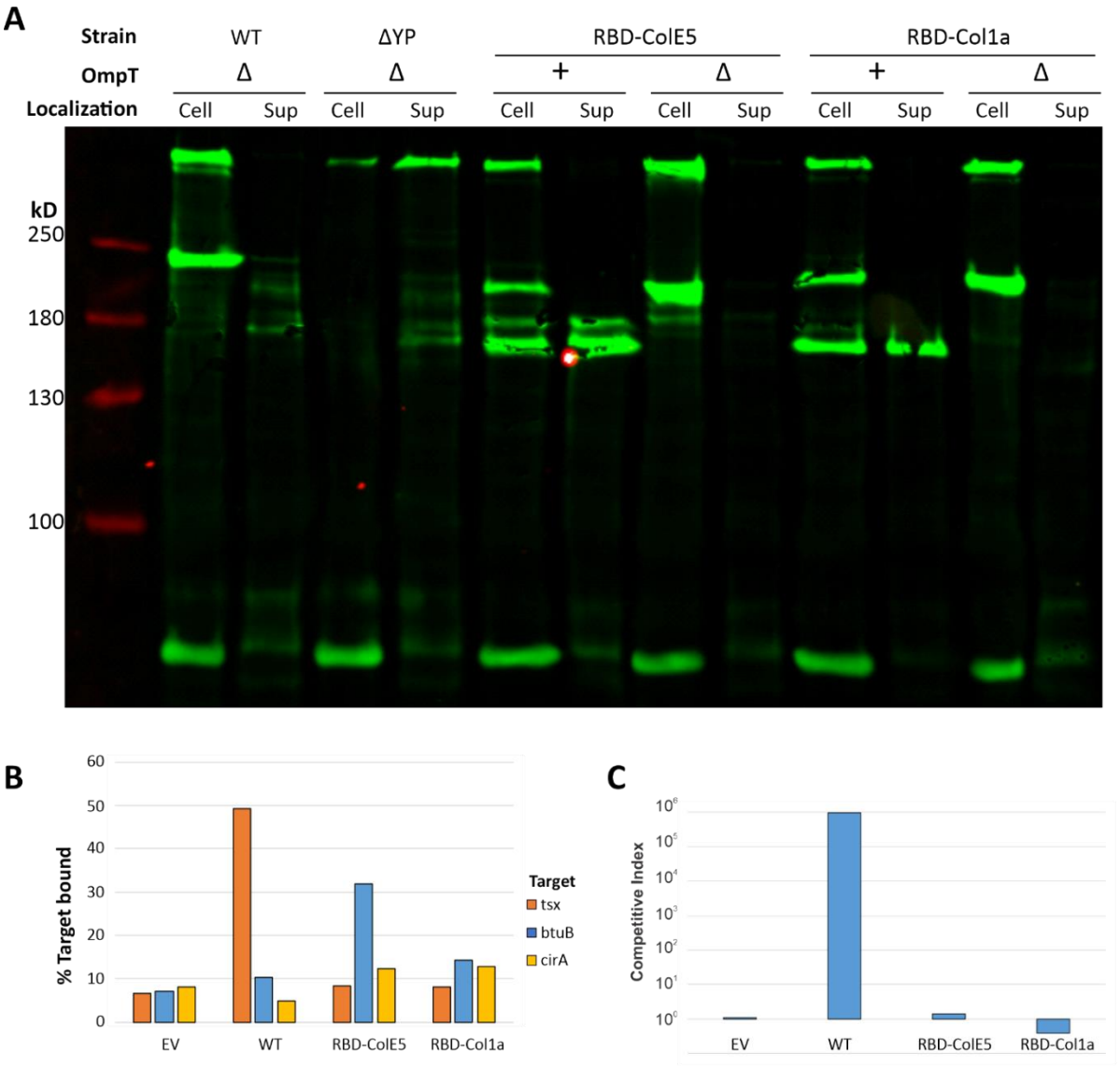

Figure 7. RBDcolicin cannot replace CdiA RBD. CdiA RBD is replaced with RBD from ColE5 and Col1a. (A) CdiA immunoblot of cell/sup fractions. $RBD^{colicin}$ chimeras are aberrantly cleaved around the cite of replacement, releasing the N-terminal fragment into the supernatant. This cleavage is OmpT-dependent. (B) Target cell adhesion measured by flow cytometry. GFP-labeled inhibitors were mixed with DsRed-labeled targets overexpressing each receptor. (C) Competition co-cultures. Inhibitors were mixed at a 1:1 ratio with targets. Competitive indices equal the final ratio of inhibitors to targets divided by the initial ratio.

Table 1. Strains used in this study.

Strains	Description	Reference
CH14016	*E. coli* MG1655 Δwzb Δtsx	(165)
CH14017	*E. coli* MG1655 Δwzb Δtsx ΔompT	(165)
CH5570	*E. coli* MG1655 Δwzb Δtsx ΔompT PpapIB-gfp-mut3	This study
ZR373	*E. coli* EPI100 Δwzb Δtsx	(165)
CH2016	*E. coli* X90 (DE3) Δrna ΔslyD::kan	(181)
CH13001	*E. coli* MC4100 rifR ΔarfB::kan::BamA (Δ2014-2043)	This study
CH9604	*E. coli E*PI100 ΔbamA:cat	This study

Table 2. Plasmids used in this study.

Plasmid	Description	Reference
pCH9216	pSH21::(Δss)bamAEco; overproduces E. coli BamA lacking the signal sequence peptide; Amp^R	(105)
pCH9231	pSH21::(Δss)bamAECL; overproduces E. cloacae BamA lacking the signal sequence peptide; Amp^R	(105)
CH9591	pZS21:bamA(ECL); Kan^R	(105)
CH9604	pZS21:bamA(*E. coli*)); Kan^R	(105)
CH2574	pET21b::CdiBAI (STEC3); Amp^R	This study
CH2575	pET21b::CdiBAI (STEC3-EC93 RBD); Amp^R	Nicole Chan
CH14563	pET21b-cdiBAI (STEC_O31 J2M139) (MCS-) 2918Nhe; Amp^R	Chapter III
CH14591	pET21b::cdiBA (STEC) D1956-amyE fusion; Amp^R	This study
CH14592	pET21b::cdiBA (STEC) K2425-amyE fusion; Amp^R	This study
CH14593	pET21b::cdiBA (STEC) S2919-amyE fusion; Amp^R	This study
CH14736	pET23a-tp22-DHFR; Amp^R	Chris Hayes
CH3809	pET21b::cdiBA (STEC) D1956-DHFR; Amp^R	This study
CH3810	pET21b::cdiBA (STEC) K2425-DHFR; Amp^R	This study
CH3811	pET21b::cdiBA (STEC) S2919-DHFR; Amp^R	This study
CH3812	pET21b::cdiBA (STEC) ΔP1658-N1757 DHFR (D1956); Amp^R	This study
CH3813	pET21b::cdiBA (STEC) ΔP1658-N1757 DHFR (K2425); Amp^R	This study
CH3814	pET21b::cdiBA (STEC) ΔP1658-N1757 DHFR (S2919); Amp^R	This study
CH3815	pET21b::cdiBA (STEC_O31 J2M139) D1956-pelE; Amp^R	This study
CH3816	pET21b::cdiBA (STEC_O31 J2M139) K2425-pelE; Amp^R	This study
CH3817	pET21b::cdiBA (STEC_O31 J2M139) S2919-pelE; Amp^R	This study

CH3818	pET21b::cdiBA (STEC_O31 J2M139) ΔP-rich D1956-pelE; Amp^R	This study
CH3819	pET21b::cdiBA (STEC_O31 J2M139) ΔP-rich K2425-pelE; Amp^R	This study
CH3820	pET21b::cdiBA (STEC_O31 J2M139) ΔP-rich S2919-pelE; Amp^R	This study
CH3821	pET21b::cdiBA (STEC_O31 J2M139) D1956-pmeA; Amp^R	This study
CH3822	pET21b::cdiBA (STEC_O31 J2M139) K2425-pmeA; Amp^R	This study
CH3823	pET21b::cdiBA (STEC_O31 J2M139) S2919-pmeA; Amp^R	This study
CH3824	pET21b::cdiBA (STEC_O31 J2M139) ΔP-rich D1956-pmeA; Amp^R	This study
CH3825	pET21b::cdiBA (STEC_O31 J2M139) ΔP-rich K2425-pmeA; Amp^R	This study
CH3826	pET21b::cdiBA (STEC_O31 J2M139) ΔP-rich S2919-pmeA; Amp^R	This study
CH14404	pET21b:cdiBAI (STEC_O31 J2M139) ΔP-rich Xho killed; Amp^R	This study
CH2522	pET21b::cdiBA (STEC3) D1956-DHFR(C7S)-Cys-FLAG; Amp^R	This study
CH2523	pET21b::cdiBA (STEC3) K2425-DHFR(C7S)-Cys-FLAG; Amp^R	This study
CH2524	pET21b::cdiBA (STEC3) S2919-DHFR(C7S)-Cys-FLAG; Amp^R	This study
CH2207	pET21b-cdiBAI (STEC_O31 J2M139) (MCS-) ΔRBD EcoBam (1726C) ; Amp^R	Chapter III
pZR435	pET21b::cdiBA(G1726C)I (STEC_O31 J2M139); Amp^R	(165)
pZR439	pET21b::cdiBA(D1959C)I (STEC_O31 J2M139); Amp^R	(165)
pZR442	pET21b::cdiBA(S2731C)I (STEC_O31 J2M139); Amp^R	(165)
CH4589	pET21b::cdiBAI(STEC3) RBD(1959C)-DHFR(C7S); Amp^R	This study
CH4590	pET21b::cdiBAI(STEC3) RBD(2731C)-DHFR(C7S); Amp^R	This study
CH4591	pET21b::cdiBAI(STEC3) RBD-YP25(1959C)-DHFR(C7S); Amp^R	This study
CH4592	pET21b::cdiBAI(STEC3) RBD-YP25(2731C)-DHFR(C7S); Amp^R	This study
CH4593	pET21b::cdiBAI(STEC3) RBD-YP1(1959C)-DHFR(C7S); Amp^R	This study
CH4594	pET21b::cdiBAI(STEC3) RBD-YP1(2731C)-DHFR(C7S); Amp^R	This study
CH5397	pET21b::cdiBAI(STEC3) ΔRBD (EcoRI/BamHI); Amp^R	This study
CH5398	pET21b::cdiBAI(STEC3) ΔRBD-YP25aa; Amp^R	This study
CH5400	pET21b::cdiBAI(STEC3) ΔRBD-YP1; Amp^R	This study
CH5402	pET21b::cdiBAI(STEC3) RBD-DHFR; Amp^R	This study
CH5404	pET21b::cdiBAI(STEC3) RBD-YP25-DHFR; Amp^R	This study
CH5406	pET21b::cdiBAI(STEC3) RBD-YP1-DHFR; Amp^R	This study

CH288	pET21(MCS-)::STEC3(RBD-ColE5); Amp^R	This study, Chris Hayes
CH5367	pET21(MCS-)::STEC3(RBD-Col1a); Amp^R	This study
pCH450	pAraBAD, Tet^R	(157)
pCH450Kpn	Kpn version of pCH450; Tet^R	Chris Hayes
CH4101	pCH450kpn-btuB; Tet^R	This study
CH4102	pCH450-cirA; Tet^R	This study

Table 3. Oligonucleotides used in this study.

Primer	Name	Sequence	Reference
CH4603	amyE-Nco-Spe-for	5' - AAA CCA TGG ATA CTA GTC TTA CAG CAC CGT CGA TCA AAA G - 3'	This study
CH4604	amyE-AflII-Spe-for	5' - AAA CTT AAG ACT AGT CTT ACA GCA CCG TCG ATC AAA AG - 3'	This study
CH4605	amyE-Nhe-Spe-for	5' - AAA GCT AGC ACT AGT CTT ACA GCA CCG TCG ATC AAA AG -3'	This study
CH4606	amyE-Xho-rev	5' - TTT CTC GAG TCA ATG GGG AAG AGA ACC GGA TAA G - 3'	This study
CH4683	DHFR-Spe-for	5' - AAA ACT AGT ATG GTT CGA CCA TTG AAC TGC - 3'	This study
CH4684	DHFR-Xho-rev	5' - TTT CTC GAG TTA GTC TTT CTT CTC GTA GA - 3'	This study
CH4692	pelE-Spe-for	5' - AAA ACT AGT GCC AGT CTG CAA ACC ACC - 3'	This study
CH4693	pelE-Xho-rev	5' - TTT CTC GAG TTA CAG TTT ACC GTA GCC CGC - 3'	This study
CH4694	pmeA-Spe-for	5' - AAA ACT AGT GCG ACC ACC TAC AAC GC -3'	This study
CH4695	pmeA-Xho-rev	5' - TTT CTC GAG TCA GGG TAA TGT CGG CGT C -3'	This study
CH4806	DHFR-C75-Spe-for	5' - GAT ACT AGT ATG GTT CGA CCA TTG AAC AGC ATC - 3'	This study
CH4807	DHFR-Cys-FLAG-rev1	5' - TCG TCT TTG TAG TCG CAG TCT TTC TTC TCG TAG ACT TCA AA - 3'	This study
CH4808	DHFR-Cys-FLAG-Xho-rev2	5' - TTT CTC GAG TTA CTT GTC GTC ATC GTC TTT GTA GTC GCA - 3'	This study
CH4904	DHFR-Eco-for	5' - AAA GAA TTC GAT GGT TCG ACC ATT GAA C - 3'	This study
CH4905	DHFR-Bam-rev	5' - TTT GGA TCC GTC TTT CTT CTC GTA GAC TTC -3'	This study
CH4906	STEC3-G1708-Bam-for	5' - AAA GGA TCC GGG CAG GCA CCA CG -3'	This study
CH4907	STEC3-P1683-Bam-for	5' - AAA GGA TCC CCG AAA CTG GAT GGT CTC G -3'	This study

CH4242	STEC-Nco/Not-rev	5' - TTT GCG GCC GCC CAT GGC ACT GAC AGA GG - 3'	(165)
CH4944	colE5-E320-Eco-for	5' - TGA GAA TTC TGA GCG AAA TTA TGA ACG CG - 3'	This study
CH4945	colE5-N438-Bam-rev	5' - ATC GGA TCC ATT ATC CTC TTT CTT CTT CCT GC - 3'	This study
CH4946	col1A-RBD-Eco-for	5' - TTT GAA TTC CAG AGC CAT TTC AGA GGC CC - 3'	This study
CH4947	col1A-RBD-Bam-rev	5' - TTT GGA TCC TTT TTC CTT CAA CAG GGC ATT AAG AGC - 3'	This study
CH5042	btuB-Kpn-for	5' - TGC GGT ACC ATG ATT AAA AAA GCT TCG CTG - 3'	This study
CH5043	btuB-Xho-rev	5' - TGG CTC GAG GTT CAG AAG GTG TAG CTG -3'	This study
CH5044	cirA-Eco-for	5' - TGG GAA TTC GGA ATG TTT AGG TTG AAC CC - 3'	This study
CH5045	cirA-Xho-rev	5' - TTC CTC GAG CAT CTT CTC ATC AGA AGC - 3'	This study

Chapter V: CdiA filament a robust toxin-delivering machinery which tolerates shortening and severing

This work has not been published yet. $tRNA^{Glu}$ northern blot was done by Quan Nhan. I produced all other data presented in the chapter.

A. Introduction

Two-partner secretion (TPS) system is an example of the type V secretion system (T5SS) in Gram-negative bacteria which specializes in export of large filamentous proteins across the outer membrane (67,182). TPS is composed of a TpsB protein which forms an outer membrane β-barrel transporter and a TpsA cargo which gets transported to the extracellular space (67,182). Secretion of the TpsA is dependent on recognition of a conserved TPS domain at the N-terminus of the cargo proteins by the periplasmic POTRA domain of the TpsB (92,168,183). Size of the TpsA proteins varies but they carry conserved FHA-1 domain which adapts a β-helical fold upon export which is thought to drive the secretion (96,99). Once exported, TpsA filaments serve diverse role such as cytolysis (184,185), adhesin (186,187), iron acquisition (188), and contact-dependent growth inhibition (70). A review by Guerin *et al.* highlights this diversity among TpsA proteins (182).

Contact-dependent growth inhibition (CDI) is a TPS system found in diverse proteobacteria (70,74). CDI+ inhibitor cells use CdiB (a TpsB transporter) to export CdiA effector (a TpsA cargo) which then delivers the C-terminal toxin (CdiA-CT) to a neighboring cell upon cell-to-cell contact (70,74). The N-terminal half of CdiA is exported which forms a 33nm long filament on cell surface (165). The receptor-binding domain which facilitates

binding to a neighboring cell is located at the tip of the filament (105,165). Receptor-binding controls the export of the remaining C-terminal half from the periplasm which then delivers the CdiA-CT to kill the target cell (165).

Previously, deletion analysis showed that a 100-residue deletion in the N-terminal CdiA filament did not hinder toxin delivery (165). It is unclear what the function of the CdiA filament is. In this chapter, I will further dissect the importance of the CdiA filament by making larger deletions and guiding protease cleavage at specific sites. It is also unclear where the TPS domain is localized after CdiA export has been initiated. Some think that the TPS domain of well-studied *Bordetella pertussis* FhaC lingers in the periplasm and maintains its interaction with the POTRA domain (94). However, this model exerts too much toll on the CdiB transporter which much accommodate a hairpin like topology of CdiA. Using the cysteine scanning and topology mapping, I will show that CdiA TPS domain gets exported to the extracellular space along with the FHA-1 domain which folds to the filament. Lastly, I will demonstrate that N-terminal half of CdiA forms a robust filament which resists proteolysis and tolerates severing at the base to stably present the RBD and deliver CdiA-CT.

B. Results

Shortened CdiA filaments still support toxin delivery

Previously, 100-residue deletion of the filament did not have any effect in toxin delivery (165). To further investigate the significance of the N-terminal CdiA which forms the 33nm filament (165), I made a series of in-frame deletions removing increasing numbers of the FHA1 repeats (Table 1). The length of the filament removed the deletions is predicted based on reported β-helical structure in which each ~20 repeat motif extends the helix by 4.8

Å (99,100). The smallest deletion (ΔL507-T662) removed 156 residues and should encode for the longest filaments among the mutants. The largest deletion (ΔL507-T1303) removed 797 residues and should encode for the shortest filament.

Surprisingly, all shortened filaments inhibited target cells (Figure 1A and B). Anti-CdiA immunoblot showed that biogenesis was undisturbed because there was no sign of aberrant cleavage by outer membrane proteinases like OmpT (Figure 1C and D). After mixing in Tsx+ targets, the periplasmic half resumed secretion as reported by maleimide-dye labelling of periplasmic 1726Cys (Figure 1C and D). The two shortest mutant filaments began to show some defective insertion into target outer membrane after receptor-dependent export. In these mutants, significant portion of the "full-length" or CT+ band is labelled with the maleimide-dye (Figure 1D). The inhibitory activity of these the shorted filaments were also weaker than the WT control (Figure 1B). Nonetheless, all six short filaments still delivered the toxin effector in a receptor-dependent manner.

The TPS domain is a part of the extracellular filament

Because the TPS domain of CdiA interacts with the POTRA domain of CdiB, it has been proposed that the TPS domain remains in the periplasm while the rest of the CdiA domain gets exported through the lumen of CdiB. However, this model puts too much spatial toll on CdiB considering our recent finding on secretion arrest of CdiA (165). If the TPS domain remains periplasmic, then the CdiB lumen must accommodate two folds of CdiA polypeptide chain and support the resumed secretion of the C-terminal CdiA after receptor-binding. Alternatively, the POTRA may recognize CdiA cargo by initial interaction with the TPS domain, then export the TPS making it a part of the extracellular filament. The TPS then

can possibly interact with one of the extracellular loops of the CdiB to present the rest of the CdiA filament facing away from the surface. Then the lumen would be dedicated for the extended region traveling back from the NT-half to the periplasmic half, later to accommodate the periplasmic half exporting during resumed secretion. In this model, a cysteine introduced in the TPS domain would be extracellularly labelled by the maleimide-dye used for topology mapping.

The crystal structure of the TPS domain from FhaB forms three faced beta helix resembling the rest of the FHA filament (95). Based on this model, I have selected 6 residues predicted to face outward and changed them to Cys: three at the bottom of the TPS beta helix and three at the top (Figure 2A and B). Even if the TPS domain is extracellular, one of more of these faces may be interacting with CdiB loops thus inaccessible to maleimide-dye. Therefore, I mutated two residues on each face, one at the top and the other at the bottom (Figure 2A).

Maleimide-dye was introduced to label the extracellular cysteines. Dye reactivity was compared to when cells were treated with PMB to permeabilize the outer membrane, exposing periplasmic cysteines. Five positions (69Cys, 75Cys, 244Cys, 252Cys, and 257Cys) were extracellularly labelled suggesting the TPS domain is exported after its initial interaction with the POTRA domain (Figure 2C). One position, 64Cys was not labeled even when the outer membrane is permeabilized most likely due to structural occlusion (Figure 2B). When CdiA with 64Cys was expressed without CdiB, whole CdiA was retained in the periplasm, and the cysteine was labeled with the dye upon PMB treatment (Figure 2D). This strongly suggests that dye inaccessibility at this position is likely due to interaction with

CdiB rather than occlusion from secondary structure around the residue. As control, 69Cys was also probed to show what a surface available residue looks like.

The extended region is tightly packed against the filament

Extracellular CdiA has been shown to be trypsin-resistant, suggesting that the filament forms a tightly packed structure on cell surface with minimal loose structure (Figure 3A, WT lanes). The extended region traversing down the filament must be packed against the filament in a tight structure. To investigate how structural disturbance introduced by deletions change protease-sensitivity, I have exposed various in-frame deletions in the N-terminal CdiA to tryptic digest (Figure 3A). As expected, the WT CdiA resisted tryptic digest but previous reported 100-residue deletions in the FHA1 (ΔD900-A999) and the receptor-binding domains (ΔN1400-S1499) (165) were susceptible to tryptic digest (Figure 3A). The 100-residue FHA1 deletion was out of sync with FHA1 repeat structure thus must have disrupted the filament's folding pattern. Interestingly, a deletion in sync with FHA repeats (ΔL507-T662) was mostly resistant to trypsin despite having a larger deletion than the 100-residue FHA1 deletion (Figure 3A and B). Subsequently larger deletions of the FHA repeats deemed the CdiA filament susceptible to tryptic digest (Figure 3B).

When trypsin was able to cleave CdiA due to deletion-induced exposure, the resulting NT half was released to the supernatant as shown in the anti-CdiA-NT immunoblot (Figure 3B). The C-terminal half of CdiA is periplasmic so it remained in the cell fraction (Figure 3B). It is notable that the N-terminal fragment after tryptic digest of ΔD900-A999 was smaller than those from digesting clean FHA1 repeat deletions (Figure 3A and B). Deletion of ΔD900-A999 begins at residue 900 while the FHA1 repeat deletions begin at residue 507.

This suggests that trypsin cleaved at around residue 900 where the filament structure has been compromised in ΔD900-A999 mutant. However, trypsin cut FHA1 repeat deletions further downstream in the extended YP domain which is traveling down the filament back into the periplasm. The clean FHA1 deletions mostly likely left the filament structure intact but created some slacks at the extended YP domain, exposing the region to trypsin.

Severed CdiA can still deliver CT-toxin

I introduced TEV protease sites at various points along the NT-half of CdiA to specifically direct protease cleavage and observe how disconnected CdiA filament functions. I made total of 6 TEV site insertions at the following positions: 505, 1270, 1279, 1305, 1383, and 1662. TEV sites in the FHA1 repeats (1270, 1279, and 1305) were resistant to TEV cleavage suggesting FHA1 domains fold tightly to form the CdiA filament (Figure 4A). TEV1383 is inserted very near the RBD and interfered with receptor-binding as shown in flow cytometry (Figure 4B). As a result, the target cell growth was not inhibited (Figure 4C).

Two TEV insertions at 505 and 1662 were susceptible to TEV cleavage (Figure 6). Both insertions still delivered the C-terminal toxin and killed target cells (Figure 4C and D). These two insertions were further investigated to see what happens to the severed CdiA filament. When CdiA 505TEV was cleaved, a short N-terminal fragment was released to the supernatant (Figure 5A, left). Predicted cleavage fragment is around 51kD which matches the anti-CdiA-NT immunoblot. As expected, the anti-CdiA-CT antibody did not react to this fragment (Figure 5A, right). Surprisingly, CdiA filament could be disconnected from its N-terminus and still deliver the toxin. The TEV cleaved CdiA TEV505 still delivered the toxin

in a receptor dependent manner (Figure 5B). The delivered toxin then cleaved $tRNA_{UUC}^{Glu}$ in *tsx+* target cells (Figure 5C).

Severed CdiA is held on cell surface by interacting with the distal portion of the extended region.

When CdiA TEV1662 was cleaved, the resulting NT fragment is much larger than TEV505 fragment (Figure 6A). Similarly, TEV1662 fragment is lost to the supernatant (Figure 6A) while the C-terminal half remains in the cell (Figure 6B). However, when TEV1383 is cleaved, the resulting NT fragment is still retained in the cell fraction (Figure 6A). This suggests that the extended region is tightly bound to the filament at the distal portion. The severed CdiA filament does not flop around with new N-terminus facing away from the cell only tethered at the YP domain. Instead the extended region can tightly hold on to the filament which then neatly oscillates with RBD facing outward. This interaction occurs at the distal portion of the extended YP domain because cleavage at 1383 retains the interaction but cleavage at 1662 disconnects the filament and the extended region from the YP domain anchor.

C. Discussion

The work presented here provide deeper insight on the structure and significance of CdiA filament form by the N-terminal half of the protein. The length of the CdiA filament was not important for the biogenesis and toxin delivery of CdiA. All six incremental deletions of FHA1 repeats delivered their toxin in a receptor-dependent manner (Figure 1). The largest deletion (ΔL507-T1303) is predicted to shorten the filament by 19.1 nm leaving

less than half of the normal CdiA filament. Even this shortest mutant displayed the CdiA effector with correct secretion arrest and exported the toxin after receptor-binding. However, subsequent assembly of FHA2 domain seemed compromised because immunoblot showed more CT remained undelivered following the export (Figure 1D).

Since the filament can be significantly reduced, the importance of CdiA filament length remains unknown. One simple explanation is that the filament prevents auto-delivery of the toxin using the self-receptors. CdiA recognizes receptors from same species (104). Thus, toxin delivery is primarily intended for neighboring non-sibling cells of the same species. If CdiA filament did not provide a structural support to point the RBD away from its surface, toxin-delivery would be waited on auto-delivery. This would be a clear evolutionary disadvantage. Alternatively, the 33nm filament may locate the RBD above the LPS layer for optical contact with a target receptor. Furthermore, the filament can help the RBD penetrate through the LPS layer on the target cell surface to contact the receptor. The *E. coli* cells used in this study is a naked K-12 variant without the O-antigen and adequate LPS layer. The short CdiA filaments may show reduced activity in natural strains of *E. coli*. This hypothesis can be tested by evaluating the short filament effectors after restoring the LPS of the CDI+ cells, target cells, or both.

Previous models of the two-partner secretion systems have depicted the TPS domain of cargo in the periplasm where it maintains its interaction with the POTRA domain of the transporter (94). Most studied example of this model is *Bordetella pertussis* FhaB. The C-terminal proto-domain of FhaC was proposed to remain in the periplasm, but maturation of the FhaC followed proteolytic cleavage of the proto-domain so that the final C-terminus is facing away from the cell surface (94). Revision of this model is inevitable when applying to

CdiA because of our previous discovery of stable secretion arrest (165). Retaining the TPS in the periplasm requires the CdiB lumen to accommodate two strands of polypeptide chain because the C-terminal half of CdiA loops back in a hairpin-like fashion. My work here shows that the TPS domain of CdiA is also exported (Figure 2). The exported TPS domain can then be interacting with extracellular loops of CdiB to orient the filament upright. The surface occluded residue 64 in the TPS could possibly suggest such an interaction with CdiB. Interestingly, this possible interaction between the N-terminal CdiA and CdiB is insufficient to stably anchor CdiA on cell surface because the filament falls off to supernatant if the YP domain is removed (165). The secretion arrest orchestrated between the YP domain and CdiB is the primary mechanism of holding on to the filament, and any TPS-CdiB interaction seems to play a minimal role in orienting the filament upright.

Once presented on the surface, CdiA forms a tightly packed structure which is trypsin-resistant (Figure 3). The RBD and the extended YP domain must be stably folded or packed against the FHA1 filament. Interruption of the FHA1 filament by deleting a random 100-resdiues deemed that portion susceptible to tryptic digest (Figure 3A). However, in-sync deletions of FHA1 repeats maintaining the structural soundness of the filament until too much of the filament was removed and the extended YP domain is cleaved by trypsin (Figure 3B). TEV insertions in the FHA1 repeats were also TEV-resistant further suggesting that the filament forms a stable protease-resistant structure (Figure 4A).

The distal portion of the extended YP domain is in a tight interaction with the CdiA filament enough so that even a severed N-terminal filament remains cell-bound. TEV1383 cuts between the FHA1 filament and the RBD (Figure 6). The distal portion of the extended region is still connected to the secretion arrest mechanism of the YP domain, so the filament

is still presented on the cell surface (Figure 6A). However, TEV1662 cuts somewhere in the middle of the extended region. This disconnects the distal portion of the extended region from the secretion arrest mechanism in the periplasmic YP-C domain. As the result, the cleaved filament along with the RBD is lost to the supernatant (Figure 6A).

Remarkably, severed CdiA filament can still delivery its toxin as long as it remains on the cell surface. TEV1383 had defective receptor-binding (Figure 4B) so TEV505 was used to analyze the effect of N-terminal cleavage of the filament (Figure 5B and C). Even though TEV505 cuts the CdiA filament at its base, it should remain presented on cell surface due to the interaction with the distal extended region. When mixed with target cells, the severed filament delivered its C-terminal toxin which then cleaved Glu tRNAs in the target cells (Figure 6).

In conclusion, CdiA filament is an impressively robust strategy to present toxin delivery activity away from self, to a neighboring cell. The filament can tolerate significant shortening in length and N-terminal cleavage by protease. As long as the RBD is presented on the cell surface via the extended region, secretion of the C-terminal CdiA resumes upon receptor-binding and delivers the toxin effector.

D. Materials and Methods

Bacterial growth conditions.

Bacterial strains were derivatives of E. coli K-12 strains MG1655. Bacteria were cultured in lysogeny broth (LB) or on LB agar at 37 °C. Unless indicated otherwise, media were supplemented with antibiotics at the following concentrations: 150 μg/mL ampicillin

(Amp), 50 µg/mL kanamycin (Kan), 25 µg/mL tetracycline (Tet), and 200 µg/mL spectinomycin (Spc).

Plasmid construction

FHA1 deletions were made with PCR and introduced to plasmid pET21b::cdiBAI^{STEC3} G1726C MCS- (pCH5237). pCH5237 is modified version of pCH14563 which carries G1726C mutation for maleimide labelling. Forward primers CH4764, CH4765, CH4778, CH4779, CH4814, and CH4381 were paired with a reverse primer, CH4381. These products were KpnI/SacI cloned to pCH5237 to generate increasing FHA1 deletions: pCH2319, pCH2320, pCH2321, pCH2322, pCH2754, and pCH2755, respectively.

Cysteines were made in the TPS domain by Gibson assembly and introduced to plasmid pET21b::cdiBAI^{STEC3} MCS- (pCH14563). Primers were designed to have 20 bp overlaps to allow DNA assembly. PCR products from primer pairs CH5072/CH5074 and CH5075/CH5073 were assembled with NotI/KpnI digested p14563 to generate pCH5297 (H64C). PCR products from primer pairs CH5072/CH5074 and CH5076/CH5073 were assembled with NotI/KpnI digested p14563 to generate pCH5298 (D69C). PCR products from primer pairs CH5072/CH5077 and CH5078/CH5073 were assembled with NotI/KpnI digested p14563 to generate pCH5299 (E75C). PCR products from primer pairs CH5072/CH5079 and CH5080/CH5073 were assembled with NotI/KpnI digested p14563 to generate pCH5300 (G244C). PCR products from primer pairs CH5072/CH5081 and CH5082/CH5073 were assembled with NotI/KpnI digested p14563 to generate pCH5301 (Y252C). PCR products from primer pairs CH5072/CH5081 and CH5083/CH5073 were

assembled with NotI/KpnI digested p14563 to generate pCH5302 (H257C). CdiA-alone constructs for H64C and D69C were made by amplifying the deletion with primer pair CH4843/CH5073 then AscI/KpnI cloned to pET21(MCS-)::cdiAI (STEC3).

TEV sites in the N-terminal CdiA were made by PCR and introduced to p14563. Primers were designed to include GS linkers to cap both sides of the TEV protease site (GS-ENLYFQ-GS). PCR fragments were amplified with primers ZR260/CH5055 then NotI/KpnI cloned to generate pCH5627 (TEV505). PCR fragments using CH4239/CH5050 and CH5056/CH4381 were sequentially cloned into pBluescript II SK+ using KpnI/BamHI and BamHI/SacI, respectively. The KpnI/SacI fragment was then subcloned to generate pCH5628 (TEV1270). PCR fragments using CH4239/CH5052 and CH5057/CH4381 were sequentially cloned into pBluescript II SK+ using KpnI/BamHI and BamHI/SacI, respectively. The KpnI/SacI fragment was then subcloned to generate pCH5629 (TEV1279). PCR fragments using CH4239/CH5054 and CH5058/CH4381 were sequentially cloned into pBluescript II SK+ using KpnI/BamHI and BamHI/SacI, respectively. The KpnI/SacI fragment was then subcloned to generate pCH5630 (TEV1305).

To clone TEV sites around the RBD, STEC3 RBD was amplified with CH4858/CH4859 then EcoRI/BamHI cloned to pCH2207 (Chapter 3) to generate pCH1028. pCH1038 has extra restriction sites around the RBD but otherwise WT. PCR fragment with CH4239/CH5009 was KpnI/EcoRI cloned to pCH1038 to generate pCH3077 (TEV1383). PCR fragment with CH4864/CH4242 was BamHI/NcoI cloned to pCH1038 to generate pCH1008 (TEV1662). Both pCH3077 and pCH1008 were subcloned by NotI/XhoI to pCH450 for arabinose induction.

Competition co-cultures.

E. coli CH14016 (MG1655 Δ*wzb* Δ*tsx*) that harbor CdiA expression plasmids were used as inhibitor cells in shaking broth co-cultures. *E. coli* CH14016 strains that carry pCH14047 (*tsx*+) were used as target cells. Cells were grown in LB media at 37 °C to mid-log phase, adjusted to OD600 ~ 0.3 in fresh pre-warmed LB media without antibiotics, mixed at a 1:1 ratio (5 mL total volume) and incubated with shaking for 3 h at 37 °C. Culture aliquots were taken at the beginning of co-culture and after 3 h to quantify viable inhibitor and target cells as colony forming units per milliliter (CFU mL^{-1}). Cell suspensions were serially diluted into 1X M9 salts and plated onto LB-agar supplemented with Amp to enumerate inhibitor cells, and LB-agar supplemented with Kan to enumerate target cells. Competitive indices were calculated as the ratio of inhibitor to target cells at 3 h divided by the initial inhibitor to target cell ratio.

Target cell mixing

E. coli MG1655 *Δwzb Δtsx* (CH14016) or MG1655 *Δwzb Δtsx ΔompT* (CH14017) carrying CdiA expression plasmids were diluted to OD600 ~ 0.05 in Amp supplemented LB media and grown to mid-log phase at 37 °C. These inhibitor cultures were mixed with *E. coli* CH14016 or CH14017 target cells that carry pCH14046 *(*Δ*tsx*) or pCH14047 (*tsx*+) at a 1:1 ratio with Spc to block new protein synthesis. After 20 min with shaking, 1 mL of the mixture was harvested by centrifugation. Cell pellets were re-suspended in 50 µL of urea-lysis buffer and subjected to one freeze-thaw cycle to extract proteins. Urea-soluble proteins (5 µL) were resolved by SDS-PAGE and analyzed by immunoblotting using anti-TPS domain antisera.

Surface topology mapping of the TPS domain.

E. coli CH14017 cells carrying CdiA expression plasmids were diluted to OD600 ~ 0.05 in Amp supplemented LB media and grown to mid-log phase at 37 °C. Cultures were then treated with Spc for 20 min to block protein synthesis. Cells were harvested by centrifugation and re-suspended at OD600 ~ 0.3 in 1.0 mL of 1X phosphate buffered saline (PBS) supplemented with 1 mM MgSO4 (PBS-Mg) to probe intact cells or PBS-Mg with 100 µg/mL polymyxin B to probe permeabilized cells. IRDye680LT-maleimide (LI-COR) was added to a final concentration of 40 µM. Labeling reactions were incubated in the dark at room temperature for 15 min, then quenched with 6 mM 2-mercaptoethanol (2-ME). Cells were collected by centrifugation and washed with PBS-Mg supplemented with 6 mM 2-ME. Cell pellets were re-suspended in 50 µL of urea-lysis buffer and subjected to one freeze-thaw cycle to extract proteins. Urea-soluble proteins (5 µL) were resolved by SDS-PAGE and analyzed by immunoblotting using anti-TPS domain antisera.

Protease cleavage

For trypsin digest, *E. coli* CH14017 cells carrying CdiA expression plasmid were grown and Spc-treated as described above. 1 mL of culture was centrifuged and resuspended in 1mL PBS-Mg. Trypsin was added to a final concentration of 20 µg/ml and incubated at RT for 20 min. Cells washed thrice with 1 mL PBS-Mg freshly added 2mM PMSF. When needed, 900 µL of supernatant was retained before washing for TCA-precipitation. Cell pellets were re-suspended in 50 µL of urea-lysis buffer and subjected to one freeze-thaw

cycle to extract proteins. Urea-soluble proteins (5 µL) were resolved by SDS-PAGE and analyzed by immunoblotting using anti-TPS domain antisera.

For TEV cleavage, *E. coli* CH14017 cells carrying CdiA expression plasmid were grown and Spc-treated as described above. 1 mL of culture was centrifuged and resuspended in 1mL PBS-Mg. TEV protease was added to a final concentration of 30 µM and incubated at 37 for 1 h. Cells spun down by centrifugation while keeping 900 µL of supernatant for TCA-precipitation. Pellets were washed once with 1 mL PBS-Mg and re-suspended in 50 µL of urea-lysis buffer and subjected to one freeze-thaw cycle to extract proteins. Urea-soluble proteins (5 µL) were resolved by SDS-PAGE and analyzed by immunoblotting.

TEV-cleaved cells were further mixed with target cells as described above to evaluate CdiA-CT delivery after TEV-cleavage. 1 mL was spun down for protein extraction with urea-lysis buffer was done as described. Remaining cell mixture (~7 mL) was kept in ice-cold methanol for RNA extraction.

Protein extraction from supernatant

To analyze culture supernatants for released CdiA mutants, retained 900 µL of the supernatant was added to 100 µL of trichloroacetic acid. Proteins were collected by centrifugation at 18,000 X g for 30 min at 4 °C. Precipitates were washed thrice with 1.0 ml of cold acetone. Air-dried pellets were dissolved in 45 µL of urea-lysis buffer, and 5 µL of each sample analyzed by SDS-PAGE and immunoblotting.

Immunoblotting

Urea-soluble protein samples (5 µL) were analyzed by SDS-PAGE on Tris-tricine 6% polyacrylamide gels run at 100 V (constant) for 3.5 h. Gels were soaked for 15 min in 25 mM Tris, 192 mM glycine (pH 8.6), 10% methanol, then electroblotted to low-fluorescence PVDF membranes using a semi-dry transfer apparatus at 17 V (constant) for 1 h. Membranes were blocked with 4% non-fat milk in PBS for 1 h at room temperature, and incubated with primary antibodies in 0.1% non-fat milk, PBS overnight at 4 °C. Rabbit polyclonal antisera (Cocalico Biologicals, Stevens, PA) to the N-terminal TPS domain was used at a 1:10,000 dilution, and anti-PT/CdiA-CT antisera was used at a 1:3,000 dilution. Blots were incubated with 800CW-conjugated goat anti-rabbit IgG (1:40,000 dilution, LICOR) in 0.1% non-fat milk in PBS. Immunoblots were visualized with a LI-COR Odyssey infrared imager.

Northern blotting

Frozen cell pellets were resuspended in guanidinium isothiocyanate (GITC)-phenol and total RNA extracted as described (181). RNAs (5 µg) were run on 50% urea-10% polyacrylamide gels buffered with 1 × Tris-borate EDTA and electroblotted to positively charged nylon membranes for Northern blot analysis. Blots were hybridized with [^{32}P]-labeled oligonucleotide probe CH1417 specific for *E. coli* $tRNA_{UUC}^{Glu}$. Blots were visualized by phosphorimaging using Bio-Rad Quantity One software.

Cell-cell adhesion by flow cytometry.

Receptor-binding studies were conducted using *E. coli* strain DL4259, which expresses gfp-mut3 from the papBA promoter (Webb et al., 2013). *E. coli* DL4259 cells were transformed with pCH450-derived CdiA expression plasmids and the resulting strains grown

at 37 °C in LB media supplemented with Tet until the cells became fluorescent. *E. coli* ZR373 cells carrying plasmid pDsRedExpress2 were used as targets. Targets were also provided with plasmid pCH14046 (Δ*tsx)* or pCH14047 (*tsx*+). Target cells were grown overnight in LB supplemented with Tet, Amp, 0.4% L-arabinose and 1 mM IPTG to induce expression of Tsx and DsRed prior to mixing with inhibitors. GFP-labeled inhibitor cells were mixed at a 5:1 ratio with DsRed-labeled target bacteria at a final OD600 ~ 0.2. Cell suspensions were shaken at 30 °C for 20 min, diluted into 1X PBS, vortexed briefly, then analyzed on an Accuri C6 flow cytometer using FL1 (533/30nm, GFP) and FL2 (585/40nm, DsRed) fluorophore filters. The fraction of target bacteria bound to inhibitor cells was calculated as the number of dual green/red fluorescent events divided by the total number of red fluorescent events. More than 2,000 red fluorescent events were scored for each cell mixture.

E. Figures and tables

Mutant	Deletion size (residues)	Predicted length shortened (nm)
ΔL507-T662	156	3.7
ΔL507-T759	253	6.1
ΔL507-T852	346	8.3
ΔL507-T1066	560	13.4
ΔL507-T1160	654	15.7
ΔL507-T1303	797	19.1

Table 1. FHA1 deletions to make shorter CdiA filaments. Each deletions in-frame of the FHA1 repeat structure. The shortened length of the filament is predicted based on reported β-helical structure in which each ~20 repeat motif extends the helix by 4.8 Å.

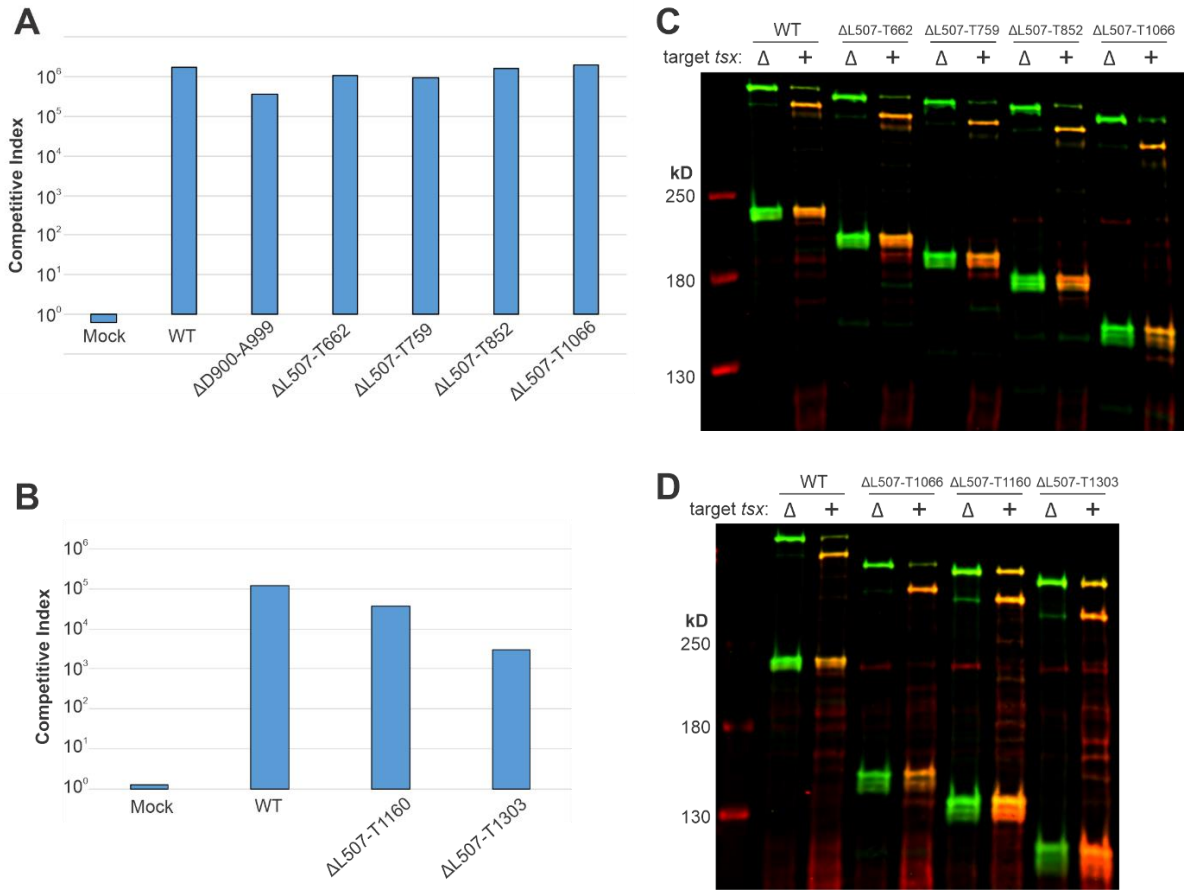

Figure 1. Shortened CdiA filaments still support toxin delivery. Increasing FHA1 repeat deletions still deliver CdiA-CT to tsx+ target cells. (A and B) Competition co-cultures. Inhibitors were mixed at a 1:1 ratio with targets. Competitive indices equal the final ratio of inhibitors to targets divided by the initial ratio. (C and D) Short FHA1 mutants were mixed with tsx- or tsx+ target cells. Periplasmic cysteine at 1726 is labelled with maleimide dye to visualize export of C-terminal half.

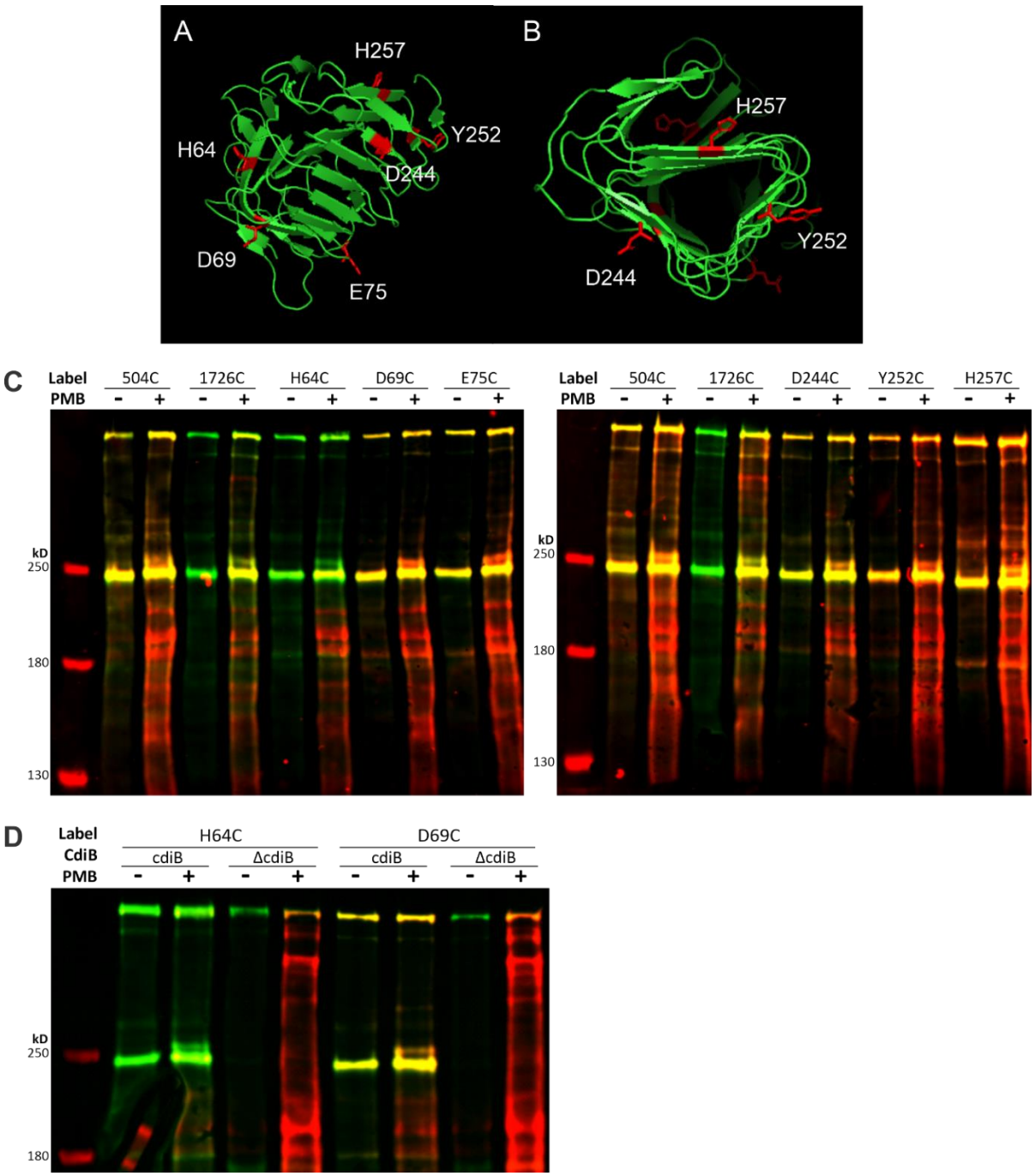

Figure 2. The TPS domain is a part of the extracellular filament. (A) Model of CdiA TPS is built based on FhaC TPS. Six residues mutated to Cys are labelled. (B) Top view of CdiA TPS model to show the residues are facing out of the β-helix. (C) Maleimide-labelling and CdiA immunoblot shows the Cys residues in TPS are extracellularly labelled except H64C. 504C is extracellular control. 1726C is periplasmic control. (D) Maleimide-labelling and CdiA immunoblot with/without CdiB. H64 is labelled in the periplasm when CdiB is not present.

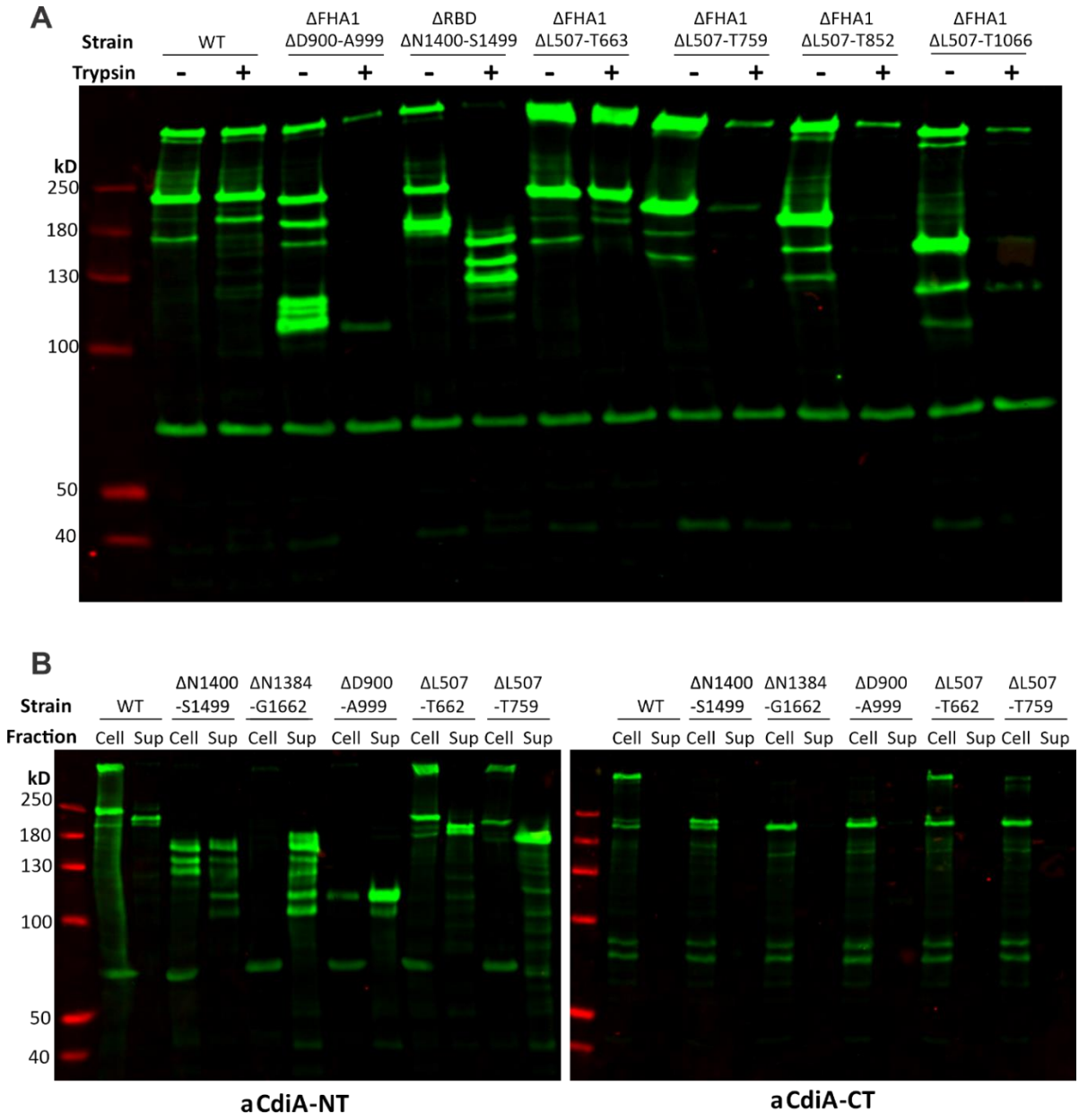

Figure 3. The extended region is tightly packed against the filament. (A) Tryptic digest of CdiA mutants and CdiA immunoblot. WT is trypsin-resistant, but deletions expose CdiA to digest (B) Cell/sup fractions after tryptic digest probed with anti-TPS (left) and anti-CT (right). Cleaved N-terminal CdiA is disconnected from the cell and gets released to supernatant. C-terminal half of CdiA is in the periplasm and resists tryptic digest.

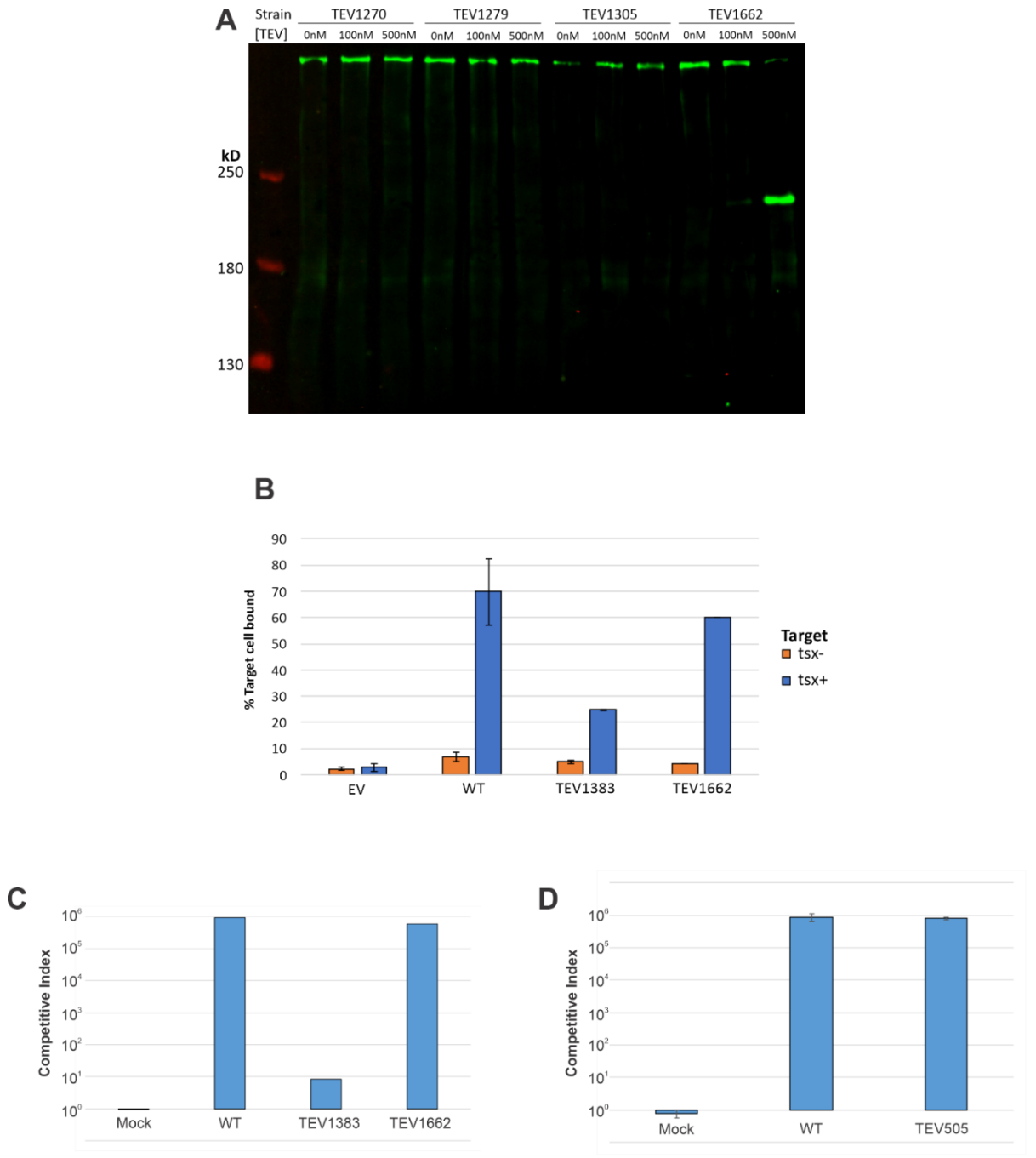

Figure 4. TEV protease sites introduced at various positions of CdiA. (A) TEV cleavage and immunoblot of TEV sites in FHA1 repeats. TEV1662 as a control for cleavage (B) Target cell adhesion measured by flow cytometry. GFP-labeled inhibitors were mixed with DsRed-labeled targets. Data are presented as mean ± SEM. (C and D) Competition co-cultures. Inhibitors were mixed at a 1:1 ratio with targets. Competitive indices equal the final ratio of inhibitors to targets divided by the initial ratio.

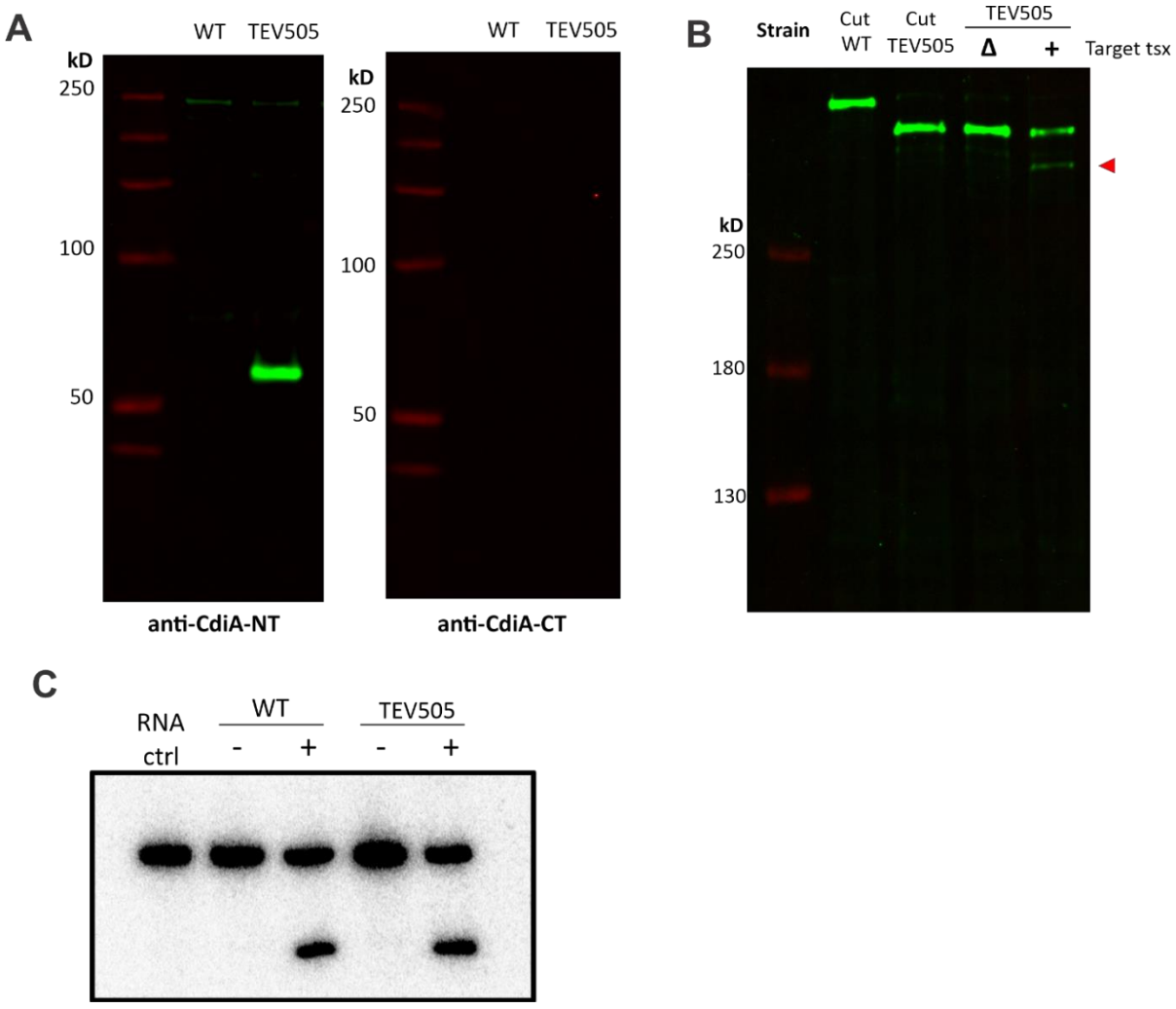

Figure 5. Severed CdiA can still deliver CT-toxin. (A) Supernatant protein samples after TEV505 CdiA is cut with TEV protease. Smaller N-terminal fragment is lost into the supernatant. (B) Anti-CdiA-CT blot shows the remaining CdiA after TEV cleavage. The TEV505 CdiA severed at the N-terminal base can still deliver CdiA-CT. Red arrow points to CdiA getting smaller after toxin delivery. (C) $tRNA^{Glu}$ northern blot from cell mixture after TEV cleavage.

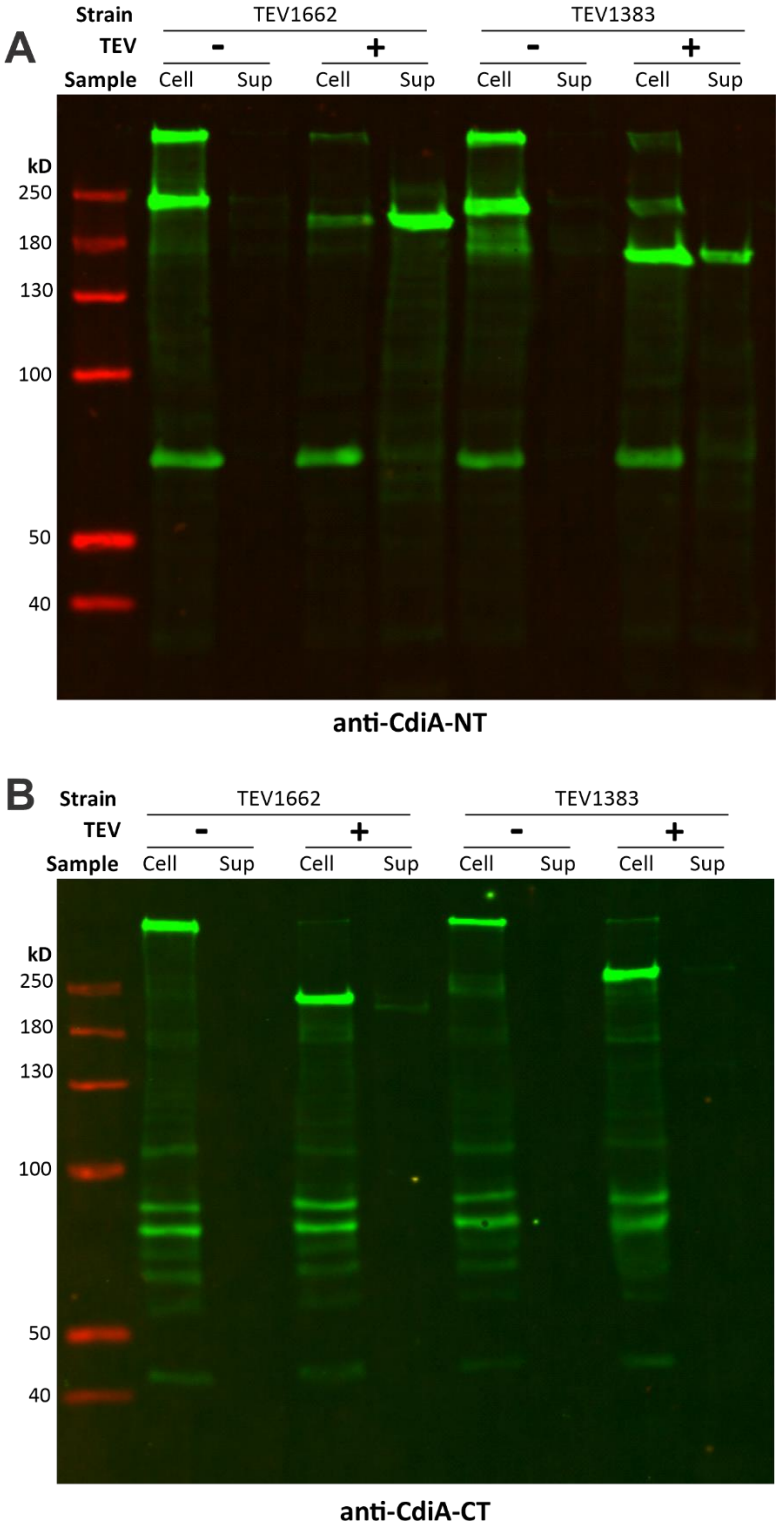

Figure 6. Severed CdiA is held on cell surface by interacting with the distal portion of the extended region. TEV cleavage of TEV1662 and TEV1383 which cuts proximal and distal portions of the CdiA, respectively. Even after cleavage at 1383, the filament is held on the cell surface presumably it is interacting with the extended region which is still connected to the cell.

Table 2. Strains used in this study.

Strains	Description	Reference
CH14016	*E. coli* MG1655 Δwzb Δtsx	(165)
CH14017	*E. coli* MG1655 Δwzb Δtsx ΔompT	(165)
DL4259	*E. coli* MC4100 l640-13 PpapIB-gfp-mut3	(113)
ZR373	*E. coli* EPI100 Δwzb Δtsx	(165)

Table 3. Plasmids used in this study.

Plasmid	Description	Reference
CH2319	pET21b-cdiBAI (STEC3) ΔL507-T662 (G1726C), Amp^R	This study
CH2320	pET21b-cdiBAI (STEC3) ΔL507-T759 (G1726C), Amp^R	This study
CH2321	pET21b-cdiBAI (STEC3) ΔL507-T852 (G1726C), Amp^R	This study
CH2322	pET21b-cdiBAI (STEC3) ΔL507-T1066 (G1726C), Amp^R	This study
CH2754	pET21b-cdiBAI (STEC3) ΔL507-T1160 (G1726C), Amp^R	This study
CH2755	pET21b-cdiBAI (STEC3) ΔL507-T1303 (G1726C), Amp^R	This study
CH5237	pET21b-cdiBAI (STEC3) MCS- G1726C, Amp^R	Chapter III
CH14563	pET21b-cdiBAI (STEC3) MCS-, Amp^R	Chapter III
CH5297	pET21b-cdiBAI (STEC3) H64C, Amp^R	This study
CH5298	pET21b-cdiBAI (STEC3) D69C, Amp^R	This study
CH5299	pET21b-cdiBAI (STEC3) E75C, Amp^R	This study
CH5300	pET21b-cdiBAI (STEC3) D244C, Amp^R	This study
CH5301	pET21b-cdiBAI (STEC3) Y252C, Amp^R	This study
CH5302	pET21b-cdiBAI (STEC3) H257C, Amp^R	This study
CH5283	pET21b-cdiAI (STEC3) H64C, Amp^R	This study
CH5284	pET21b-cdiAI (STEC3) D69C, Amp^R	This study
CH1067	pET21(MCS-)::cdiAI (STEC3), Amp^R	Chris Hayes
CH14028	pET21b-cdiBAI (STEC3) ΔFHA-1: ΔAsp900-Ala999, Amp^R	Cell 2018
CH14029	pET21b-cdiBAI (STEC3 ΔRBD: ΔAsn1400-Ser1499, Amp^R	Cell 2018
CH5627	pET21b-cdiBAI (STEC3) 505-GS-TEV, Amp^R	This study
CH5628	pET21b-cdiBAI (STEC3) 1270-GS-TEV, Amp^R	This study
CH5629	pET21b-cdiBAI (STEC3) 1279-GS-TEV, Amp^R	This study
CH5630	pET21b-cdiBAI (STEC3) 1305-GS-TEV, Amp^R	This study
CH1038	pET21(MCS-)::STEC3(RBD-Eco/Bam), Amp^R	Chris Hayes
CH2207	pET21b-cdiBAI (STEC3) (MCS-) ΔRBD EcoBam (1726C), Amp^R	Chapter III
CH3077	pET21(MCS-)-STEC3-TEV(L1383) (1726C), Amp^R	This study
CH1008	pET21(MCS-)::STEC3-TEV(1662)-C1726, Amp^R	Chris Hayes

CH4504	pCH450-cdiBAI (STEC3) TEV(1383), Tet^R	This study
CH4505	pCH450-cdiBAI (STEC3) TEV(1662), Tet^R	This study
pCH450	pAraBAD, Tet^R	(157)
CH14046	pZS21, Kan^R	Chapter III
CH14047	pZS21::tsx, Kan^R	Chapter III

Table 4. Oligonucleotides used in this study.

Primer	Name	Sequence	Reference
CH4764	STEC3-G757-Kpn-for2	5' - GCA GGT ACC ACG CAG GGA CA - 3'	This study
CH4765	STEC3-G1065-Kpn-for	5' - GAC GGT ACC ATT CAG GGC AAC GG -3'	This study
CH4778	STEC3-G661-Kpn-for	5' - AAC GGT ACC CTG TAC AGC GCT GC -3'	This study
CH4779	STEC3-G851-Kpn-for	5' - AGC GGT ACC GTC ACA GGT CTG AG -3'	This study
CH4814	STEC3-L1159-Kpn-for	5' - AGC GGT ACC CTG CTG GGT AAT CAG GG - 3'	This study
CH4815	STEC3-G1302-Kpn-for	5' - ACC GGT ACC ACG GGT AGT CTG ATG TTA - 3'	This study
CH4381	STEC(3)-Y1657-Xho-rev	5' - TTT CTC GAG ATA GTT CCC CTC CAC GAT GC - 3'	(165)
CH5072	STEC3-Not-GA-for	5' - CCT CTA GTC GAC AAG CTT GC - 3;	This study
CH5073	STEC3-Kpn-GA-rev	5'- GTT CCT TTG CCC CGG AGA GG -3'	This study
CH5074	STEC3-S63-rev	5'- CGA AAT CCC GGC CCC GTT CG -3'	This study
CH5075	STEC3-H64C-for	5'- CGA ACG GGG CCG GGA TTT CGT GTA ACA GGT TTA CGG ATT ACA ACG TC -3'	This study
CH5076	STEC3-D69C-for	5'- CGA ACG GGG CCG GGA TTT CGC ATA ACA GGT TTA CGT GTT ACA ACG TCG GGA AGG AAG -3'	This study
CH5077	STEC3-K74-rev	5'- CTT CCC GAC GTT GTA ATC CG -3'	This study
CH5078	STEC3-E75C-for	5'- CGG ATT ACA ACG TCG GGA AGT GTG GGC TGA TTC TCA ATA ATG CCA -3'	This study
CH5079	STEC3-V243-rev	5'- AAC AGC AAC TTT CGG CAC AT -3'	This study
CH5080	STEC3-G244C-for	5'- ATG TGC CGA AAG TTG CTG TTT GTA CCG GCG CGC TCG -3'	This study

CH5081	STEC3-M251-rev	5'- CAT TCC ACC GAG CGC GCC GG -3'	This study
CH5082	STEC3-Y252C-for	5'- CCG GCG CGC TCG GTG GAA TGT GTG CCA GGC GTA TTC ATC TGA C -3'	This study
CH5083	STEC3-H257C-for	5'- CCG GCG CGC TCG GTG GAA TGT ACG CCA GGC GTA TTT GTC TGA CCT CCA CTG AAA GTG -3'	This study
CH4843	STEC3-cdiB(R587)-Asc-for	5' - TTT ACT GGC GCG CCG CCG TCG CGT TT -3'	This study
ZR260	J2M139 CDI-Not-for	5' - TTT GCG GCC GCA ATG TCT GGT TGT GGC AGG - 3'	(165)
CH5055	STEC3-TEV-G505-Kpn-rev	5' - TTT GGT ACC GCT ACC CTG AAA ATA CAG ATT TTC AGA ACC GCT GTT GTT TAT CTG CGT GGC - 3'	This study
CH4239	STEC-Kpn-for	5' - CAG CGG TAC CCT CTC CG - 3'	(165)
CH4381	STEC(3)-Y1657-Xho-rev	5' - TTT CTC GAG ATA GTT CCC CTC CAC GAT GC - 3'	(165)
CH5050	STEC3-G1270-Bam-rev	5' - CAT CGC AAT CCC GGA TCC GCT CAG TGC CG -3'	This study
CH5052	STEC3-G1279-Bam-rev	5' - CCT GCC TGC AGG GAT CCG CTG GCA TTC -3'	This study
CH5054	STEC3-G1305-Bam-rev	5' - CCG TTA ACA TCA GGG ATC CCG TCG TGC CGG -3'	This study
CH5056	STEC3-TEV-G1270-Bam-for	5' - TTT GGA TCC GAA AAT CTG TAT TTT CAG GGC AGC GGG ATT GCG ATG -3'	This study
CH5057	STEC3-TEV-G1279-Bam-for	5' - TTT GGA TCC GAA AAT CTG TAT TTT CAG GGC AGC CTG CAG GCA GGC -3'	This study
CH5058	STEC3-TEV-G1305-Bam-for	5' - TTT GGA TCC GAA AAT CTG TAT TTT CAG GGT AGT CTG ATG TTA ACG GCC -3'	This study
CH4858	STEC3-N1384(RBD)-Eco-for	5' - ACT GAA TTC GCG GGA GGG CAT AAA TGA G	This study
CH4859	STEC3-P1660(RBD)-Bam-rev	5' - GTT GGA TCC AGG CAG GGG ATA GTT CCC	This study
CH4239	STEC-Kpn-for	5' - CAG CGG TAC CCT CTC CG - 3'	(165)
CH5009	STEC3-L1383-TEV-Eco-rev	5' - TTT GAA TTC GAC TGA AAA TAC AGA TTT TCC AGT AAA TGT CCG GTT CTG ATG G - 3'	This study

CH4864	STEC3-1662-TEV-Bam-for	5' - TTT GGA TCC GAA AAT CTG TAT TTT CAG TCT AAC AAT GGT TAT TTT GTC CCG TCA GC -3'	This study
CH4242	STEC-Nco/Not-rev	5' - TTT GCG GCC GCC CAT GGC ACT GAC AGA GG - 3'	(165)
CH1417	tRNA-Glu probe	5' - CCC CTG TTA CCG CCG TG	(138)

Chapter VI. Conclusion

Protein secretion across the outer membrane is a fundamental cellular process in Gram-negative bacteria. The type V secretion system (T5SS), specifically the two-partner secretion (TPS) system is highly specialized mechanism of exporting large filamentous effectors using β-barrel outer membrane transporters. Secretion initiation of the effector proteins by TPS-POTRA interaction is highly conserved, yet the exported effectors display an impressive diversity of function, mechanism, and localization. This thesis, which has discussed one particular example of the contact-dependent growth inhibition (CDI) system, speaks to the depth and diversity of the TPS systems found in many Gram-negative bacteria.

In nature, bacteria occupy densely populated environment and must compete for limited resources and space. CDI system would confer evolutionary advantage to the cells which target closely related neighbors in proximity and deliver toxin effectors.

Collaboration with Zach Ruhe and Poorna Subramanian in Chapter II has revealed the first electron tomography image of CdiA on cell surface as well as the striking topology of this protein. My work has traced the CdiA protein as it binds to a target receptor and deliver the CdiA-CT toxin effector. Receptor-binding resumes export of the periplasmic CdiA which harbors mechanism of toxin transport across the outer membrane of target cells. Disruption of the periplasmic half causes downstream CdiA to linger in the extracellular space, eventually to be cleaved by an outer membrane protease, OmpT. Further work by Zach Ruhe has shown that the periplasmic FHA2 repeats are directly deposited into the target outer membrane. These findings suggest that previously uncharacterized FHA2 domain's function is to form a translocon in the target outer membrane to deliver a C-terminal toxin effector.

Another seminal discovery was locating the secretion arrest domain in the YP region. The topology of CdiA in which the C-terminal half is retained in the periplasm requires the secretion to stop in the middle of the protein until receptor-binding. This secretion arrest is attributed to the YP region because when the YP region is removed, the periplasm CdiA was prematurely exported and the whole filament fell off the cell.

Chapter III further dissected this secretion arrest mechanism. I have shown that the sequence of the YP region is crucial for its function. The preciously location of the secretion arrest could not be further narrowed down beyond a 25 residue stretch in the 2nd half of the YP-C domain. The YP region was also impressively robust because some periplasm residues could be pulled out without disrupting secretion arrest and the region also tolerated many smaller deletions. It seems that the entire secondary structure of the YP region contribute to the secretion arrest mechanism. We also report that the secretion arrest requires coordination between cognate YP region and CdiB pair. The YP region required cognate TpsB transporter to arrest secretion of its TpsA cargo. These findings support that secretion arrest may be highly conserved mode of export in other TPS systems including the FHA system. We also report a more sophisticated function of the CdiB transporter. In our system, CdiB not only exports the CdiA cargo, but it precisely controls secretion in a receptor-dependent manner at least indirectly. Interaction between CdiB and YP region halts export of the periplasmic CdiA which resumes upon receptor-binding.

During CdiA biogenesis, the extended YP region is most likely go through the lumen of CdiB. The 25 residues of YP region most crucial for secretion arrest is in the periplasm, possibly interacting with the periplasmic POTRA domain of CdiB. I aimed to capture this interaction using Bacterial 2 hybrid system. I cloned CdiB residues S88-G259 (POTRA) and

CdiA residues A1697-V1952 (YP region) and fused to T25/T18 subunits of adenylate cyclase from *Bordetella pertussis*. As a positive control, I also cloned CdiA TPS domain (V33-T322) which is known to interact with the POTRA domain. I exhaustively tested all possible combinations of bacterial 2 hybrid by making both C-terminal and N-terminal fusions of both subunits of adenylate cyclase to both POTRA and the YP region. However, my experiments only reported POTRA-TPS interaction but not POTRA-YP interaction (data not shown). POTRA-TPS interaction occurs to initiate cargo transport so it is not surprising to reliably see their interaction. In contrast, POTRA-YP interaction may only occur after the N-terminal CdiA is exported thus presenting the YP region to CdiB with limited structural freedom. Any interaction between the POTRA domain and freely diffusing YP region may only be transient.

To capture such transient interactions between CdiB and the YP region, I have also mutated some resides in the YP region to *p*-benzoyl-L-phenylalanine (pBPA) for UV crosslinking. Residues 1726 and 1837 were chosen for crosslinking. Residue 1726 is a hallmark periplasmic residue while 1837 seems to enhance defects in secretion arrest when mutated to Gly. CDI+ cells expressing the orthogonal residues were exposed to 365nm wavelength UV for up to 20 minutes. Unfortunately, there was no sign of CdiB crosslinking to these residues. But this does not rule out the YP domain is interacting with CdiB. Residues 1726 and 1837 does not seem to be proximity of CdiB themselves. More residues need to be scanned with pBPA to test possible CdiB-YP interaction.

Chapter IV aimed to understand receptor-induced secretion of the C-terminal CdiA. We show that isolated receptor could release the secretion arrest and the periplasmic CdiA is exported unfolded. Heterologous domains could replace the periplasmic CdiA to engineer a

receptor-dependent trigger. A CdiA-enzyme chimera keeps the enzymatic activity in the periplasm and exports it outside in response to a receptor. I have used CdiA-PmeA to build a plate-based screening that reports periplasmic half secretion on a pectin agar plate. p*cdiBA-pmeA* construct can be mutagenized and selected for clones that secretion PmeA extracellularly. ΔYP CdiA-PmeA serves as a positive control. I expect to find mutations in CdiB and the YP region which will reveal molecular mechanism of secretion arrest. Residues found critical for secretion arrest will be candidates for orthogonal translation to pBPA for UV crosslinking. Crosslinking study using residues identified by mutagenesis will reveal interaction surfaces between CdiB and the YP region.

It is still unclear how receptor-biding domain initiates C-terminal half export. We tested two possible models of receptor-induced export: Induced folding of the RBD and mechanism pulling at the RBD. Current set of data is insufficient to distinguish between the two models of secretion restart. Although DHFR domain replacing the RBD could be folded by introducing MTX, it did not induce export of the periplasmic CdiA. Shortening the extended region to increase the effect of folding prevented DHFR folding altogether. Therefore, it is uncertain whether DHFR folding is sufficiently mimicking CdiA RBD folding. Replacing the RBD to colicin RBDs caused OmpT-dependent cleavage at the cite of replacement. Even when ompT is knocked out, colicin RBDs failed to exhibit target cell binding comparable to WT CdiA RBD. Another possible alternative to test the mechanical pulling model is using single molecule experiment with an optical tweezer. A dielectric particle could be fused at the RBD then pulled with a focused laser beam.

Chapter V shows the robustness of CdiA in engaging a target and delivering CdiA-CT toxin. CdiA tolerated significant shortening of its N-terminal filament as well as severing

at the base of filament by a proteolytic digest. As long as the RBD was presented on the surface, CdiA-CT delivered. My work here also deepens our understanding of what the N-terminal CdiA looks like on cell surface. TPS domain of CdiA is extracellular. Also, the extended region is packed tightly against the filament and keeps the filament cell-bound even when disconnect at the base.

Secretion arrest and restart dictate the timing of the toxin delivery by controlling FHA2 folding in the target outer membrane. Even when secretion arrest was faulty, secreted CdiA could deliver CdiA-CT toxin in a receptor-dependent manner because exported FHA2 can fold into an adjacent target cell. In principle, unfolded CdiA molecule could be introduced to target cells and made to refold and deliver CdiA-CT. For a preliminary study, I have concentrated cell-free CdiA molecules by expressing the ΔYP mutant and TCA-precipitating them from the supernatant. Concentrated ΔYP was resuspended in urea. This mutant contains intact RBD, FHA2, pre-toxin domain, and CdiA-CT. When unfolded ΔYP CdiA urea extract was quickly introduced to target cells to dilute urea and allow refolding, CdiA-CT was delivered to a receptor+ target cells but not receptor- control cells (data not shown). This experiment was replicated with the same batch of urea lysate, but I could not repeat TCA precipitation and urea extract to replicate same results. The protein precipitation method may need to be fine-tuned to reliably preserve the activity of C-terminal CdiA.

Finally, my findings in this thesis raises more questions about the energetics of TPS systems. Export of TpsA cargos are thought to be driven by β-helix folding of the TPS and Fha1 domains. However, this energetic drive from sequential β-folding is discontinuous in CdiA because its secretion is halted at the YP region. Despite interrupted secretion, CdiA remains secretion-compatible because receptor-binding readily resumes secretion of the

periplasmic half. Most probably source of energy to drive C-terminal CdiA export is FHA2 folding into the target outer membrane. FHA2 repeats are also predicted to adapt β-strands and they are shown to get deposited in target outer membrane. Once receptor-binding overcomes secretion arrest and exports FHA2, FHA2 repeats can fold into β-barrel like translocon in target cell which could fuel full secretion of CdiA including the CdiA-CT. The C-terminal secretion seems to be independent of the N-terminal secretion since significant deletions of and complete cleavage at the N-terminal Fha1 filament did not hinder C-terminal export after receptor-binding. Whatever the precious mechanism of receptor-induce secretion is, CdiA is a fascinating example of protein secretion across the outer membrane.

References

1. Henderson, J. C. *et al.* The Power of Asymmetry: Architecture and Assembly of the Gram-Negative Outer Membrane Lipid Bilayer. *Annu. Rev. Microbiol.* **70,** 255–278 (2016).
2. Rojas, E. R. *et al.* The outer membrane is an essential load-bearing element in Gram-negative bacteria. *Nature* **559,** 617–621 (2018).
3. Delcour, A. H. Outer membrane permeability and antibiotic resistance. *Biochim. Biophys. Acta - Proteins Proteomics* **1794,** 808–816 (2009).
4. Costa, T. R. D. *et al.* Secretion systems in Gram-negative bacteria: structural and mechanistic insights. *Nat. Rev. Microbiol.* **13,** 343–359 (2015).
5. Papanikou, E., Karamanou, S. & Economou, A. Bacterial protein secretion through the translocase nanomachine. *Nat. Rev. Microbiol.* **5,** 839–851 (2007).
6. Abdallah, A. M. *et al.* Type VII secretion - Mycobacteria show the way. *Nat. Rev. Microbiol.* **5,** 883–891 (2007).
7. Gerlach, R. G. & Hensel, M. Protein secretion systems and adhesins: The molecular armory of Gram-negative pathogens. *Int. J. Med. Microbiol.* **297,** 401–415 (2007).
8. Remaut, H. *et al.* Fiber Formation across the Bacterial Outer Membrane by the Chaperone/Usher Pathway. *Cell* **133,** 640–652 (2008).
9. Desvaux, M., Hébraud, M., Talon, R. & Henderson, I. R. Secretion and subcellular localizations of bacterial proteins: a semantic awareness issue. *Trends Microbiol.* **17,** 139–145 (2009).
10. Goyal, P. *et al.* Structural and mechanistic insights into the bacterial amyloid secretion channel CsgG. *Nature* **516,** 250–253 (2014).
11. Abby, S. S. *et al.* Identification of protein secretion systems in bacterial genomes. *Sci. Rep.* **6,** 1–14 (2016).
12. Sato, K. *et al.* A protein secretion system linked to bacteroidete gliding motility and pathogenesis. *Proc. Natl. Acad. Sci. U. S. A.* **107,** 276–281 (2010).
13. Mark, B. M. & Zhu, Y. Gliding motility and por secretion system genes are widespread among members of the phylum bacteroidetes. *J. Bacteriol.* **195,** 270–278 (2013).
14. Lasica, A. M., Ksiazek, M., Madej, M. & Potempa, J. The Type IX Secretion System (T9SS): Highlights and Recent Insights into Its Structure and Function. *Front. Cell. Infect. Microbiol.* **7,** (2017).
15. Thomas, S., Holland, I. B. & Schmitt, L. The Type 1 secretion pathway - The hemolysin system and beyond. *Biochim. Biophys. Acta - Mol. Cell Res.* **1843,** 1629–1641 (2014).
16. Thanabalu, T., Koronakis, E., Hughes, C. & Koronakis, V. *Substrate-induced assembly of a contiguous channel for protein export from E.coli: reversible bridging of an inner-membrane translocase to an outer membrane exit pore*. *EMBO J.* **17,** (1998).
17. Kenny, B., Haigh, R. & Holland, I. B. Analysis of the haemolysin transport process through the secretion from Escherichia coli of PCM, CAT or ?-galactosidase fused to the Hly C-terminal signal domain. *Mol. Microbiol.* **5,** 2557–2568 (1991).
18. Dalbey, R. E. & Kuhn, A. Protein Traffic in Gram-negative bacteria - how exported and secreted proteins find their way. *FEMS Microbiol. Rev.* **36,** 1023–1045 (2012).

19. He, S. Y., Nomura, K. & Whittam, T. S. Type III protein secretion mechanism in mammalian and plant pathogens. *Biochim. Biophys. Acta - Mol. Cell Res.* **1694,** 181–206 (2004).
20. Büttner, C. R., Sorg, I., Cornelis, G. R., Heinz, D. W. & Niemann, H. H. Structure of the Yersinia enterocolitica Type III Secretion Translocator Chaperone SycD. *J. Mol. Biol.* **375,** 997–1012 (2008).
21. Kubori, T. *et al.* Supramolecular structure of the salmonella typhimurium type III protein secretion system. *Science (80-.).* **280,** 602–605 (1998).
22. Yip, C. K. *et al.* Structural characterization of the molecular platform for type III secretion system assembly. *Nature* **435,** 702–707 (2005).
23. Koster, M. *et al.* The outer membrane component, YscC, of the Yop secretion machinery of *Yersinia enterocolitica* forms a ring-shaped multimeric complex. *Mol. Microbiol.* **26,** 789–797 (1997).
24. Spreter, T. *et al.* A conserved structural motif mediates formation of the periplasmic rings in the type III secretion system. *Nat. Struct. Mol. Biol.* **16,** 468–476 (2009).
25. Tardy, F. *et al.* Yersinia enterocolitica type III secretion-translocation system: channel formation by secreted Yops. *EMBO J.* **18,** 6793–6799 (1999).
26. Pettersson, J. *et al.* Modulation of virulence factor expression by pathogen target cell contact. *Science (80-.).* **273,** 1231–1233 (1996).
27. Christie, P. J., Whitaker, N. & González-Rivera, C. Mechanism and structure of the bacterial type IV secretion systems. *Biochim. Biophys. Acta - Mol. Cell Res.* **1843,** 1578–1591 (2014).
28. Trokter, M., Felisberto-Rodrigues, C., Christie, P. J. & Waksman, G. Recent advances in the structural and molecular biology of type IV secretion systems. *Curr. Opin. Struct. Biol.* **27,** 16–23 (2014).
29. Tzfira, T., Vaidya, M. & Citovsky, V. Involvement of targeted proteolysis in plant genetic transformation by agrobacterium. *Nature* **431,** 87–92 (2004).
30. Christie, P. J. Type IV secretion: The Agrobacterium VirB/D4 and related conjugation systems. *Biochim. Biophys. Acta - Mol. Cell Res.* **1694,** 219–234 (2004).
31. Boyer, F., Fichant, G., Berthod, J., Vandenbrouck, Y. & Attree, I. Dissecting the bacterial type VI secretion system by a genome wide in silico analysis: What can be learned from available microbial genomic resources? *BMC Genomics* **10,** 104 (2009).
32. Zheng, J. & Leung, K. Y. Dissection of a type VI secretion system in Edwardsiella tarda. *Mol. Microbiol.* **66,** 1192–1206 (2007).
33. Zoued, A. *et al.* Architecture and assembly of the Type VI secretion system. *Biochim. Biophys. Acta - Mol. Cell Res.* **1843,** 1664–1673 (2014).
34. Pukatzki, S. *et al.* Identification of a conserved bacterial protein secretion system in Vibrio cholerae using the Dictyostelium host model system. *Proc. Natl. Acad. Sci. U. S. A.* **103,** 1528–1533 (2006).
35. Ma, L. S., Lin, J. S. & Lai, E. M. An IcmF family protein, ImpLM, is an integral inner membrane protein interacting with ImpKL, and its Walker a motif is required for type VI secretion system-mediated Hcp secretion in Agrobacterium tumefaciens. *J. Bacteriol.* **191,** 4316–4329 (2009).
36. Leiman, P. G. *et al.* Type VI secretion apparatus and phage tail-associated protein complexes share a common evolutionary origin. *Proc. Natl. Acad. Sci. U. S. A.* **106,** 4154–4159 (2009).

37. Brunet, Y. R., Hénin, J., Celia, H. & Cascales, E. Type VI secretion and bacteriophage tail tubes share a common assembly pathway. *EMBO Rep.* **15,** 315–321 (2014).
38. Shneider, M. M. *et al.* PAAR-repeat proteins sharpen and diversify the type VI secretion system spike. *Nature* **500,** 350–353 (2013).
39. Basler, M., Pilhofer, M., Henderson, G. P., Jensen, G. J. & Mekalanos, J. J. Type VI secretion requires a dynamic contractile phage tail-like structure. *Nature* **483,** 182–186 (2012).
40. Collier, D. N., Bankaitis, V. A., Weiss, J. B. & Bassford, P. J. The antifolding activity of SecB promotes the export of the E. coli maltose-binding protein. *Cell* **53,** 273–283 (1988).
41. Liu, G., Topping, T. B., Cover, W. H. & Randall, L. L. Retardation of folding as a possible means of suppression of a mutation in the leader sequence of an exported protein. *J. Biol. Chem.* **263,** 14790–14793 (1988).
42. Hardy, S. J. & Randall, L. L. A kinetic partitioning model of selective binding of nonnative proteins by the bacterial chaperone SecB. *Science (80-.).* **251,** 439 LP – 443 (1991).
43. Hartl, F. U., Lecker, S., Schiebel, E., Hendrick, J. P. & Wickner, W. The binding cascade of SecB to SecA to SecY E mediates preprotein targeting to the E. coli plasma membrane. *Cell* **63,** 269–279 (1990).
44. Zimmer, J., Nam, Y. & Rapoport, T. A. Structure of a complex of the ATPase SecA and the protein-translocation channel. *Nature* **455,** 936–943 (2008).
45. Mogensen, J. E. & Otzen, D. E. Interactions between folding factors and bacterial outer membrane proteins. *Mol. Microbiol.* **57,** 326–346 (2005).
46. Amaral, F., Jácome, C., Ângela, M., Tillmann, A. & Ufpel, F. Bacterial Secretion Systems – An overview. **4,** 1–32 (2015).
47. Luirink, J. & Sinning, I. SRP-mediated protein targeting: structure and function revisited. *Biochim. Biophys. Acta* **1694,** 17–35 (2004).
48. Müller, M. Twin-arginine-specific protein export in Escherichia coli. *Res. Microbiol.* **156,** 131–136 (2005).
49. Wu, L. F., Ize, B., Chanal, A., Quentin, Y. & Fichant, G. Bacterial twin-arginine signal peptide-dependent protein translocation pathway: Evolution and mechanism. *J. Mol. Microbiol. Biotechnol.* **2,** 179–189 (2000).
50. Korotkov, K. V., Sandkvist, M. & Hol, W. G. J. The type II secretion system: Biogenesis, molecular architecture and mechanism. *Nat. Rev. Microbiol.* **10,** 336–351 (2012).
51. Abendroth, J. *et al.* The three-dimensional structure of the cytoplasmic domains of EpsF from the type 2 secretion system of Vibrio cholerae. *J. Struct. Biol.* **166,** 303–315 (2009).
52. Abendroth, J., Bagdasarian, M., Sandkvist, M. & Hol, W. G. J. The structure of the cytoplasmic domain of EpsL, an inner membrane component of the type II secretion system of Vibrio cholerae: An unusual member of the actin-like ATPase superfamily. *J. Mol. Biol.* **344,** 619–633 (2004).
53. Abendroth, J., Murphy, P., Sandkvist, M., Bagdasarian, M. & Hol, W. G. J. The X-ray structure of the type II secretion system complex formed by the N-terminal domain of EpsE and the cytoplasmic domain of EpsL of Vibrio cholerae. *J. Mol. Biol.* **348,** 845–855 (2005).

54. Campos, M., Nilges, M., Cisneros, D. A. & Francetic, O. Detailed structural and assembly model of the type II secretion pilus from sparse data. *Proc. Natl. Acad. Sci. U. S. A.* **107,** 13081–13086 (2010).
55. Cisneros, D. A., Pehau-Arnaudet, G. & Francetic, O. Heterologous assembly of type IV pili by a type II secretion system reveals the role of minor pilins in assembly initiation. *Mol. Microbiol.* **86,** 805–818 (2012).
56. Korotkov, K. V. *et al.* Structural and Functional Studies on the Interaction of GspC and GspD in the Type II Secretion System. *PLoS Pathog.* **7,** e1002228 (2011).
57. Sauvonnet, N., Poquet, I. & Pugsley, A. P. Extracellular secretion of pullulanase is unaffected by minor sequence changes but is usually prevented by adding reporter proteins to its N- or C- terminal end. *J. Bacteriol.* **177,** 5238–5246 (1995).
58. Shevchik, V. E. & Robert-Baudouy, J. *Specific interaction between OutD, an Erwinia chrysanthemi outer membrane protein of the general secretory pathway, and secreted proteins ism into the periplasm, where they can be transiently Guy Condemine on the MTB machinery*. *EMBO J.* **16,** (1997).
59. Palomäki, T., Pickersgill, R., Riekki, R., Romantschuk, M. & Saarilahti, H. T. A putative three-dimensional targeting motif of polygalacturonase (PehA), a protein secreted through the type II (GSP) pathway in *Erwinia carotovora*. *Mol. Microbiol.* **43,** 585–596 (2002).
60. Reichow, S. L., Korotkov, K. V., Hol, W. G. J. & Gonen, T. Structure of the cholera toxin secretion channel in its closed state. *Nat. Struct. Mol. Biol.* **17,** 1226–1232 (2010).
61. van Ulsen, P., Rahman, S. ur, Jong, W. S. P., Daleke-Schermerhorn, M. H. & Luirink, J. Type V secretion: From biogenesis to biotechnology. *Biochim. Biophys. Acta - Mol. Cell Res.* **1843,** 1592–1611 (2014).
62. Desvaux, M. *et al.* The unusual extended signal peptide region of the type V secretion system is phylogenetically restricted. *FEMS Microbiol. Lett.* **264,** 22–30 (2006).
63. Desvaux, M. *et al.* A conserved extended signal peptide region directs posttranslational protein translocation via a novel mechanism. *Microbiology* **153,** 59–70 (2007).
64. Baud, C. *et al.* Translocation path of a substrate protein through its Omp85 transporter. *Nat. Commun.* **5,** 1–9 (2014).
65. Aoki, S. K., Webb, J. S., Braaten, B. A. & Low, D. A. Contact-dependent growth inhibition causes reversible metabolic downregulation in Escherichia coli. *J. Bacteriol.* **191,** 1777–1786 (2009).
66. Henderson, I. R., Navarro-Garcia, F., Desvaux, M., Fernandez, R. C. & Ala'Aldeen, D. Type V Protein Secretion Pathway : the Autotransporter Story Type V Protein Secretion Pathway : the Autotransporter Story. *Microbiol. Mol. Biol. Rev.* **68,** 692–744 (2004).
67. Jacob-Dubuisson, F., Fernandez, R. & Coutte, L. Protein secretion through autotransporter and two-partner pathways. *Biochim. Biophys. Acta - Mol. Cell Res.* **1694,** 235–257 (2004).
68. Mazar, J. & Cotter, P. A. Topology and maturation of filamentous haemagglutinin suggest a new model for two-partner secretion. *Mol. Microbiol.* **62,** 641–654 (2006).
69. Buscher, A. Z., Grass, S., Heuser, J., Roth, R. & St. Geme, J. W. Surface anchoring of a bacterial adhesin secreted by the two-partner secretion pathway. *Mol. Microbiol.* **61,**

470–483 (2006).
70. Aoki, S. K. *et al.* Contact-dependent inhibition of growth in Escherichia coli. *Sci. (New York, NY)* **309,** 1245–1248 (2005).
71. Aoki, S. K. *et al.* Contact-dependent growth inhibition requires the essential outer membrane protein BamA (YaeT) as the receptor and the inner membrane transport protein AcrB. *Mol. Microbiol.* **70,** 323–340 (2008).
72. Jacob-Dubuisson, F., Guérin, J., Baelen, S. & Clantin, B. Two-partner secretion: As simple as it sounds? *Res. Microbiol.* **164,** 583–595 (2013).
73. Willett, J. L. E., Ruhe, Z. C., Goulding, C. W., Low, D. A. & Hayes, C. S. Contact-Dependent Growth Inhibition (CDI) and CdiB/CdiA Two-Partner Secretion Proteins. *J. Mol. Biol.* **427,** 3754–3765 (2015).
74. Aoki, S. K. *et al.* A widespread family of polymorphic contact-dependent toxin delivery systems in bacteria. *Nature* **468,** 439–442 (2010).
75. Poole, S. J. *et al.* Identification of functional toxin/immunity genes linked to contact-dependent growth inhibition (cdi) and rearrangement hotspot (rhs) systems. *PLoS Genet.* **7,** (2011).
76. Pinto, C. *et al.* Formation of the β-barrel assembly machinery complex in lipid bilayers as seen by solid-state NMR. *Nat. Commun.* **9,** 4135 (2018).
77. Lee, J. *et al.* Characterization of a stalled complex on the β-barrel assembly machine. *Proc. Natl. Acad. Sci.* **113,** 8717–8722 (2016).
78. Doerner, P. A. & Sousa, M. C. Extreme Dynamics in the BamA β-Barrel Seam. *Biochemistry* **56,** 3142–3149 (2017).
79. Wzorek, J. S., Lee, J., Tomasek, D., Hagan, C. L. & Kahne, D. E. Membrane integration of an essential β-barrel protein prerequires burial of an extracellular loop. *Proc. Natl. Acad. Sci. U. S. A.* **114,** 2598–2603 (2017).
80. Noinaj, N. *et al.* Structural insight into the biogenesis of β-barrel membrane proteins. *Nature* **501,** 385–390 (2013).
81. Gu, Y. *et al.* Structural basis of outer membrane protein insertion by the BAM complex. *Nature* **531,** 64–69 (2016).
82. Han, L. *et al.* Structure of the BAM complex and its implications for biogenesis of outer-membrane proteins. *Nat. Struct. Mol. Biol.* **23,** 192–196 (2016).
83. Bakelar, J., Buchanan, S. K. & Noinaj, N. The structure of the β-barrel assembly machinery complex. *Science (80-.).* **351,** 180–186 (2016).
84. Iadanza, M. G. *et al.* Lateral opening in the intact β-barrel assembly machinery captured by cryo-EM. *Nat. Commun.* **7,** 1–12 (2016).
85. Kim, S. *et al.* Structure and function of an essential component of the outer membrane protein assembly machine. *Science (80-.).* **317,** 961–964 (2007).
86. Höhr, A. I. C. *et al.* Membrane protein insertion through a mitochondrial β-barrel gate. *Science (80-.).* **359,** (2018).
87. Tsirigotaki, A., De Geyter, J., Šoštarić, N., Economou, A. & Karamanou, S. Protein export through the bacterial Sec pathway. *Nat. Rev. Microbiol.* **15,** 21–36 (2017).
88. Schiffrin, B., Brockwell, D. J. & Radford, S. E. Outer membrane protein folding from an energy landscape perspective. *BMC Biol.* **15,** 1–16 (2017).
89. Clantin, B. *et al.* Structure of the membrane protein FhaC: A member of the Omp85-TpsB transporter superfamily. *Science (80-.).* **317,** 957–961 (2007).
90. Konninger, U. W., Hobbie, S., Benz, R. & Braun, V. The haemolysin-secreting ShlB

protein of the outer membrane of Serratia marcescens : determination of surface-exposed residues and formation of ion-permeable pores by ShlB mutants in artificial lipid bilayer membranes. *Mol. Microbiol.* **32,** 1212–1225 (1999).
91. Surana, N. K. *et al. Evidence for conservation of architecture and physical properties of Omp85-like proteins throughout evolution*. (2004). at <www.pnas.orgcgidoi10.1073pnas.0404679101>
92. Delattre, A. S. *et al.* Substrate recognition by the POTRA domains of TpsB transporter FhaC. *Mol. Microbiol.* **81,** 99–112 (2011).
93. Knowles, T. J. *et al.* Fold and function of polypeptide transport-associated domains responsible for delivering unfolded proteins to membranes. *Mol. Microbiol.* **68,** 1216–1227 (2008).
94. Mazar, J. & Cotter, P. A. New insight into the molecular mechanisms of two-partner secretion. *Trends Microbiol.* **15,** 508–515 (2007).
95. Willery, E., Locht, C., Villeret, V. & Clantin, B. The crystal structure of filamentous hemagglutinin secretion domain and its implications for the two-partner secretion pathway. (2004).
96. Hodak, H. *et al.* Secretion signal of the filamentous haemagglutinin, a model two-partner secretion substrate. *Mol. Microbiol.* **61,** 368–382 (2006).
97. Jacob-Dubuisson, F., Buisine, C., Willery, E., Renauld-Mongénie, G. & Locht, C. Lack of functional complementation between Bordetella pertussis filamentous hemagglutinin and Proteus mirabilis HpmA hemolysin secretion machineries. *J. Bacteriol.* **179,** 775–783 (1997).
98. Relman, D. A., Domenighinit, M., Tuomanen, E., Rappuoli ¶, R. & Falkow, S. *Filamentous hemagglutinin of Bordetella pertussis: Nucleotide sequence and crucial role in adherence (Bordetella/deletion mutant/cell recognition site)*. *Biochemistry* **86,** (1989).
99. Makhov, A. M. *et al.* Filamentous Hemagglutinin of Bordetella pertussis. A Bacterial Adhesin Formed as a 50-nm Monomeric Rigid Rod Based on a 19-residue Repeat Motif Rich in Beta Strands and Turns. *J. Mol. Biol.* **241,** 110–124 (1994).
100. Kajava, A. V. *et al.* Beta-helix model for the filamentous haemagglutinin adhesin of Bordetella pertussis and related bacterial secretory proteins. *Mol. Microbiol.* **42,** 279–292 (2001).
101. Renauld-Mongénie, G., Cornette, J., Mielcarek, N., Menozzi, F. D. & Locht, C. Distinct roles of the N-terminal and C-terminal precursor domains in the biogenesis of the Bordetella pertussis filamentous hemagglutinin. *J. Bacteriol.* **178,** 1053–1060 (1996).
102. Guédin, S., Willery, E., Locht, C. & Jacob-Dubuisson, F. Evidence that a globular conformation is not compatible with FhaC-mediated secretion of the Bordetella pertussis filamentous haemagglutinin. *Mol. Microbiol.* **29,** 763–774 (1998).
103. Aoki, S. K., Poole, S. J., Hayes, C. S. & Low, D. A. Toxin on a stick: modular CDI toxin delivery systems play roles in bacterial competition. *Virulence* **2,** 356–9 (2011).
104. Ruhe, Z. C., Wallace, A. B., Low, D. A. & Hayes, C. S. Receptor polymorphism restricts contact-dependent growth inhibition to members of the same species. *MBio* **4,** 1–9 (2013).
105. Ruhe Zachary C., Nguyen Josephine Y., Jing Xiong, K. S. & Beck Christina M., Perkins Basil R., Low David A., H. C. S. CdiA Effectors Use Modular

ReceptorBinding Domains To Recognize Target Bacteria. *MBio* **8,** 1–16 (2017).
106. Beck, C. M. *et al.* CdiA Effectors from Uropathogenic Escherichia coli Use Heterotrimeric Osmoporins as Receptors to Recognize Target Bacteria. 1–26 (2016). doi:10.1371/journal.ppat.1005925
107. Ni, D. *et al.* Structural and functional analysis of the ??-barrel domain of BamA from Escherichia coli. *FASEB J.* **28,** 2677–2685 (2014).
108. Koskiniemi, S. *et al.* Genetic analysis of the CDI pathway from Burkholderia pseudomallei 1026b. *PLoS One* **10,** 1–18 (2015).
109. Chauleau, M., Mora, L., Serba, J. & De Zamaroczy, M. FtsH-dependent processing of RNase colicins d and e3 means that only the cytotoxic domains are imported into the cytoplasm. *J. Biol. Chem.* **286,** 29397–29407 (2011).
110. Bonsor, D. a, Meenan, N. a & Kleanthous, C. Colicins exploit native disorder to gain cell entry: a hitchhiker's guide to translocation. *Biochem. Soc. Trans.* **36,** 1409–1413 (2008).
111. Ruhe, Z. C., Nguyen, J. Y., Beck, C. M., Low, D. A. & Hayes, C. S. The proton-motive force is required for translocation of CDI toxins across the inner membrane of target bacteria. *Mol. Microbiol.* **94,** 466–481 (2014).
112. Beck, C. M., Diner, E. J., Kim, J. J., Low, D. A. & Hayes, C. S. The F pilus mediates a novel pathway of CDI toxin import. *Mol. Microbiol.* **93,** 276–290 (2014).
113. Webb, J. S. *et al.* Delivery of CdiA Nuclease Toxins into Target Cells during Contact-Dependent Growth Inhibition. *PLoS One* (2013). doi:10.1371/journal.pone.0057609
114. Willett, J. L. E., Gucinski, G. C., Fatherree, J. P., Low, D. A. & Hayes, C. S. Contact-dependent growth inhibition toxins exploit multiple independent cell-entry pathways. *Proc. Natl. Acad. Sci. U. S. A.* **112,** 11341–6 (2015).
115. Tikhonova, E. B. & Zgurskaya, H. I. AcrA, AcrB, and TolC of Escherichia coli form a stable intermembrane multidrug efflux complex. *J. Biol. Chem.* **279,** 32116–32124 (2004).
116. Ma, D. *et al.* Genes acrA and acrB encode a stress-induced efflux system of Escherichia coli. *Mol. Microbiol.* **16,** 45–55 (1995).
117. Zgurskaya, H. I. & Nikaido, H. Bypassing the periplasm: Reconstitution of the AcrAB multidrug efflux pump of Escherichia coli. *Proc. Natl. Acad. Sci. U. S. A.* **96,** 7190–7195 (1999).
118. Yu, E. W., McDermott, G., Zgurskaya, H. I., Nikaido, H. & Koshland, D. E. Structural basis of multiple drug-binding capacity of the AcrB multidrug efflux pump. *Science (80-.).* **300,** 976–980 (2003).
119. Nikolakakis, K. *et al.* The toxin/immunity network of Burkholderia pseudomallei contact-dependent growth inhibition (CDI) systems. *Mol. Microbiol.* **84,** 516–529 (2012).
120. Beck, C. M. *et al.* CdiA from enterobacter cloacae delivers a toxic ribosomal RNase into target bacteria. *Structure* **22,** 707–718 (2014).
121. Morse, R. P. *et al.* Structural basis of toxicity and immunity in contact-dependent growth inhibition (CDI) systems. *Proc. Natl. Acad. Sci. U. S. A.* **109,** 21480–21485 (2012).
122. Diner, E. J., Beck, C. M., Webb, J. S., Low, D. A. & Hayes, C. S. Identification of a target cell permissive factor required for contact-dependent growth inhibition (CDI). *Genes Dev.* **26,** 515–525 (2012).

123. Braun, V. & Patzer, S. I. Intercellular communication by related bacterial protein toxins: Colicins, contact-dependent inhibitors, and proteins exported by the type VI secretion system. *FEMS Microbiol. Lett.* **345,** 13–21 (2013).
124. Zhang, D., Iyer, L. M. & Aravind, L. A novel immunity system for bacterial nucleic acid degrading toxins and its recruitment in various eukaryotic and DNA viral systems. *Nucleic Acids Res.* **39,** 4532–4552 (2011).
125. Zhang, D., de Souza, R. F., Anantharaman, V., Iyer, L. M. & Aravind, L. Polymorphic toxin systems: Comprehensive characterization of trafficking modes, processing, mechanisms of action, immunity and ecology using comparative genomics. *Biol. Direct* **7,** 1–76 (2012).
126. Ruhe, Z. C. *et al.* CDI Systems Are Stably Maintained by a Cell-Contact Mediated Surveillance Mechanism. *PLoS Genet.* (2016). doi:10.1371/journal.pgen.1006145
127. Ruhe, Z. C. *et al.* CdiA promotes receptor-independent intercellular adhesion. *Mol. Microbiol.* **98,** 175–192 (2015).
128. García-Bayona, L., Guo, M. S. & Laub, M. T. Contact-dependent killing by Caulobacter crescentus via cell surface-associated, glycine zipper proteins. *Elife* **6,** (2017).
129. Jamet, A. *et al.* A New Family of Secreted Toxins in Pathogenic Neisseria Species. *PLoS Pathog.* **11,** e1004592 (2015).
130. Souza, D. P. *et al.* ARTICLE Bacterial killing via a type IV secretion system. (2015). doi:10.1038/ncomms7453
131. Hood, R. D. *et al.* A Type VI Secretion System of Pseudomonas aeruginosa Targets a Toxin to Bacteria. *Cell Host Microbe* **7,** 25–37 (2010).
132. MacIntyre, D. L., Miyata, S. T., Kitaoka, M. & Pukatzki, S. The Vibrio cholerae type VI secretion system displays antimicrobial properties. *Proc. Natl. Acad. Sci. U. S. A.* **107,** 19520–19524 (2010).
133. Koskiniemi, S. *et al.* Rhs proteins from diverse bacteria mediate intercellular competition. *Proc. Natl. Acad. Sci. U. S. A.* **110,** 7032–7037 (2013).
134. Cao, Z., Casabona, M. G., Kneuper, H., Chalmers, J. D. & Palmer, T. The type VII secretion system of Staphylococcus aureus secretes a nuclease toxin that targets competitor bacteria. *Nat. Microbiol.* **2,** 1–11 (2016).
135. Whitney, J. C. *et al.* A broadly distributed toxin family mediates contact-dependent antagonism between gram-positive bacteria. *Elife* **6,** (2017).
136. Neil, R. B. & Apicella, M. A. Role of HrpA in biofilm formation of Neisseria meningitidis and regulation of the hrpBAS transcripts. *Infect. Immun.* **77,** 2285–2293 (2009).
137. Rojas, C. M., Ham, J. H., Deng, W. L., Doyle, J. J. & Collmer, A. HecA, a member of a class of adhesins produced by diverse pathogenic bacteria, contributes to the attachment, aggregation, epidermal cell killing, and virulence phenotypes of Erwinia chrysanthemi EC16 on Nicotiana clevelandii seedlings. *Proc. Natl. Acad. Sci. U. S. A.* **99,** 13142–13147 (2002).
138. Michalska, K. *et al.* Functional plasticity of antibacterial EndoU toxins. *Mol. Microbiol.* **109,** 509–527 (2018).
139. Albrecht, R. *et al.* Structure of BamA, an essential factor in outer membrane protein biogenesis. *Acta Crystallogr. Sect. D Biol. Crystallogr.* **70,** 1779–1789 (2014).
140. Ye, J. & Van Den Berg, B. Crystal structure of the bacterial nucleoside transporter

Tsx. *EMBO J.* **23,** 3187–3195 (2004).
141. Kramer, R. A. *et al.* Identification of essential acidic residues of outer membrane protease OmpT supports a novel active site. *FEBS Lett.* **505,** 426–430 (2001).
142. Vandeputte-Rutten, L. *et al.* Crystal structure of the outer membrane protease OmpT from Escherichia coli suggests a novel catalytic site. *EMBO J.* (2001). at <https://www.ncbi.nlm.nih.gov/pmc/articles/PMC125623/>
143. Yeo, H. J. *et al.* The structure of the Haemophilus influenzae HMW1 pro-piece reveals a structural domain essential for bacterial two-partner secretion. *J. Biol. Chem.* **282,** 31076–31084 (2007).
144. Yang, J. *et al.* The I-TASSER suite: Protein structure and function prediction. *Nat. Methods* **12,** 7–8 (2014).
145. Basler, M., Pilhofer, M., Henderson, G. P., Jensen, G. J. & Mekalanos, J. J. Type VI secretion requires a dynamic contractile phage tail-like structure. *Nature* **483,** 182–186 (2012).
146. Russell, A. B., Peterson, S. B. & Mougous, J. D. Type VI secretion system effectors: Poisons with a purpose. *Nat. Rev. Microbiol.* **12,** 137–148 (2014).
147. Pathak, D. T., Wei, X., Dey, A. & Wall, D. Molecular Recognition by a Polymorphic Cell Surface Receptor Governs Cooperative Behaviors in Bacteria. *PLoS Genet.* **9,** (2013).
148. Vassallo, C. *et al.* Cell rejuvenation and social behaviors promoted by LPS exchange in myxobacteria. *Proc. Natl. Acad. Sci. U. S. A.* **112,** E2939–E2946 (2015).
149. Vassallo, C. N. *et al.* Infectious polymorphic toxins delivered by outer membrane exchange discriminate kin in myxobacteria. *Elife* **6,** (2017).
150. Cascales, E. *et al.* Colicin Biology. *Microbiol. Mol. Biol. Rev.* **71,** 158–229 (2007).
151. Housden, N. G. & Kleanthous, C. Colicin translocation across the Escherichia coli outer membrane. in *Biochem. Soc. Trans.* **40,** 1475–1479 (Biochem Soc Trans, 2012).
152. Melvin, J. A., Scheller, E. V., Noël, C. R. & Cotter, P. A. New insight into filamentous hemagglutinin secretion reveals a role for full-length FhaB in Bordetella virulence. *MBio* **6,** (2015).
153. Noël, C. R., Mazar, J., Melvin, J. A., Sexton, J. A. & Cotter, P. A. The prodomain of the Bordetella two-partner secretion pathway protein FhaB remains intracellular yet affects the conformation of the mature C-terminal domain. *Mol. Microbiol.* **86,** 988–1006 (2012).
154. Shiomi, D. *et al.* Mutations in cell elongation genes mreB, mrdA and mrdB suppress the shape defect of RodZ-deficient cells. *Mol. Microbiol.* **87,** 1029–1044 (2013).
155. Cherepanov, P. P. & Wackernagel, W. Gene disruption in Escherichia coli: TcR and KmR cassettes with the option of Flp-catalyzed excision of the antibiotic-resistance determinant. *Gene* **158,** 9–14 (1995).
156. Baba, T. *et al.* Construction of Escherichia coli K-12 in-frame, single-gene knockout mutants: The Keio collection. *Mol. Syst. Biol.* **2,** (2006).
157. Hayes, C. S. & Sauer, R. T. Cleavage of the A site mRNA codon during ribosome pausing provides a mechanism for translational quality control. *Mol. Cell* **12,** 903–911 (2003).
158. Garza-Sánchez, F., Schaub, R. E., Janssen, B. D. & Hayes, C. S. tmRNA regulates synthesis of the ArfA ribosome rescue factor. *Mol. Microbiol.* **80,** 1204–1219 (2011).
159. Iancu, C. V. *et al.* Electron cryotomography sample preparation using the Vitrobot.

Nat. Protoc. **1,** 2813–2819 (2007).
160. Kremer, J. R., Mastronarde, D. N. & McIntosh, J. R. Computer visualization of three-dimensional image data using IMOD. *J. Struct. Biol.* **116,** 71–76 (1996).
161. Tivol, W. F., Briegel, A. & Jensen, G. J. An improved cryogen for plunge freezing. *Microsc. Microanal.* **14,** 375–379 (2008).
162. Zheng, S. Q. *et al.* UCSF tomography: An integrated software suite for real-time electron microscopic tomographic data collection, alignment, and reconstruction. *J. Struct. Biol.* **157,** 138–147 (2007).
163. Agulleiro, J. I. & Fernandez, J. J. Fast tomographic reconstruction on multicore computers. *Bioinforma. Appl. NOTE* **27,** 582–583 (2011).
164. Robert, V. *et al.* Assembly Factor Omp85 Recognizes Its Outer Membrane Protein Substrates by a Species-Specific C-Terminal Motif. *PLoS Biol.* **4,** e377 (2006).
165. Ruhe, Z. C. *et al.* Programmed Secretion Arrest and Receptor-Triggered Toxin Export during Antibacterial Contact-Dependent Growth Inhibition. *Cell* **175,** 921-933.e14 (2018).
166. Hayes, C. S., Peng, Z. Y. & Setlow, P. Equilibrium and kinetic binding interactions between DNA and a group of novel, nonspecific DNA-binding proteins from spores of Bacillus and Clostridium species. *J. Biol. Chem.* **275,** 35040–35050 (2000).
167. Frenkiel-Krispin, D. *et al.* Structure of the DNA-SspC complex: Implications for DNA packaging, protection, and repair in bacterial spores. *J. Bacteriol.* **186,** 3525–3530 (2004).
168. Ur Rahman, S., Arenas, J., Öztürk, H., Dekker, N. & Van Ulsen, P. The polypeptide transport-associated (POTRA) domains of TpsB transporters determine the system specificity of two-partner secretion systems. *J. Biol. Chem.* **289,** 19799–19809 (2014).
169. Browning, D. F. *et al.* Cross-species chimeras reveal BamA POTRA and β-barrel domains must be fine-tuned for efficient OMP insertion. *Mol. Microbiol.* **97,** 646–659 (2015).
170. Ganesan, I. Evaluating the Functional Pore Size of Chloroplast TOC and TIC Protein Translocons. 1–35 (2017).
171. Häusler, T., Stierhof, Y. D., Wirtz, E. & Clayton, C. Import of a DHFR hybrid protein into glycosomes in vivo is not inhibited by the folate-analogue aminopterin. *J. Cell Biol.* **132,** 311–324 (1996).
172. Touchette, N. A., Perry, K. M. & Matthews, C. R. Folding of Dihydrofolate Reductase from Escherichia coli. *Biochemistry* **25,** 5445–5452 (1986).
173. Rajagopalan, P. T. R. *et al.* Interaction of dihydrofolate reductase with methotrexate: Ensemble and single-molecule kinetics. *Proc. Natl. Acad. Sci.* **99,** 13481–13486 (2002).
174. Cody, V., Luft, J. R. & Pangborn, W. Understanding the role of Leu22 variants in methotrexate resistance: Comparison of wild-type and Leu22Arg variant mouse and human dihydrofolate reductase ternary crystal complexes with methotrexate and NADPH. *Acta Crystallogr. Sect. D Biol. Crystallogr.* **61,** 147–155 (2005).
175. Fujimoto, Z. *et al.* Crystal structure of a catalytic-site mutant alpha-amylase from Bacillus subtilis complexed with maltopentaose. *J. Mol. Biol.* **277,** 393–407 (1998).
176. Boos, W. & Shuman, H. Maltose/maltodextrin system of Escherichia coli: transport, metabolism, and regulation. *Microbiol. Mol. Biol. Rev.* **62,** 204–29 (1998).
177. Lindeberg, M. & Collmer, A. Analysis of eight out genes in a cluster required for

pectic enzyme secretion by Erwinia chrysanthemi: Sequence comparison with secretion genes from other gram-negative bacteria. *J. Bacteriol.* **174,** 7385–7397 (1992).
178. Korotkov, K. V. & Sandkvist, M. Architecture, Function, and Substrates of the Type II Secretion System. *EcoSal Plus* **8,** (2019).
179. Hagerman, A. E., Blau, D. M. & McClure, A. L. Plate assay for determining the time of production of protease, cellulase, and pectinases by germinating fungal spores. *Anal. Biochem.* **151,** 334–342 (1985).
180. Vorhölter, F. J. *et al.* Involvement of bacterial TonB-dependent signaling in the generation of an oligogalacturonide damage-associated molecular pattern from plant cell walls exposed to Xanthomonas campestris pv. campestris pectate lyases. *BMC Microbiol.* **12,** (2012).
181. Garza-Sánchez, F., Janssen, B. D. & Hayes, C. S. Prolyl-tRNAPro in the A-site of SecM-arrested ribosomes inhibits the recruitment of transfer-messenger RNA. *J. Biol. Chem.* **281,** 34258–34268 (2006).
182. Guérin, J., Bigot, S., Schneider, R., Jacob-Dubuisson, F. & Buchanan, S. K. Two-Partner Secretion: Combining Efficiency and Simplicity in the Secretion of Large Proteins for Bacteria-Host and Bacteria-Bacteria Interactions. *Front. Cell. Infect. Microbiol.* **7,** 1–23 (2017).
183. Grass, S., Rempe, K. A. & St. Geme, J. W. Structural determinants of the interaction between the TpsA and TpsB proteins in the Haemophilus influenzae HMW1 two-partner secretion system. *J. Bacteriol.* **197,** 1769–1780 (2015).
184. Braun, V., Hobbie, S. & Ondraczek, R. Serratia marcescens forms a new type of cytolysin. *FEMS Microbiol. Lett.* **100,** 299–305 (1992).
185. Uphoff, T. S. & Welch, R. A. Nucleotide sequencing of the Proteus mirabilis calcium-independent hemolysin genes (hpmA and hpmB) reveals sequence similarity with the Serratia marcescens hemolysin genes (shlA and shlB). *J. Bacteriol.* **172,** 1206–1216 (1990).
186. Locht, C., Berlin, P., Menozzi, F. D. & Renauld, G. The filamentous haemagglutinin, a multifaceted adhesin produced by virulent Bordetella spp. *Mol. Microbiol.* **9,** 653–660 (1993).
187. St. Geme, J. W. & Yeo, H. J. A prototype two-partner secretion pathway: the Haemophilus influenzae HMW1 and HMW2 adhesin systems. *Trends Microbiol.* **17,** 355–360 (2009).
188. Cope, L. D. *et al.* The 100 kDa haem:haemopexin-binding protein of Haemophilus Influenzae: structure and localization. *Mol. Microbiol.* **13,** 863–873 (1994).